



Search for new phenomena in events with two opposite-charge leptons, jets and missing transverse momentum in pp collisions at $\sqrt{s} = 13$ TeV with the ATLAS detector

The ATLAS Collaboration

The results of a search for direct pair production of top squarks and for dark matter in events with two opposite-charge leptons (electrons or muons), jets and missing transverse momentum are reported, using 139 fb^{-1} of integrated luminosity from proton–proton collisions at $\sqrt{s} = 13$ TeV, collected by the ATLAS detector at the Large Hadron Collider during Run 2 (2015–2018). This search considers the pair production of top squarks and is sensitive across a wide range of mass differences between the top squark and the lightest neutralino. Additionally, spin-0 mediator dark-matter models are considered, in which the mediator is produced in association with a pair of top quarks. The mediator subsequently decays to a pair of dark-matter particles. No significant excess of events is observed above the Standard Model background, and limits are set at 95% confidence level. The results exclude top squark masses up to about 1 TeV, and masses of the lightest neutralino up to about 500 GeV. Limits on dark-matter production are set for scalar (pseudoscalar) mediator masses up to about 250 (300) GeV.

1 Introduction

The Standard Model (SM) of particle physics is extremely successful in describing the phenomena of elementary particles and their interactions. Its predictive power has been proven with high precision by a wide range of experiments. However, despite its success, several important questions remain unanswered within the SM. One particularly striking omission is that it does not provide any explanation for dark matter (DM) [1, 2]. This is a non-baryonic, non-luminous matter component of the universe, for which there is strong evidence from a range of astrophysical observations. A weakly interacting dark-matter candidate particle can be produced at the Large Hadron Collider (LHC) [3] in a variety of ways, as described, for example, by supersymmetry (SUSY) [4–9] or DM models. At the LHC, one of the most promising modes is the production of DM particle pairs in association with on- or off-shell top quarks. Previous searches for DM candidates in association with a top quark pair have been performed by the ATLAS [10–16] and CMS [17–26] collaborations. However, those previous searches were statistically limited, or sensitive only up to limited particle masses. They also suffered from significant regions in which no limit could be placed because the kinematics of the decays made the signal events particularly difficult to identify. This paper aims to extend the sensitivity beyond that of the previous searches to higher masses, and to cover the regions in which the previous ATLAS results had no sensitivity [27, 28]. It achieves this in part by exploiting a larger dataset, corresponding to 139 fb^{-1} of proton–proton collision data collected by the ATLAS experiment during Run 2 of the LHC (2015–2018) at a centre-of-mass energy $\sqrt{s} = 13 \text{ TeV}$. Further improvements in sensitivity are obtained by using a new discriminating variable, the ‘object-based $E_{\text{T}}^{\text{miss}}$ significance’ [29], lowering the lepton p_{T} thresholds, and optimising a dedicated selection to target signal models in the most difficult kinematic regions.

Signal models and kinematic regions

For DM production, the simplified benchmark models [30–32] assume the existence of a mediator particle which couples both to the SM and to the dark sector [33–35]. The couplings of the mediator to the SM fermions are then severely restricted by precision flavour measurements. An ansatz that automatically relaxes these constraints is Minimal Flavour Violation [36]. This assumption implies that the interaction between any new neutral spin-0 state and SM matter is proportional to the fermion masses via Yukawa-type couplings.¹ It follows that colour-neutral mediators would be produced mainly through loop-induced gluon fusion or in association with heavy-flavour quarks. Here, the DM particles χ are assumed to be pair produced through the exchange of a spin-0 mediator, which can be a colour-neutral scalar or pseudoscalar particle (denoted by ϕ or a , respectively), in association with a top quark pair: $pp \rightarrow \chi\bar{\chi}t\bar{t}$ (Figure 1(a)).

Alternatively, dark-matter particles are also predicted in supersymmetry, a space-time symmetry that for each SM particle postulates the existence of a partner particle whose spin differs by one-half unit. To avoid violation of baryon number (B) and lepton number (L) conservation, a multiplicative quantum number R -parity [37], defined as $R = (-1)^{3(B-L)+2S}$, is assumed to be conserved. SUSY particles are then produced in pairs, and the lightest supersymmetric particle (LSP) is stable and, if only weakly interacting, a candidate for dark matter [38, 39]. In the framework of a generic R -parity-conserving Minimal Supersymmetric Standard Model (MSSM) [40, 41], the supersymmetric scalar partners of right-handed and left-handed quarks (squarks), \tilde{q}_{R} and \tilde{q}_{L} , can mix to form two mass eigenstates, \tilde{q}_1 and \tilde{q}_2 , with \tilde{q}_1 defined

¹ Following Ref. [34], couplings to W and Z bosons, as well as explicit dimension-4 ϕ - h or a - h couplings, are set to zero in this simplified model. In addition, the coupling of the mediator to the dark sector is not taken to be proportional to the mass of the DM candidates.

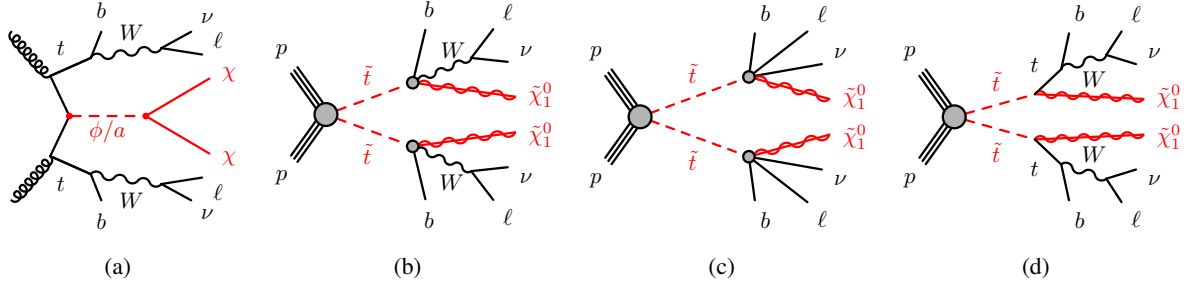


Figure 1: Diagrams representing the signal models targeted by the searches: (a) the spin-0 mediator models, where the mediator decays into a pair of dark-matter particles and is produced in association with a pair of top quarks ($pp \rightarrow \chi\bar{\chi}t\bar{t}$), (b) the three-body \tilde{t}_1 decay mode into an on-shell W boson, a b -quark and the lightest neutralino ($\tilde{t}_1 \rightarrow bW\tilde{\chi}_1^0$), (c) the four-body \tilde{t}_1 decay mode ($\tilde{t}_1 \rightarrow b\bar{\ell}\nu\tilde{\chi}_1^0$) where $\bar{\ell}$ and ν are a anti-lepton with its neutrino and (d) the two-body \tilde{t}_1 decay into an on-shell top quark and the lightest neutralino ($\tilde{t}_1 \rightarrow t\tilde{\chi}_1^0$). For all the diagrams (a-d) the distinction between particle and anti-particle is omitted.

to be the lighter one. In the case of the supersymmetric partner of the top quark, \tilde{t} , large mixing effects can lead to one of the top squark mass eigenstates, \tilde{t}_1 , being significantly lighter than the other squarks. The charginos and neutralinos are mixtures of the bino, winos and Higgsinos that are superpartners of the U(1) and SU(2) gauge bosons and the Higgs bosons, respectively. Their mass eigenstates are referred to as $\tilde{\chi}_i^\pm$ ($i = 1, 2$) and $\tilde{\chi}_j^0$ ($j = 1, 2, 3, 4$) in order of increasing mass. In a large variety of models, the LSP, which is the DM candidate, is the lightest neutralino $\tilde{\chi}_1^0$. Searches for direct pair production of the top squark and DM particles can be performed in final states with two leptons (electrons or muons) of opposite electric charge, jets and missing transverse momentum (Figures 1(b)–1(d)). Depending on the mass difference between the top squark and the lighter SUSY particles, different decay modes are relevant. For $m(W) + m(b) < m(\tilde{t}_1) - m(\tilde{\chi}_1^0) < m(t)$, the three-body decay $\tilde{t}_1 \rightarrow bW\tilde{\chi}_1^0$ occurs through an off-shell top quark (Figure 1(b)). For smaller mass differences, i.e. $m(\tilde{t}_1) - m(\tilde{\chi}_1^0) < m(W) + m(b)$, the four-body decay channel $\tilde{t} \rightarrow bff'\tilde{\chi}_1^0$, where f and f' are two fermions from the off-shell (W^*) decay, is assumed to occur (Figure 1(c)). In this search, f and f' are a charged lepton and its associated anti-neutrino (or vice versa). For each of these two decay modes a dedicated event selection is performed to maximise the sensitivity. These selections are referred to as *three-body* and *four-body* selections in this paper. Direct pair production of top squarks which decay into an on-shell top quark and the lightest neutralino $\tilde{t}_1 \rightarrow t\tilde{\chi}_1^0$, will occur when $m(\tilde{t}_1) - m(\tilde{\chi}_1^0) > m(t)$ (Figure 1(d)). The signature of the $t\bar{t}$ +DM process is similar to that of the simplified model shown in Figure 1(a), so the same selection is also used to constrain the $\tilde{t}_1 \rightarrow t\tilde{\chi}_1^0$ model and it is referred to as the *two-body* selection.

The paper proceeds as follows; after a description of the ATLAS detector in Section 2, the data and simulated Monte Carlo (MC) samples used in the analysis are detailed in Section 3 and the object identification is documented in Section 4. The search strategy, the SM background estimations, and the systematic uncertainties are discussed in Sections 5, 6 and 7. The results and their statistical interpretations are presented in Sections 8 and 9. Finally, Section 10 presents the conclusions.

2 ATLAS detector

The ATLAS detector [42] at the LHC covers nearly the entire solid angle around the collision point.² It consists of an inner tracking detector surrounded by a thin superconducting solenoid, electromagnetic and hadronic calorimeters, and a muon spectrometer with three large superconducting toroidal magnets.

The inner-detector system (ID) is immersed in a 2 T axial magnetic field and provides charged-particle tracking in the range $|\eta| < 2.5$. The high-granularity silicon pixel detector covers the vertex region and typically provides four measurements per track, the first hit normally being in the insertable B-layer installed before Run 2 [43, 44]. It is followed by the silicon microstrip tracker, which usually provides eight measurements per track. These silicon detectors are complemented by the transition radiation tracker (TRT), which enables radially extended track reconstruction up to $|\eta| = 2.0$. The TRT also provides electron identification information based on the fraction of hits (typically 30 in total) above a higher energy-deposit threshold corresponding to transition radiation.

The calorimeter system covers the pseudorapidity range $|\eta| < 4.9$. Within the region $|\eta| < 3.2$, electromagnetic calorimetry is provided by barrel and endcap high-granularity lead/liquid-argon (LAr) calorimeters, with an additional thin LAr presampler covering $|\eta| < 1.8$ to correct for energy loss in material upstream of the calorimeters. Hadronic calorimetry is provided by the steel/scintillating-tile calorimeter, segmented into three barrel structures within $|\eta| < 1.7$, and two copper/LAr hadronic endcap calorimeters. The solid angle coverage is completed with forward copper/LAr and tungsten/LAr calorimeter modules optimised for electromagnetic and hadronic measurements respectively.

The muon spectrometer (MS) comprises separate trigger and high-precision tracking chambers measuring the deflection of muons in a magnetic field generated by the superconducting air-core toroids. The field integral of the toroids ranges between 2.0 and 6.0 T m across most of the detector. A set of precision chambers covers the region $|\eta| < 2.7$ with three layers of monitored drift tubes, complemented by cathode-strip chambers in the forward region, where the background is highest. The muon trigger system covers the range $|\eta| < 2.4$ with resistive-plate chambers in the barrel, and thin-gap chambers in the endcap regions.

Interesting events are selected to be recorded by the first-level trigger system implemented in custom hardware, followed by selections made by algorithms implemented in software in the high-level trigger [45]. The first-level trigger accepts events from the 40 MHz bunch crossings at a rate below 100 kHz, which the high-level trigger reduces in order to record events to disk at about 1 kHz.

3 Data and simulated event samples

The data used in this analysis were collected by the ATLAS detector during pp collisions at a centre-of-mass energy of $\sqrt{s} = 13$ TeV from 2015 to 2018. The average number $\langle\mu\rangle$ of pp interactions per bunch crossing (pile-up) varies from 14 during 2015 to 38 during 2017–2018. Only events taken in stable beam conditions,

² ATLAS uses a right-handed coordinate system with its origin at the nominal interaction point (IP) in the centre of the detector and the z -axis along the beam pipe. The x -axis points from the IP to the centre of the LHC ring, and the y -axis points upwards. Cylindrical coordinates (r, ϕ) are used in the transverse plane, ϕ being the azimuthal angle around the z -axis. The pseudorapidity is defined in terms of the polar angle θ as $\eta = -\ln \tan(\theta/2)$, and the rapidity in terms of energy E and momentum p as $y = 0.5 \ln[(E + p_z)/(E - p_z)]$. Angular distance is measured in units of $\Delta R \equiv \sqrt{(\Delta y)^2 + (\Delta\phi)^2}$ or $\Delta R_\eta \equiv \sqrt{(\Delta\eta)^2 + (\Delta\phi)^2}$. A vector energy \vec{E} is defined by combining the energy deposited in the calorimeter with its deposit direction.

and for which all relevant detector systems were operational, are considered in this analysis. After data-quality requirements the data sample amounts to a total integrated luminosity of 139 fb^{-1} . The uncertainty in the combined 2015–2018 integrated luminosity is 1.7% [46], obtained using the LUCID-2 detector [47].

The two-body and three-body selections use events accepted by a trigger that requires a minimum of two electrons, two muons, or an electron and a muon [45]. Different trigger-level thresholds for the transverse momentum of the leptons were used in different data-taking periods, ranging between 8 and 22 GeV. Tighter thresholds are applied in the lepton offline selection, to ensure that the trigger efficiency is ‘on plateau’ in all of the relevant kinematic region. Missing transverse momentum triggers [48] are used in the four-body selection to increase the acceptance of low- p_T leptons. The missing transverse momentum trigger threshold varied depending on data-taking conditions in the four years: 70 GeV for data collected during 2015; in the range 90–110 GeV for data collected during 2016, and 110 GeV for data collected during 2017 and 2018. Tighter offline requirements on the missing transverse momentum are defined accordingly to ensure event selection on the plateau region of the trigger efficiency curve.

Simulated event samples are used for SM background estimations and to model the signal samples. Standard Model MC samples were processed through a full GEANT4 [49] simulation of the ATLAS detector, while a fast simulation based on parameterisation of the calorimeter response and GEANT4 simulation for all the other detector components [50] is used for the SUSY and DM signal samples. MC events are reconstructed using the same algorithms used for the data. To compensate for small residual differences between data and simulation in the lepton reconstruction efficiency, energy scale, energy resolution, trigger modelling, and b -tagging efficiency, the simulated events are reweighted using correction factors derived from data [51–53].

The events targeted by this analysis are characterised by two leptons with opposite electric charge, jets and missing transverse momentum. The main SM background contributions are expected to come from top quark pair production ($t\bar{t}$), associated production of a Z boson and a top quark pair ($t\bar{t}Z$), single-top decay in the Wt production channel (Wt), $Z/\gamma^* + \text{jets}$ production and diboson processes (VV with $V = W, Z$).

Matrix element and showering generators used for the SM backgrounds and signals are listed in Table 1 along with the relevant parton distribution function (PDF) sets, the configuration of underlying-event and hadronisation parameters (tunes), and the cross-section order in α_s used to normalise the event yields. Additional MC samples are used to estimate systematic uncertainties, as detailed in Section 7.

The SUSY top squark pair signal samples were generated from leading-order (LO) matrix elements with up to two extra partons using MADGRAPH5_aMC@NLO 2.6.2 [54]. MADGRAPH5_aMC@NLO was interfaced to PYTHIA 8.212 + MADSPIN [55, 56] for the signal samples used in the three-body and four-body selections, while it was interfaced to PYTHIA 8.212 for the SUSY signal samples used for the interpretation of the two-body selection results. Signal cross-sections were calculated to next-to-next-to-leading order (NNLO) in α_s , adding the resummation of soft gluon emission at next-to-next-to-leading-logarithm accuracy (NNLO+NNLL) [57–64]. The nominal cross section and the uncertainty are derived using the PDF4LHC15 PDF set, following the recommendations presented in Ref. [65]. Jet–parton matching was performed following the CKKW-L prescription [66]. The A14 tune [67] was used for the modelling of parton showering, hadronisation and the underlying event. Parton luminosities were provided by the NNPDF2.3LO PDF set [68].

The dark-matter signal samples were also generated from leading-order matrix elements, with up to one extra parton, using MADGRAPH5_aMC@NLO 2.6.2 interfaced to PYTHIA 8.212. In the DM samples generation the couplings of the scalar and pseudoscalar mediators to the SM and DM particles (g_q and

g_χ) are set to one. The kinematics of the mediator decay are not strongly dependent on the values of the couplings; however, the particle kinematic distributions are sensitive to the nature of the mediator and to the mediator and DM particle masses. The cross-sections were computed at NLO [69, 70].

Inelastic pp interactions were generated and overlaid onto the hard-scattering process to simulate the effect of multiple proton–proton interactions occurring during the same (in-time) or a nearby (out-of-time) bunch crossing. These were produced using PYTHIA 8.186 [71] and EvtGen [72] with the NNPDF2.3LO set of PDFs [68] and the A3 tune [73]. The MC samples were reweighted so that the distribution of the average number of interactions per bunch crossing reproduces the observed distribution in the data.

Table 1: Simulated signal and background event samples with the corresponding matrix element and parton shower (PS) generators, cross-section order in α_s used to normalise the event yield, and the generator and PS PDF sets used.

| Physics process | Generator | Parton shower | Normalisation | PDF (generator) | PDF (PS) |
|---|-------------------------------|---------------------------------|-------------------|-------------------|-------------------|
| SUSY Signals (three-body, four-body) | MADGRAPH5_aMC@NLO [54]. | PYTHIA 8.212 + MadSPIN [55, 56] | NNLO+NNLL [57–64] | NNPDF2.3LO [68] | NNPDF2.3LO [68] |
| SUSY Signals (two-body) | MADGRAPH5_aMC@NLO | PYTHIA 8.212 | NNLO+NNLL [57–64] | NNPDF2.3LO | NNPDF2.3LO |
| DM Signals (two-body) | MADGRAPH5_aMC@NLO | PYTHIA 8.212 | NLO [69, 70] | NNPDF2.3LO | NNPDF2.3LO |
| $t\bar{t}$ | POWHEG-Box v2 [74–76] | PYTHIA 8.230 | NNLO+NNLL [77] | NNPDF3.0NLO [78] | NNPDF2.3LO |
| $t\bar{t} + V$ ($V = W, Z$) | MADGRAPH5_aMC@NLO | PYTHIA 8.210 | NLO [54, 79] | NNPDF3.0NLO | NNPDF2.3LO |
| Single top | POWHEG-Box v2 [74–76, 80, 81] | PYTHIA 8.230 | NLO+NNLL [82–86] | NNPDF3.0NLO | NNPDF2.3LO |
| $Z/\gamma^* (\rightarrow \ell\ell) + \text{jets}$ | SHERPA 2.2.1 [87, 88] | SHERPA 2.2.1 | NNLO [89] | NNPDF3.0NNLO [78] | NNPDF3.0NNLO [78] |
| Diboson VV ($V = W, Z$) | SHERPA 2.2.1 or 2.2.2 [87] | SHERPA 2.2.1 or 2.2.2 | NLO [90] | NNPDF3.0NNLO | NNPDF3.0NNLO |
| Triboson VVV ($V = W, Z$) | SHERPA 2.2.2 | SHERPA 2.2.2 | NLO [87, 90] | NNPDF3.0NNLO | NNPDF3.0NNLO |
| $t\bar{t}H$ | POWHEG-Box v2 [74, 75, 91] | PYTHIA 8.230 | NLO [54, 79] | NNPDF3.0NLO | NNPDF2.3LO |
| $t\bar{t}WW$ | MADGRAPH5_aMC@NLO | PYTHIA 8.186 [71] | NLO [54] | NNPDF2.3LO | NNPDF2.3LO |
| $t\bar{t}WZ$ | MADGRAPH5_aMC@NLO | PYTHIA 8.212 | NLO [54] | NNPDF3.0NLO | NNPDF2.3LO |
| $tZ, t\bar{t}\bar{t}, t\bar{t}t$ | MADGRAPH5_aMC@NLO | PYTHIA 8.230 | NLO [54] | NNPDF3.0NLO | NNPDF2.3LO |

4 Object identification

Candidate events are required to have a reconstructed vertex with at least two associated tracks, each with $p_T > 500$ MeV and originating from the beam collision region in the x – y plane. The primary vertex in the event is the vertex with the highest scalar sum of the squared transverse momenta of associated tracks.

The leptons selected for analysis are classified as baseline or signal leptons depending on an increasingly stringent set of reconstruction quality criteria and kinematic selections, so that signal leptons are a subset of the baseline leptons. Baseline leptons are used in the calculation of missing transverse momentum ($\mathbf{p}_T^{\text{miss}}$), to resolve ambiguities between the analysis objects in the event, as described later, and for the fake/non-prompt (FNP) lepton background estimation described in Section 6. Signal leptons are used for the final event selection.

Baseline electron candidates are reconstructed from three-dimensional clusters of energy deposition in the electromagnetic calorimeter matched to ID tracks. These electron candidates are required to have pseudorapidity $|\eta| < 2.47$, $E_T > 4.5$ GeV, and to pass a *Loose* likelihood-based identification requirement [51] with an additional condition on the number of hits in the B-layer. The tracks associated with electron candidates are required to have a longitudinal impact parameter³ relative to the primary vertex $|z_0 \sin \theta| < 0.5$ mm, where θ is the track’s polar angle.

³ The transverse impact parameter is defined as the distance of closest approach in the transverse plane between a track and the beam-line. The longitudinal impact parameter corresponds to the z -coordinate distance between the point along the track at which the transverse impact parameter is defined and the primary vertex.

Baseline muon candidates are reconstructed by matching ID tracks, in the pseudorapidity region $|\eta| < 2.4$ for the two-body and three-body selections and $|\eta| < 2.7$ for the four-body selection, with MS tracks or energy deposits in the calorimeter compatible with a minimum-ionising particle (calo-tagged muon). The resulting tracks are required to have a $p_T > 4$ GeV and a $|z_0 \sin \theta| < 0.5$ mm from the primary vertex. Muon candidates are required to satisfy the *Medium* identification requirement, defined in Ref. [52], based on the numbers of hits in the different ID and MS subsystems, and on the significance of the charge-to-momentum ratio q/p .

Additional tighter selections are applied to the baseline lepton candidates to select the signal electrons or muons. Signal electrons are required to satisfy a *Medium* likelihood-based identification requirement [51] and the track associated with a signal electron is required to have a significance $|d_0|/\sigma(d_0) < 5$, where d_0 is the transverse impact parameter relative to the reconstructed primary vertex and $\sigma(d_0)$ is its uncertainty. Isolation criteria are applied to electrons by placing an upper limit on the sum of the transverse energy of the calorimeter energy clusters in a cone of size $\Delta R_\eta = \sqrt{(\Delta\eta)^2 + (\Delta\phi)^2} = 0.2$ around the electron (excluding the deposit from the electron itself) and the scalar sum of the p_T of tracks within a cone of $\Delta R_\eta = 0.2$ around the electron (excluding its own track). The isolation criteria are optimised such that the isolation selection efficiency is uniform across η . This varies from 90% for $p_T = 25$ GeV to 99% for $p_T = 60$ GeV in events with a Z boson decaying into pair of electrons [51].

For signal muons a significance in the transverse impact parameter $|d_0|/\sigma(d_0) < 3$ is required. Isolation criteria applied to muons require the scalar sum of the p_T of tracks inside a cone of $\Delta R_\eta = 0.3$ around the muon (excluding its own track) to be less than 15% of the muon p_T . In addition, the sum of the transverse energy of the calorimeter energy clusters in a cone of $\Delta R_\eta = 0.2$ around the muon (excluding the energy from the lepton itself) must be less than 30% of the muon p_T [52].

Jets are reconstructed from three-dimensional clusters of energy in the calorimeter [92] using the anti- k_t jet clustering algorithm [93] as implemented in the FastJet package [94], with a radius parameter $R = 0.4$. The reconstructed jets are then calibrated by the application of a jet energy scale derived from 13 TeV data and simulation [95]. Only jet candidates with $p_T > 20$ GeV and $|\eta| < 2.8$ are considered.⁴

To reduce the effects of pile-up, for jets with $|\eta| \leq 2.5$ and $p_T < 120$ GeV a significant fraction of the tracks associated with each jet are required to have an origin compatible with the primary vertex, as defined by the jet vertex tagger (JVT) [96]. This requirement reduces the fraction of jets from pile-up to 1%, with an efficiency for pure hard-scatter jets of about 90%. Finally, in order to remove events impacted by detector noise and non-collision backgrounds, specific jet-quality requirements [97, 98] are applied, designed to provide an efficiency of selecting jets from proton–proton collisions above 99.5% (99.9%) for $p_T > 20$ (100) GeV.

The MV2C10 boosted decision tree algorithm [53] identifies jets containing b -hadrons (b -jets) by using quantities such as the impact parameters of associated tracks, and well-reconstructed secondary vertices. A selection that provides 77% efficiency for tagging b -jets in simulated $t\bar{t}$ events is used. The corresponding rejection factors against jets originating from c -quarks, from τ -leptons, and from light quarks and gluons in the same sample at this working point are 4.9, 15 and 110, respectively.

To avoid reconstruction ambiguities and double counting of analysis objects, an overlap removal procedure is applied to the baseline leptons and jets in the order which follows. First, the calo-tagged muons are removed if sharing the track with electrons and, next, all electrons sharing an ID track with a muon are removed. Jets which are not b -tagged (with the tagging parameters corresponding to an efficiency of 85%)

⁴ Hadronic τ -lepton decay products are treated as jets.

and which lie within a cone of $\Delta R = \sqrt{(\Delta y)^2 + (\Delta\phi)^2} = 0.2$ around an electron candidate are removed. All jets lying within $\Delta R = 0.2$ of an electron are removed if the electron has $p_T > 100$ GeV. Finally, any lepton candidate is removed in favour of a jet candidate if it lies a distance $\Delta R < \min(0.4, 0.04 + 10/p_T(\ell))$ from the jet, where $p_T(\ell)$ is the p_T of the lepton.

The missing transverse momentum ($\mathbf{p}_T^{\text{miss}}$), with magnitude E_T^{miss} , is defined as the negative vector sum of the transverse momenta for all baseline electrons, photons, muons and jets. Low-momentum tracks from the primary vertex that are not associated with reconstructed analysis objects are also included in the calculation. The E_T^{miss} value is adjusted for the calibration of the selected physics objects [99]. Linked to the E_T^{miss} value is the ‘object-based E_T^{miss} significance’, called simply ‘ E_T^{miss} significance’ in this paper. This quantity measures the significance of E_T^{miss} based upon the transverse momentum resolution of all objects used in the calculation of the $\mathbf{p}_T^{\text{miss}}$. It is defined as

$$E_T^{\text{miss}} \text{ significance} = \frac{|\mathbf{p}_T^{\text{miss}}|}{\sqrt{\sigma_L^2(1 - \rho_{LT}^2)}}$$

where σ_L is the (longitudinal) component parallel to the $\mathbf{p}_T^{\text{miss}}$ of the total transverse momentum resolution for all objects in the event and the quantity ρ_{LT} is the correlation factor between the parallel and perpendicular components of the transverse momentum resolution for each object. On an event-by-event basis, given the full event composition, E_T^{miss} significance evaluates the p -value that the observed E_T^{miss} is consistent with the null hypothesis of zero real E_T^{miss} , as further detailed in Ref. [29]. In this way E_T^{miss} significance helps to separate events with true E_T^{miss} , arising from weakly interacting particles such as dark matter or neutralinos, from those where E_T^{miss} is consistent with particle mismeasurement, resolution or identification inefficiencies, thus providing better background rejection.

5 Event selection

Different event selections are inspired by previous published strategies [27, 28] reoptimised to fully exploit the larger available dataset. For all selections, an improvement in the sensitivity is obtained with the introduction of the E_T^{miss} significance variable, which enables further optimisation of the selection variables. The four-body sensitivity also benefits from a reduction in the lepton p_T threshold in the region with small mass differences $\Delta m(\tilde{\tau}_1, \tilde{\chi}_1^0)$ between $\tilde{\tau}_1$ and $\tilde{\chi}_1^0$. The threshold for the muon (electron) p_T was lowered from 7 GeV to 4 GeV (4.5 GeV).

Events are required to have exactly two signal leptons (two electrons, two muons, or one electron and one muon) with opposite electric charge. In the two-body and three-body selections, an invariant mass $m_{\ell\ell}$ greater than 20 GeV condition is applied to remove leptons from Drell–Yan and low-mass resonances, while in the four-body selection, given the softer p_T spectrum of the leptons, $m_{\ell\ell}$ is required to be higher than 10 GeV. Events with same flavour (SF) lepton pairs ($e^\pm e^\mp$ and $\mu^\pm \mu^\mp$) with $m_{\ell\ell}$ between 71.2 and 111.2 GeV are rejected to reduce the Z boson background, except for the four-body selection. No additional $m_{\ell\ell}$ selection is imposed on the different flavour (DF) lepton pairs ($e^\pm \mu^\mp$). Different jet (b -jet) multiplicities, labelled as n_{jets} ($n_{b\text{-jets}}$), are required in the three selections, as detailed below.

5.1 Discriminators and kinematic variables

Final event selections are obtained by separating signal from SM background using different kinematic variables. Two variables are constructed from the E_T^{miss} and the p_T of the leading leptons and jets:

$$R_{2\ell} = E_T^{\text{miss}} / (p_T(\ell_1) + p_T(\ell_2)) \quad \text{and} \quad R_{2\ell 4j} = E_T^{\text{miss}} / \left(E_T^{\text{miss}} + p_T(\ell_1) + p_T(\ell_2) + \sum_{i=1, \dots, N \leq 4} p_T(j_i) \right)$$

where $p_T(\ell_1)$ and $p_T(\ell_2)$ are the leading and sub-leading lepton transverse momenta respectively and $p_T(j_{i=1, \dots, N \leq 4})$ are the transverse momenta of the up to four leading jets, in decreasing order. For some backgrounds, e.g. $Z/\gamma^* + \text{jets}$, the variable $R_{2\ell}$ has a distribution that peaks at lower values than the signal, and it is thus used to reject those backgrounds. Similarly, $R_{2\ell 4j}$ is employed for its high rejection power against multi-jet events.

Another variable employed is $\mathbf{p}_{T, \text{boost}}^{\ell\ell}$, which is defined as the vectorial sum of $\mathbf{p}_T^{\text{miss}}$ and the leptons' transverse momentum vectors $\mathbf{p}_T(\ell_1)$ and $\mathbf{p}_T(\ell_2)$. Its magnitude, $p_{T, \text{boost}}^{\ell\ell}$, can be interpreted as the magnitude of the vector sum of all the transverse hadronic activity in the event. The azimuthal angle between the $\mathbf{p}_T^{\text{miss}}$ vector and the $\mathbf{p}_{T, \text{boost}}^{\ell\ell}$ vector is defined as $\Delta\phi_{\text{boost}}$. This variable is useful for selecting events where the non hadronic component (e, μ, ν and χ or $\tilde{\chi}_1^0$) is collimated.

The lepton-based transverse mass [100, 101] is a kinematic variable used to bound the masses of a pair of identical particles which have each decayed into a visible and an invisible particle. This quantity is defined as

$$m_{T2}(\mathbf{p}_{T,1}, \mathbf{p}_{T,2}, \mathbf{p}_T^{\text{miss}}) = \min_{\mathbf{q}_{T,1} + \mathbf{q}_{T,2} = \mathbf{p}_T^{\text{miss}}} \left\{ \max [m_T(\mathbf{p}_{T,1}, \mathbf{q}_{T,1}), m_T(\mathbf{p}_{T,2}, \mathbf{q}_{T,2})] \right\},$$

where m_T indicates the transverse mass,⁵ $\mathbf{p}_{T,1}$ and $\mathbf{p}_{T,2}$ are the transverse momentum vectors of two visible particles, and $\mathbf{q}_{T,1}$ and $\mathbf{q}_{T,2}$ are transverse momentum vectors with $\mathbf{p}_T^{\text{miss}} = \mathbf{q}_{T,1} + \mathbf{q}_{T,2}$. The minimisation is performed over all the possible decompositions of $\mathbf{p}_T^{\text{miss}}$. In this paper, $\mathbf{p}_{T,1}$ and $\mathbf{p}_{T,2}$ are the transverse momentum vectors of the two leptons and $m_{T2}(\mathbf{p}_T(\ell_1), \mathbf{p}_T(\ell_2), \mathbf{p}_T^{\text{miss}})$ is referred to simply as $m_{T2}^{\ell\ell}$. For the $m_{T2}^{\ell\ell}$ calculation, the invisible particles are assumed to be massless. The $m_{T2}^{\ell\ell}$ distribution is expected to have an endpoint corresponding to the W mass for backgrounds such as $t\bar{t}$ while it is expected to reach higher values in the case of SUSY events, due to the presence of the neutralinos [102, 103].

The three-body selection uses a number of 'super-razor' variables [104], which are derived with a series of assumptions made in order to approximate the centre-of-mass energy frame (Razor Frame) of two parent particles (i.e. top squarks) and the decay frames. Each parent particle is assumed to decay into a set of visible (only leptons are considered in this case) and invisible particles (i.e. neutrinos and neutralinos). These variables are R_{p_T} , the Lorentz factor γ_{R+1} , the azimuthal angle $\Delta\phi_\beta^R$ and M_Δ^R . The first variable is $R_{p_T} = |\vec{J}_T| / (|\vec{J}_T| + \sqrt{\hat{s}_R}/4)$ with \vec{J}_T as the vector sum of the transverse momenta of the visible particles and the missing transverse momentum, and $\sqrt{\hat{s}_R}$ as an estimate of the system's energy in the razor frame R , defined as the frame in which the two visible leptons have equal and opposite longitudinal momentum (p_z). The value of $|\vec{J}_T|$ vanishes for events where leptons are the only visible particles, such as diboson events, leading to R_{p_T} values that tend toward zero. Instead, in events that contain additional activity, such as $t\bar{t}$, this variable tends towards unity. The Lorentz factor, γ_{R+1} , is associated with the boost from the razor frame R to the approximation of the two decay frames of the parent particles and is expected to have

⁵ The transverse mass is defined by the equation $m_T(\mathbf{p}_T, \mathbf{q}_T) = \sqrt{2|\mathbf{p}_T||\mathbf{q}_T|(1 - \cos(\Delta\phi))}$, where $\Delta\phi$ is the angle between particles of negligible mass with transverse momenta \mathbf{p}_T and \mathbf{q}_T .

values tending towards unity for back-to-back visible particles or when they have different momenta. Lower values of γ_{R+1} are otherwise expected when the two visible particles are collinear and have comparable momentum. The azimuthal angle $\Delta\phi_{\beta}^R$ is defined between the razor boost from the laboratory to the R frame and the sum of the visible momenta as evaluated in the R frame. It is a good discriminator when used in searches for signals from models with small mass differences between the massive pair-produced particle and the invisible particle produced in the decay. Finally, the last variable is $M_{\Delta}^R = \sqrt{\hat{s}_R}/\gamma_{R+1}$, which is particularly powerful in discriminating between signal events and $t\bar{t}$ and diboson background, since it has a kinematic end-point that is proportional to the mass-splitting between the parent particle and the invisible particle.

5.2 Two-body event selection

This selection targets the dark-matter signal model that assumes the production of a pair of dark-matter particles through the exchange of a spin-0 mediator, in association with a pair of top quarks (Figure 1(a)). It is also used for a search for top squarks decaying into an on-shell top and neutralino (Figure 1(d)).

For each event, the leading lepton, ℓ_1 , is required to have $p_T(\ell_1) > 25$ GeV, while for the sub-leading lepton, ℓ_2 , the requirement is $p_T(\ell_2) > 20$ GeV. The event selection also requires at least one reconstructed b -jet, $\Delta\phi_{\text{boost}}$ lower than 1.5 and E_T^{miss} significance greater than 12, and finally $m_{T2}^{\ell\ell}$ greater than 110 GeV. Following the classification of the events, two sets of signal regions (SRs) are defined: a set of exclusive SRs *binned* in the $m_{T2}^{\ell\ell}$ variable, to maximise model-dependent search sensitivity, and a set of *inclusive* SRs, to be used for model-independent results. For the binned SRs, events are separated according to the lepton flavours, different flavour or same flavour, and by the range $[x, y)$ of the $m_{T2}^{\ell\ell}$ interval: SR – DF $_{[x,y]}^{2\text{-body}}$ or SR – SF $_{[x,y]}^{2\text{-body}}$. For the inclusive signal regions, referred to as SR $_{[x,\infty)}^{2\text{-body}}$ with x being the lower bound placed on the $m_{T2}^{\ell\ell}$ variable, DF and SF events are combined. The common definition of these two sets of signal regions is shown in Table 2.

Table 2: Two-body selection. Common definition of the binned and the inclusive sets of signal regions.

| | SR $^{2\text{-body}}$ | |
|-----------------------------------|-----------------------|----------|
| | DF | SF |
| Leptons flavour | | |
| $p_T(\ell_1)$ [GeV] | > 25 | |
| $p_T(\ell_2)$ [GeV] | > 20 | |
| $m_{\ell\ell}$ [GeV] | > 20 | |
| $ m_{\ell\ell} - m_Z $ [GeV] | – | > 20 |
| $n_{b\text{-jets}}$ | | ≥ 1 |
| $\Delta\phi_{\text{boost}}$ [rad] | | < 1.5 |
| E_T^{miss} significance | | > 12 |
| $m_{T2}^{\ell\ell}$ [GeV] | | > 110 |

5.3 Three-body event selection

The three-body decay mode of the top squark shown in Figure 1(b) is dominant in the region where $m(\tilde{t}_1) > m(\tilde{\chi}_1^0) + m(W) + m(b)$ and $m(\tilde{t}_1) < m(\tilde{\chi}_1^0) + m(t)$. The signal kinematics in this region resemble that of WW production when $\Delta m(\tilde{t}, \tilde{\chi}_1^0) \sim m(W)$ and that of $t\bar{t}$ production when $\Delta m(\tilde{t}, \tilde{\chi}_1^0) \sim m(t)$. The signal selection was optimised to reject these dominant backgrounds while not degrading signal efficiency. The b -jet multiplicity is highly dependent on the mass-splitting between the top squark and the neutralino, $\Delta m(\tilde{t}_1, \tilde{\chi}_1^0) = m(\tilde{t}_1) - m(\tilde{\chi}_1^0)$, since for lower $\Delta m(\tilde{t}_1, \tilde{\chi}_1^0)$ the b -jets have lower momentum and cannot be reconstructed efficiently. Accordingly, two orthogonal signal regions were defined: $\text{SR}_W^{3\text{-body}}$ targeting $\Delta m(\tilde{t}, \tilde{\chi}_1^0) \sim m(W)$, applying a b -jet veto, and $\text{SR}_t^{3\text{-body}}$ targeting $\Delta m(\tilde{t}, \tilde{\chi}_1^0) \sim m(t)$, allowing for b -jets. Separation between same-flavour and different-flavour events is also kept to optimise model-dependent search sensitivity, thus defining four different SRs: $\text{SR-DF}_W^{3\text{-body}}$, $\text{SR-SF}_W^{3\text{-body}}$, $\text{SR-DF}_t^{3\text{-body}}$ and $\text{SR-SF}_t^{3\text{-body}}$. The signal regions make use of a common set of requirements on the p_T of the two leptons, E_T^{miss} significance and γ_{R+1} . The definitions of these regions are summarised in Table 3.

Table 3: Three-body selection. Signal regions definition.

| | $\text{SR}_W^{3\text{-body}}$ | | $\text{SR}_t^{3\text{-body}}$ | |
|----------------------------------|-------------------------------|--------|-------------------------------|----------|
| | DF | SF | DF | SF |
| Leptons flavour | | | | |
| $p_T(\ell_1)$ [GeV] | > 25 | | > 25 | |
| $p_T(\ell_2)$ [GeV] | > 20 | | > 20 | |
| $m_{\ell\ell}$ [GeV] | > 20 | | > 20 | |
| $ m_{\ell\ell} - m_Z $ [GeV] | – | > 20 | – | > 20 |
| $n_{b\text{-jets}}$ | | = 0 | | ≥ 1 |
| $\Delta\phi_\beta^R$ [rad] | | > 2.3 | | > 2.3 |
| E_T^{miss} significance | | > 12 | | > 12 |
| $1/\gamma_{R+1}$ | | > 0.7 | | > 0.7 |
| R_{p_T} | | > 0.78 | | > 0.70 |
| M_Δ^R [GeV] | | > 105 | | > 120 |

5.4 Four-body event selection

In the kinematic region defined by $m(\tilde{t}_1) < m(\tilde{\chi}_1^0) + m(b) + m(W)$ and $m(\tilde{t}_1) > m(\tilde{\chi}_1^0) + m(b)$, the top squarks are assumed to decay via a four-body process through an off-shell top quark and W boson as shown in Figure 1(c). In this region the final-state leptons from the virtual W boson decay are expected to have lower momentum and can be efficiently selected when imposing both a lower and upper bound on the p_T of the leptons. A transverse momentum lower bound of 4.5 GeV (4 GeV) is applied for electrons (muons), together with an upper bound, which is optimised separately for the leading and the sub-leading leptons. Two separate signal regions are defined to cover different $\Delta m(\tilde{t}_1, \tilde{\chi}_1^0)$ ranges: the first one, $\text{SR}_{\text{Small } \Delta m}^{4\text{-body}}$, targets small values of $\Delta m(\tilde{t}_1, \tilde{\chi}_1^0)$ and requires $p_T(\ell_1) < 25$ GeV and $p_T(\ell_2) < 10$ GeV; the second one, $\text{SR}_{\text{Large } \Delta m}^{4\text{-body}}$, targets larger values of $\Delta m(\tilde{t}_1, \tilde{\chi}_1^0)$ and instead requires $p_T(\ell_2) > 10$ GeV. This condition also

ensures orthogonality between the two SRs. The presence of an energetic initial-state radiation (ISR) jet recoiling against the system of the two top squarks is required, introducing an imbalance in the event kinematics with an enhanced value of E_T^{miss} that allows signal events to be distinguished from SM processes. For this reason, for each event, the leading jet j_1 is considered to be a jet from ISR and required to have $p_T > 150$ GeV. A further reduction of the SM background is achieved with selections on E_T^{miss} significance, $p_{T,\text{boost}}^{\ell\ell}$, $R_{2\ell}$ and $R_{2\ell 4j}$ variables. An additional requirement is applied to improve the sub-leading lepton isolation, using the following isolation variable:

$$\min \Delta R_{\ell_2, j_i} = \min_{j_i \in [\text{jets}]} \Delta R_{\eta}(\ell_2, j_i)$$

where ‘[jets]’ contains all the jets in the event. This reduces the probability of lepton misidentification or selecting a lepton originating from heavy-flavour or π/K decays in jets. The definitions of these regions are summarised in Table 4.

Table 4: Four-body selection. Signal regions definition.

| | $\text{SR}_{\text{Small } \Delta m}^{4\text{-body}}$ | $\text{SR}_{\text{Large } \Delta m}^{4\text{-body}}$ |
|---------------------------------------|--|--|
| $p_T(\ell_1)$ [GeV] | < 25 | < 100 |
| $p_T(\ell_2)$ [GeV] | < 10 | [10, 50] |
| $m_{\ell\ell}$ [GeV] | | > 10 |
| $p_T(j_1)$ [GeV] | | > 150 |
| $\min \Delta R_{\ell_2, j_i}$ | | > 1 |
| E_T^{miss} significance | | > 10 |
| $p_{T,\text{boost}}^{\ell\ell}$ [GeV] | | > 280 |
| E_T^{miss} [GeV] | | > 400 |
| $R_{2\ell}$ | > 25 | > 13 |
| $R_{2\ell 4j}$ | > 0.44 | > 0.38 |

6 Background estimation

The MC predictions for the dominant SM background processes are improved using a data-driven normalisation procedure, while non-dominant processes are estimated directly using MC simulation. A simultaneous profile likelihood fit [105] is used to constrain the MC yields with the observed data in dedicated background control regions (CRs). The fit is performed using standard minimisation software [106, 107] where the normalisations of the targeted backgrounds are allowed to float, while the MC simulation is used to describe the shape of kinematic variables. Systematic uncertainties that could affect the expected yields in the different regions are taken into account in the fit through nuisance parameters. Each uncertainty source is described by a single nuisance parameter, and correlations between nuisance parameters, background processes and selections are taken into account. A list of the systematic uncertainties considered in the fits is provided in Section 7. The SM background thus modelled is validated in dedicated validation regions (VRs) which are disjoint from both the control and signal regions.

Important sources of reducible background are events with jets which are misidentified as leptons. The fake/non-prompt (FNP) lepton background comes from π/K and heavy-flavour hadron decays and photon

conversions. This is particularly important for the low- p_T leptons targeted by the four-body selection. The FNP background is mainly suppressed by the lepton isolation requirements described in Section 4, but a non-negligible residual contribution is expected. This is estimated from data using the ‘fake factor’ method [108–111] which uses two orthogonal lepton definitions, labelled as ‘Id’ and ‘anti-Id’, to define a control data sample enriched in fake leptons. The Id lepton corresponds to the signal lepton identification criteria used in this analysis. Anti-Id electrons fail either the signal identification or isolation requirement, while anti-Id muons fail the isolation requirement. The sample used for the fake-factor computation is enriched in Z +jets events. Events with three leptons are selected, with the two same-flavour leptons of opposite electric charge (SFOS leptons) identified as the Z boson decay products (ℓ_1^Z and ℓ_2^Z , in order of decreasing p_T) satisfying the Id requirements, and the third unpaired lepton, called the *probe* lepton (ℓ^{probe}), satisfying either the Id or anti-Id criteria. The fake factor is defined as the ratio of the Id lepton yield to the anti-Id probe lepton yield. Residual contributions from processes producing prompt leptons are subtracted using the MC predictions. Fake factors are measured separately for electrons and muons and as a function of the lepton p_T and η . These are derived in the CR^{FNP} region whose selection is summarised in Table 5. The FNP estimates in each analysis region are derived by applying the fake factors to events satisfying that region’s criteria but replacing at least one of the signal leptons by an anti-Id one.

Table 5: FNP selection. Detailed definition of the CR^{FNP} region.

| | CR^{FNP} |
|---|---|
| Lepton multiplicity | 3 |
| $ m_{\ell\ell} - m_Z $ [GeV] | < 10 for SFOS pair |
| $p_T(\ell_1^Z)$ [GeV] | > 25 |
| $p_T(\ell_2^Z)$ [GeV] | > 20 |
| $p_T(\ell^{\text{probe}})$ [GeV] | > 4.5 (4.0) e (μ) |
| $\Delta R_\eta(\ell^{\text{probe}}, \ell_i)$ | > 0.2 |
| $m_T(\ell^{\text{probe}}, E_T^{\text{miss}})$ [GeV] | < 40 |
| Additional requirements | $p_T(\ell^{\text{probe}}) < 16$ GeV or $E_T^{\text{miss}} < 50$ GeV |

The three selections in this paper use different sets of CRs and VRs, specifically designed to be kinematically similar to the respective SRs. The definitions of the regions used in each analysis and the results of the fits are described in the following subsections.

6.1 Estimation of the backgrounds in the two-body selection

The main background sources for the two-body selection are $t\bar{t}$ and $t\bar{t}Z$ with invisible decay of the Z boson. These processes are normalised to data in dedicated CRs: $\text{CR}_{t\bar{t}}^{2\text{-body}}$ and $\text{CR}_{t\bar{t}Z}$. The $t\bar{t}$ normalisation factor is extracted from different-flavour dilepton events. In order to test the reliability of the $t\bar{t}$ background prediction, two validation regions $\text{VR}_{t\bar{t},\text{DF}}^{2\text{-body}}$ and $\text{VR}_{t\bar{t},\text{SF}}^{2\text{-body}}$ are defined. The $t\bar{t}Z$ production events with invisible decay of the Z boson are expected to dominate the tail of the $m_{T2}^{\ell\ell}$ distribution in the SRs and are normalised in the dedicated control region $\text{CR}_{t\bar{t}Z}$. Given the difficulty in achieving sufficient purity for this SM process because of the high contamination from $t\bar{t}$ events, a strategy based on a three-lepton

final state is adopted. Events are selected if characterised by three charged leptons including at least one pair of SFOS leptons having invariant mass consistent with that of the Z boson ($|m_{\ell\ell} - m_Z| < 20$ GeV). If more than one pair is identified, the one with $m_{\ell\ell}$ closest to the Z boson mass is chosen. Events are further required to have a jet multiplicity, n_{jets} , greater than or equal to three with at least two b -tagged jets. These selections target $t\bar{t}Z$ production with the Z boson decaying into two leptons and $t\bar{t}$ decaying in the semileptonic channel. In order to select $t\bar{t}Z$ events whose kinematics, regardless of subsequent $t\bar{t}$ and Z decays, emulate the kinematics of this background in the SRs, the momenta of the two leptons of the SFOS pair ($\mathbf{p}(\ell_1^Z), \mathbf{p}(\ell_2^Z)$) are vectorially added to the $\mathbf{p}_T^{\text{miss}}$, effectively treating them like the neutrino pair from the Z boson decay. A variable called $E_{T,\text{corr}}^{\text{miss}} = |(\mathbf{p}_T^{\text{miss}} + \mathbf{p}(\ell_1^Z) + \mathbf{p}(\ell_2^Z))_T|$ is constructed. Events characterised by high $m_{T2}^{\ell\ell}$ in the SRs are emulated by requiring high $E_{T,\text{corr}}^{\text{miss}}$ values in $\text{CR}_{t\bar{t}Z}$. In order to check the $t\bar{t}Z$ background estimation, the validation region $\text{VR}_{t\bar{t}Z}^{2\text{-body}}$ was defined. For this region, events with four leptons are selected and required to have at least one pair of SFOS leptons compatible with the Z boson decay. A variant of the m_{T2} variable called $m_{T2}^{4\ell}$ is defined from the $\mathbf{p}_{T,\text{corr}}^{\text{miss}} = (\mathbf{p}_T^{\text{miss}} + \mathbf{p}(\ell_1^Z) + \mathbf{p}(\ell_2^Z))_T$ and the momenta of the remaining two leptons. The definition of the control and validation regions used in the two-body selection is summarised in Table 6. The expected signal contamination in the CRs is generally below $\sim 1\%$. The signal contamination in the VRs is less than 15% (7%) for a DM signal model with scalar (pseudoscalar) mediator mass of 100 GeV and DM mass of 1 GeV.

Table 6: Two-body selection. Control and validation regions definition. The common selection defined in Section 5 also applies to all regions.

| | $\text{CR}_{t\bar{t}}^{2\text{-body}}$ | $\text{CR}_{t\bar{t}Z}$ | $\text{VR}_{t\bar{t},\text{DF}}^{2\text{-body}}$ | $\text{VR}_{t\bar{t},\text{SF}}^{2\text{-body}}$ | $\text{VR}_{t\bar{t}Z}^{2\text{-body}}$ |
|---|--|--|--|--|---|
| Lepton multiplicity | 2 | 3 | 2 | | 4 |
| Lepton flavour | DF | at least one SFOS pair | DF | SF | at least one SFOS pair |
| $p_T(\ell_1)$ [GeV] | > 25 | > 25 | > 25 | | > 25 |
| $p_T(\ell_2)$ [GeV] | > 20 | > 20 | > 20 | | > 20 |
| $p_T(\ell_3)$ [GeV] | – | > 20 | – | | > 20 |
| $p_T(\ell_4)$ [GeV] | – | – | – | | > 20 |
| $m_{\ell\ell}$ | > 20 | – | > 20 | | – |
| $ m_{\ell\ell} - m_Z $ [GeV] | – | < 20 for at least one SFOS pair | – | > 20 | < 20 for the SFOS pair |
| $n_{b\text{-jets}}$ | ≥ 1 | ≥ 2 with $n_{\text{jets}} \geq 3$ | ≥ 1 | | > 0 |
| $\Delta\phi_{\text{boost}}$ [rad] | ≥ 1.5 | – | < 1.5 | | – |
| E_T^{miss} significance | > 8 | – | > 12 | | – |
| $E_{T,\text{corr}}^{\text{miss}}$ [GeV] | – | > 140 | – | | – |
| $m_{T2}^{\ell\ell}$ [GeV] | [100, 120] | – | [100, 110] | | – |
| $m_{T2}^{4\ell}$ [GeV] | – | – | – | | > 110 |

Figure 2 illustrates the modelling of the shape of two important variables after the background fit: (a) shows the $\Delta\phi_{\text{boost}}$ distribution with the $\text{CR}_{t\bar{t}}^{2\text{-body}}$ selection, and (b) shows the $m_{\ell\ell}$ distribution of the SFOS leptons in the $\text{CR}_{t\bar{t}Z}$ selection. Good agreement is found between the data and the background model for all of the selection variables.

The results of the fit are reported in Table 7 for the two-body CRs and VRs. The normalisations for fitted backgrounds are found to be consistent with the theoretical predictions when uncertainties are considered: the normalisation factors obtained from the fit for $t\bar{t}$ and $t\bar{t}Z$ are 0.88 ± 0.08 and 1.07 ± 0.14 respectively.

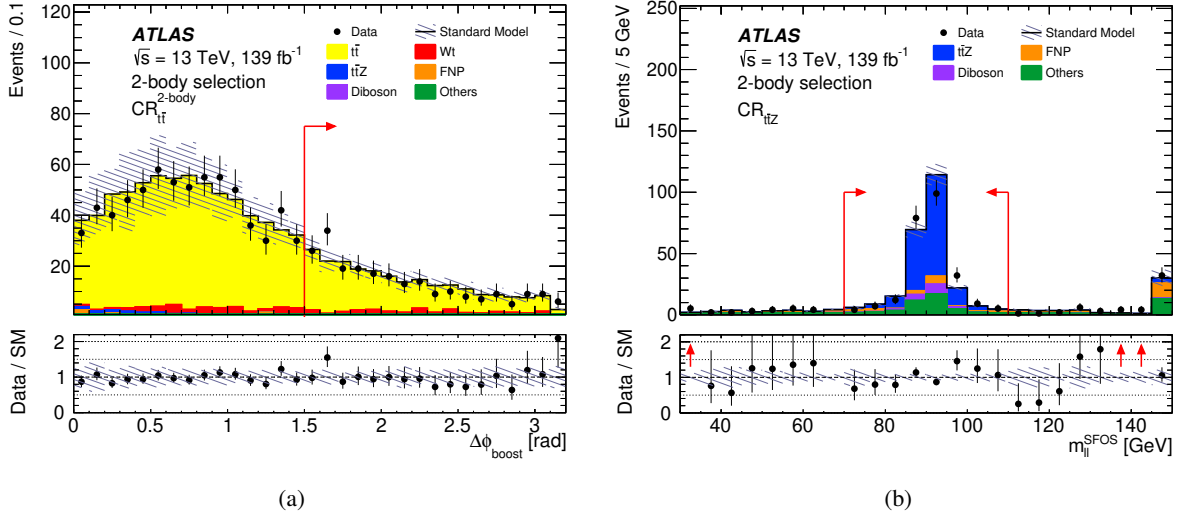


Figure 2: Two-body selection. Distributions of (a) $\Delta\phi_{\text{boost}}$ in $\text{CR}_{t\bar{t}}^{2\text{-body}}$ and (b) $m_{\ell\ell}$ of the two same-flavour and opposite-charge leptons candidate in $\text{CR}_{t\bar{t}Z}$, each after the background fit. The contributions from all SM backgrounds are shown as a histogram stack. “Others” includes the contributions from VVV , $t\bar{t}t$, $t\bar{t}\bar{t}$, $t\bar{t}W$, $t\bar{t}WW$, $t\bar{t}WZ$, $t\bar{t}H$, and tZ . The hatched bands represent the total statistical and detector-related systematic uncertainty. The rightmost bin of (b) includes overflow events. In the upper panels, red arrows indicate the control region selection criteria. The bottom panels show the ratio of the observed data to the total SM background prediction, with hatched bands representing the total uncertainty in the background prediction; red arrows show data outside the vertical-axis range.

Good agreement, within one standard deviation of the SM background prediction, is observed in the VRs (see Figure 3).

Table 7: Two-body selection. Background fit results for $\text{CR}_{t\bar{t}}^{2\text{-body}}$, $\text{CR}_{t\bar{t}Z}$, $\text{VR}_{t\bar{t},\text{DF}}^{2\text{-body}}$, $\text{VR}_{t\bar{t},\text{SF}}^{2\text{-body}}$ and $\text{VR}_{t\bar{t}Z}^{2\text{-body}}$. “Others” includes contributions from VVV , $t\bar{t}t$, $t\bar{t}\bar{t}$, $t\bar{t}W$, $t\bar{t}WW$, $t\bar{t}WZ$, $t\bar{t}H$, and tZ processes. Combined statistical and systematic uncertainties are given. Entries marked ‘-’ indicate a negligible background contribution (less than 0.001 events). The individual uncertainties can be correlated, and do not necessarily add up in quadrature to the total background uncertainty.

| | $\text{CR}_{t\bar{t}}^{2\text{-body}}$ | $\text{CR}_{t\bar{t}Z}$ | $\text{VR}_{t\bar{t},\text{DF}}^{2\text{-body}}$ | $\text{VR}_{t\bar{t},\text{SF}}^{2\text{-body}}$ | $\text{VR}_{t\bar{t}Z}^{2\text{-body}}$ |
|----------------------------|--|-------------------------|--|--|---|
| Observed events | 230 | 247 | 45 | 38 | 26 |
| Total (post-fit) SM events | 230 ± 15 | 246 ± 16 | 50 ± 15 | 42 ± 11 | 25.7 ± 3.4 |
| Post-fit, $t\bar{t}$ | 196 ± 17 | – | 44 ± 15 | 36 ± 11 | – |
| Post-fit, $t\bar{t}Z$ | 0.49 ± 0.23 | 170 ± 22 | 1.7 ± 0.6 | 1.9 ± 0.6 | 14.0 ± 2.1 |
| Wt | 31 ± 7 | – | 2.7 ± 1.2 | 2.6 ± 1.2 | – |
| Diboson | 1.0 ± 0.6 | 17 ± 4 | 0.50 ± 0.25 | 0.59 ± 0.32 | 8.7 ± 3.0 |
| Others | 1.1 ± 0.5 | 44 ± 12 | 1.0 ± 0.6 | 0.8 ± 0.5 | 3.01 ± 0.87 |
| Fake and non-prompt | $0.0^{+0.5}_{-0.0}$ | 16 ± 8 | $0.0^{+0.5}_{-0.0}$ | $0.0^{+0.5}_{-0.0}$ | $0.0^{+0.5}_{-0.0}$ |

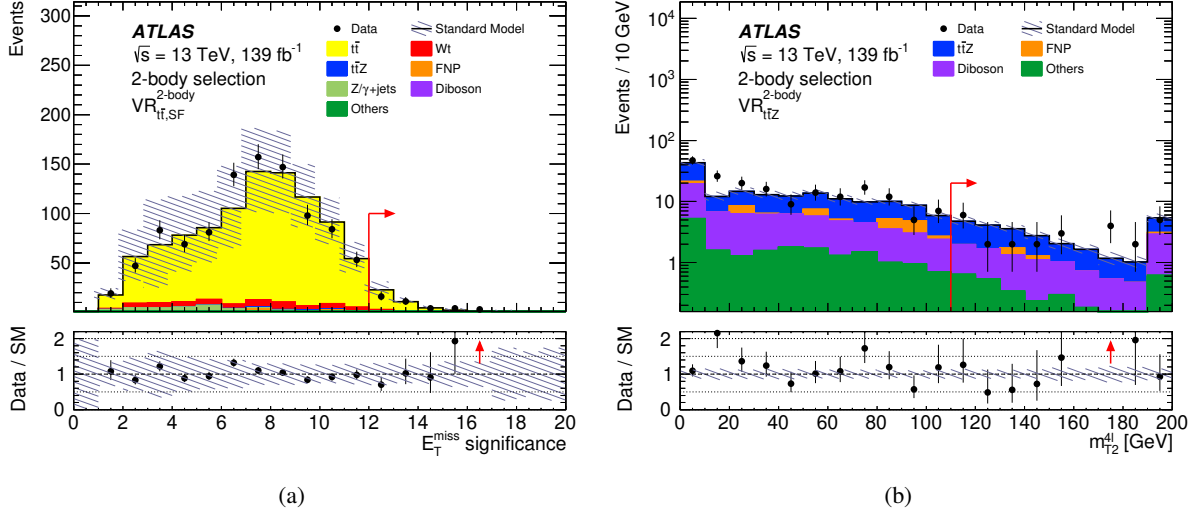


Figure 3: Two-body selection. Distributions of the E_T^{miss} significance in (a) $VR_{t\bar{t},SF}^{2-body}$ and (b) $m_{T2}^{4\ell}$ in $VR_{t\bar{t}Z}^{2-body}$, each after the background fit. The contributions from all SM backgrounds are shown as a histogram stack. “Others” includes contributions from VVV , $t\bar{t}$, $t\bar{t}t\bar{t}$, $t\bar{t}W$, $t\bar{t}WW$, $t\bar{t}WZ$, $t\bar{t}H$, and tZ processes. The hatched bands represent the total statistical and detector-related systematic uncertainty. The rightmost bin of each plot includes overflow events. In the upper panels, red arrows indicate the validation region selection criteria. The bottom panels show the ratio of the observed data to the total SM background prediction, with hatched bands representing the total uncertainty in the background prediction; red arrows show data outside the vertical-axis range.

6.2 Estimation of the backgrounds in the three-body selection

The dominant SM backgrounds in the three-body signal regions are diboson, $t\bar{t}$ and $t\bar{t}Z$ production. Dedicated CRs were defined, labelled as CR_{VV}^{3-body} and $CR_{t\bar{t}}^{3-body}$, which are kinematically close to the SRs and which have good purity in diboson and $t\bar{t}$ events respectively. The orthogonality between CRs and SRs is mainly ensured by the inversion of the $\Delta\phi_\beta^R$ cut. The normalisation of the $t\bar{t}Z$ background is extracted using the same control region $CR_{t\bar{t}Z}$ defined for the two-body selection in Section 6.1. Dedicated validation regions were defined to test the modelling of these processes: VR_{VV}^{3-body} for the diboson background, and $VR(1)_{t\bar{t}}^{3-body}$ and $VR(2)_{t\bar{t}}^{3-body}$ for the validation of the $t\bar{t}$ background, where $VR(1)_{t\bar{t}}^{3-body}$ is characterised by a b -jet veto while at least one b -jet is required in $VR(2)_{t\bar{t}}^{3-body}$. The definition of the control and validation regions is summarised in Table 8. The expected signal contamination is below 2% in the CRs and reaches a maximum of 10% in the VRs for a top squark mass of ~ 430 GeV.

Table 9 shows the expected and observed numbers of events in each of the control and validation regions after the background fit. The normalisation factors extracted from the fit of the backgrounds for the diboson, $t\bar{t}$ and $t\bar{t}Z$ production processes are 0.92 ± 0.28 , 0.96 ± 0.09 and 1.06 ± 0.15 respectively. The total number of fitted background events in the validation regions is in agreement with the observed number of data events. Figure 4 shows the distributions of $\Delta\phi_\beta^R$ for the CR_{VV}^{3-body} and $CR_{t\bar{t}}^{3-body}$ selections after the background fit, illustrating the MC modelling of the shape for this variable. Figure 5 shows distributions of R_{PT} in $VR(1)_{t\bar{t}}^{3-body}$ and $VR(2)_{t\bar{t}}^{3-body}$, and of $\Delta\phi_\beta^R$ in VR_{VV}^{3-body} , after the background fit. Good agreement, within one standard deviation of the SM background prediction, is observed in the validation regions.

Table 8: Three-body selection. Control and validation regions definitions. The common selection defined in Section 5 also applies to all regions. A further control region $\text{CR}_{t\bar{t}Z}$ was defined previously in Table 7.

| | $\text{CR}_{t\bar{t}}^{3\text{-body}}$ | $\text{CR}_{VV}^{3\text{-body}}$ | $\text{VR}(1)_{t\bar{t}}^{3\text{-body}}$ | $\text{VR}(2)_{t\bar{t}}^{3\text{-body}}$ | $\text{VR}_{VV}^{3\text{-body}}$ |
|---|--|----------------------------------|---|---|----------------------------------|
| Lepton flavour | DF | DF+SF | DF | DF | DF+SF |
| $p_{\text{T}}(\ell_1)$ [GeV] | > 25 | > 25 | > 25 | > 25 | > 25 |
| $p_{\text{T}}(\ell_2)$ [GeV] | > 20 | > 20 | > 20 | > 20 | > 20 |
| $m_{\ell\ell}$ [GeV] | > 20 | > 20 | > 20 | > 20 | > 20 |
| $ m_{\ell\ell} - m_Z $ [GeV] | – | > 20 (SF only) | – | – | > 20 (SF only) |
| $n_{b\text{-jets}}$ | ≥ 2 | = 0 | = 0 | ≥ 1 | = 0 |
| M_{Δ}^{R} [GeV] | > 80 | > 100 | [80, 105] | [80, 120] | > 100 |
| $R_{p_{\text{T}}}$ | – | > 0.3 | > 0.7 | > 0.7 | > 0.7 |
| $1/\gamma_{\text{R}+1}$ | > 0.7 | > 0.7 | > 0.7 | > 0.7 | [0.45, 0.7] |
| $E_{\text{T}}^{\text{miss}}$ significance | > 10 | > 10 | > 12 | > 12 | > 12 |
| $\Delta\phi_{\beta}^{\text{R}}$ [rad] | < 2.3 | < 2.3 | > 2.3 | > 2.3 | > 2.3 |

Table 9: Three-body selection. Background fit results for $\text{CR}_{VV}^{3\text{-body}}$, $\text{CR}_{t\bar{t}}^{3\text{-body}}$, $\text{CR}_{t\bar{t}Z}$, $\text{VR}_{VV}^{3\text{-body}}$, $\text{VR}(1)_{t\bar{t}}^{3\text{-body}}$ and $\text{VR}(2)_{t\bar{t}}^{3\text{-body}}$. ‘‘Others’’ includes contributions from VVV , $t\bar{t}t$, $t\bar{t}\bar{t}$, $t\bar{t}W$, $t\bar{t}WW$, $t\bar{t}WZ$, $t\bar{t}H$, and tZ processes. Combined statistical and systematic uncertainties are given. Entries marked ‘–’ indicate a negligible background contribution (less than 0.001 events). The individual uncertainties can be correlated, and do not necessarily add up in quadrature to the total background uncertainty.

| | $\text{CR}_{t\bar{t}}^{3\text{-body}}$ | $\text{CR}_{VV}^{3\text{-body}}$ | $\text{CR}_{t\bar{t}Z}$ | $\text{VR}(1)_{t\bar{t}}^{3\text{-body}}$ | $\text{VR}(2)_{t\bar{t}}^{3\text{-body}}$ | $\text{VR}_{VV}^{3\text{-body}}$ |
|----------------------------|--|----------------------------------|-------------------------|---|---|----------------------------------|
| Observed events | 192 | 169 | 247 | 41 | 137 | 84 |
| Total (post-fit) SM events | 192 ± 14 | 169 ± 13 | 247 ± 16 | 38.3 ± 5.9 | 142 ± 25 | 97 ± 15 |
| Post-fit, $t\bar{t}$ | 180 ± 14 | 65 ± 14 | – | 25 ± 5 | 130 ± 24 | 44 ± 11 |
| Post-fit, $t\bar{t}Z$ | 1.57 ± 0.33 | 1.36 ± 0.31 | 172 ± 23 | $0.07^{+0.12}_{-0.07}$ | 1.6 ± 0.7 | 1.0 ± 0.4 |
| Post-fit, diboson | 0.063 ± 0.035 | 74 ± 21 | 16 ± 7 | 11 ± 4 | 0.9 ± 0.5 | 41 ± 14 |
| Wt | 9.0 ± 1.4 | 7.6 ± 2.3 | – | 1.9 ± 0.6 | 8.1 ± 2.0 | 8.1 ± 1.1 |
| $Z/\gamma^* + \text{jets}$ | – | 13 ± 5 | – | – | – | $0.04^{+0.05}_{-0.04}$ |
| Others | 1.39 ± 0.21 | 3.57 ± 0.24 | 43 ± 12 | 0.27 ± 0.06 | 1.11 ± 0.18 | 1.15 ± 0.11 |
| Fake and non-prompt | $0.00^{+0.22}_{-0.00}$ | 5.0 ± 1.9 | 16 ± 8 | $0.00^{+0.27}_{-0.00}$ | $0.00^{+0.27}_{-0.00}$ | 1.8 ± 1.5 |

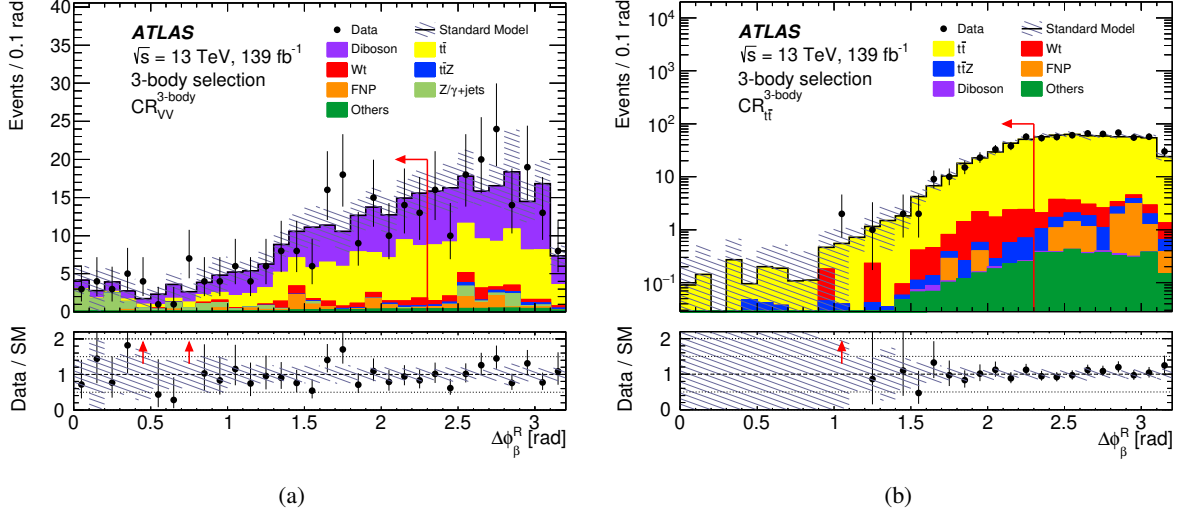


Figure 4: Three-body selection. Distributions of (a) $\Delta\phi_\beta^R$ in the $CR_{VV}^{3\text{-body}}$ selection, and (b) in the $CR_{t\bar{t}}^{3\text{-body}}$ selection, after the background fit. The contributions from all SM backgrounds are shown as a histogram stack. “Others” includes contributions from VVV , $t\bar{t}t$, $t\bar{t}t\bar{t}$, $t\bar{t}W$, $t\bar{t}WW$, $t\bar{t}WZ$, $t\bar{t}H$, and tZ processes. The hatched bands represent the total statistical and detector-related systematic uncertainty. In the upper panels, red arrows indicate the control region selection criteria. The bottom panels show the ratio of the observed data to the total SM background prediction, with hatched bands representing the total uncertainty in the background prediction; red arrows show data outside the vertical-axis range.

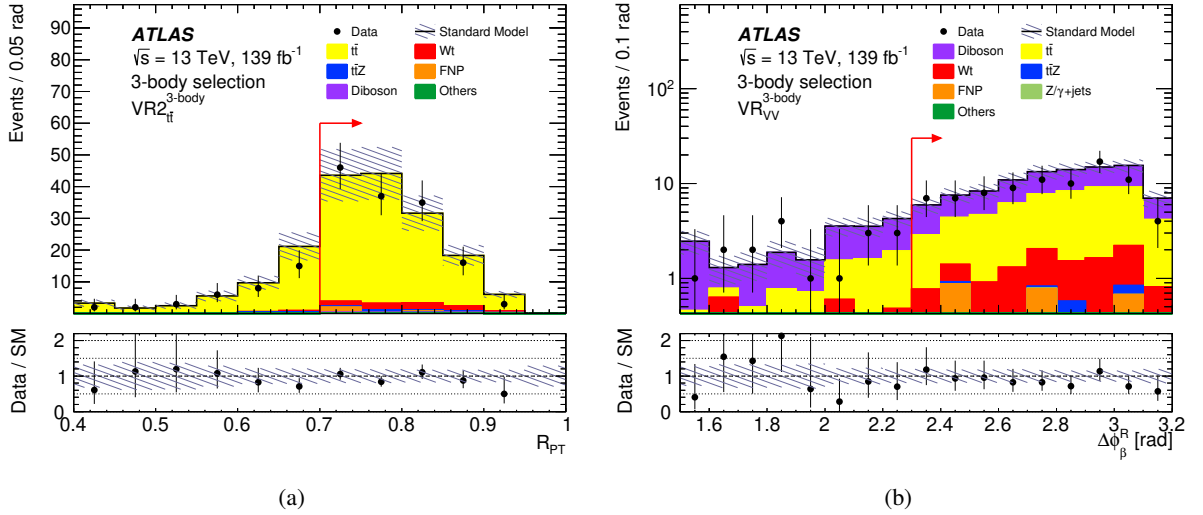


Figure 5: Three-body selection. Distributions of (a) R_{PT} in the validation region $VR(2)_{t\bar{t}}^{3\text{-body}}$ and (b) $\Delta\phi_\beta^R$ in the validation region $VR_{VV}^{3\text{-body}}$, after the background fit. The contributions from all SM backgrounds are shown as a histogram stack. “Others” includes contributions from VVV , $t\bar{t}t$, $t\bar{t}t\bar{t}$, $t\bar{t}W$, $t\bar{t}WW$, $t\bar{t}WZ$, $t\bar{t}H$, and tZ processes. The hatched bands represent the total statistical and detector-related systematic uncertainty. The bottom panels show the ratio of the observed data to the total SM background prediction, with hatched bands representing the total uncertainty in the background prediction.

6.3 Estimation of the backgrounds in the four-body selection

The dominant irreducible SM background sources for the four-body selection are $t\bar{t}$ and diboson: these backgrounds are normalised in two dedicated background-enriched control regions labelled as $\text{CR}_{t\bar{t}}^{4\text{-body}}$ and $\text{CR}_{VV}^{4\text{-body}}$. Some of the requirements defining the kinematics of the SRs are relaxed in order to allow the selection of $t\bar{t}$ events in $\text{CR}_{t\bar{t}}^{4\text{-body}}$, while the $R_{2\ell}$ selection is adjusted to maintain complete orthogonality with the SRs. The diboson contribution in $\text{CR}_{VV}^{4\text{-body}}$ is enhanced by limiting the number of jets in the event and the sub-leading jet p_T , and by the additional veto on b -jets. The background predictions are tested in validation regions: $\text{VR}_{t\bar{t}}^{4\text{-body}}$ for $t\bar{t}$ validation and $\text{VR}_{VV}^{4\text{-body}}$ and $\text{VR}_{VV,3\ell}^{4\text{-body}}$ for diboson validation, with the latter two selecting, respectively, events with two and three leptons in the final state. For $\text{VR}_{VV,3\ell}^{4\text{-body}}$ a new set of variables is defined in order to mimic the dibosons' kinematics in the signal regions. The two SFOS leptons with an invariant mass closest to m_Z are considered as the two leptons coming from the decay of the Z boson. The momentum of the lepton ($\mathbf{p}(\ell_{\text{paired}}^Z)$) of the selected pair having the same electric charge as the non-paired lepton is added to the $\mathbf{p}_T^{\text{miss}}$ in order to define $E_{T,1\ell,\text{corr}}^{\text{miss}} = \left| \left(\mathbf{p}_T^{\text{miss}} + \mathbf{p}(\ell_{\text{paired}}^Z) \right)_T \right|$ and $R_{\ell,\text{corr}}$ is defined as the ratio of $E_{T,1\ell,\text{corr}}^{\text{miss}}$ to the sum of the transverse momenta of two remaining OS leptons. The invariant mass of the remaining two leptons, called $m_{\ell\ell,\text{corr}}$, is also used. The definition of the control and validation regions used in the four-body selection is summarised in Table 10. In the $t\bar{t}$ control region the signal contamination is $\sim 1\%$ or less. In $\text{CR}_{VV}^{4\text{-body}}$, the typical signal contamination is about $\sim 1 - 2\%$, but reaches a maximum value of $\sim 5\%$ for a top squark mass of ~ 400 GeV and lightest-neutralino mass of ~ 310 GeV at the boundary of the region excluded by the previous analysis. Signal contamination in the validation regions is below 10%.

Table 11 shows the expected and observed numbers of events in each of the control and validation regions after the background fit. The normalisation factors extracted by the fit for the diboson and $t\bar{t}$ production processes are 1.00 ± 0.25 and 0.90 ± 0.12 respectively. The distributions of E_T^{miss} in $\text{CR}_{t\bar{t}}^{4\text{-body}}$ and $R_{2\ell}$ in $\text{CR}_{VV}^{4\text{-body}}$, after the background fit, are shown in Figure 6. The distributions of $p_T(\ell_2)$ in $\text{VR}_{t\bar{t}}^{4\text{-body}}$, n_{jets} in $\text{VR}_{VV}^{4\text{-body}}$ and $E_{T,1\ell,\text{corr}}^{\text{miss}}$ in $\text{VR}_{VV,3\ell}^{4\text{-body}}$, after the background fit, are shown in Figure 7. Good agreement between data and the SM predictions is observed.

Table 10: Four-body selection. Control and validation regions definition. The common selection defined in Section 5 also applies to all regions.

| | $\text{CR}_{t\bar{t}}^{4\text{-body}}$ | $\text{CR}_{VV}^{4\text{-body}}$ | $\text{VR}_{t\bar{t}}^{4\text{-body}}$ | $\text{VR}_{VV}^{4\text{-body}}$ | $\text{VR}_{VV,3\ell}^{4\text{-body}}$ |
|---|--|----------------------------------|--|----------------------------------|--|
| Lepton multiplicity | 2 | 2 | 2 | 2 | 3 |
| Lepton flavour | DF+SF | DF+SF | DF+SF | DF+SF | at least one SFOS pair |
| $p_T(\ell_1)$ [GeV] | < 100 | < 100 | < 100 | < 100 | < 100 |
| $p_T(\ell_2)$ [GeV] | < 50 | < 50 | < 50 | < 50 | < 100 |
| $p_T(\ell_3)$ [GeV] | – | – | – | – | < 100 |
| $m_{\ell\ell}$ [GeV] | > 10 | > 45 | > 10 | > 45 | > 10 |
| $ m_{\ell\ell} - m_Z $ [GeV] | – | > 10 for SF only | – | > 10 for SF only | – |
| E_T^{miss} [GeV] | > 350 | > 250 | > 250 | > 250 | > 250 |
| $p_T(j_1)$ [GeV] | > 150 | > 150 | > 150 | > 150 | > 150 |
| $\min \Delta R_{\ell_2, j_1}$ | > 1 | > 1 | > 1 | > 1 | > 1 |
| n_{jets} | – | ≤ 2 | – | ≤ 4 | < 5 |
| $n_{b\text{-jets}}$ | ≥ 2 | = 0 | ≥ 1 | = 0 | = 0 |
| $b\text{-tagged } j_1$ | – | – | True | – | – |
| $p_T(j_2)$ [GeV] | – | < 40 if j_2 exists | – | – | – |
| E_T^{miss} significance | > 10 | > 10 | > 10 | > 10 | > 5 |
| $p_{T,\text{boost}}^{\ell\ell}$ [GeV] | > 280 | > 280 | > 280 | > 280 | – |
| $R_{2\ell}$ | < 5 | < 4 | > 5 | [4, 5] | – |
| $R_{2\ell 4j}$ | – | – | [0.3, 0.38] | – | – |
| $E_{T,1\ell,\text{corr}}^{\text{miss}}$ [GeV] | – | – | – | – | > 300 |
| $R_{2\ell,\text{corr}}$ | – | – | – | – | > 5 |
| $m_{\ell\ell,\text{corr}}$ [GeV] | – | – | – | – | > 10 |

Table 11: Four-body selection. Background fit results for $\text{CR}_{t\bar{t}}^{4\text{-body}}$, $\text{CR}_{VV}^{4\text{-body}}$, $\text{VR}_{t\bar{t}}^{4\text{-body}}$, $\text{VR}_{VV}^{4\text{-body}}$ and $\text{VR}_{VV,3\ell}^{4\text{-body}}$. The ‘Others’ category contains the contributions from VVV , $t\bar{t}t$, $t\bar{t}t\bar{t}$, $t\bar{t}W$, $t\bar{t}WW$, $t\bar{t}WZ$, $t\bar{t}H$, and tZ . Combined statistical and systematic uncertainties are given. Entries marked ‘–’ indicate a negligible background contribution (less than 0.001 events). The individual uncertainties can be correlated, and do not necessarily add up in quadrature to the total background uncertainty.

| | $\text{CR}_{t\bar{t}}^{4\text{-body}}$ | $\text{CR}_{VV}^{4\text{-body}}$ | $\text{VR}_{t\bar{t}}^{4\text{-body}}$ | $\text{VR}_{VV}^{4\text{-body}}$ | $\text{VR}_{VV,3\ell}^{4\text{-body}}$ |
|----------------------------|--|----------------------------------|--|----------------------------------|--|
| Observed events | 149 | 163 | 86 | 168 | 25 |
| Total (post-fit) SM events | 149 ± 12 | 162 ± 13 | 86 ± 20 | 173 ± 14 | 27 ± 5 |
| Post-fit, $t\bar{t}$ | 115 ± 13 | 39 ± 13 | 41 ± 19 | 57 ± 14 | – |
| Post-fit, diboson | 0.7 ± 0.5 | 89 ± 18 | 1.5 ± 0.6 | 75 ± 18 | 19 ± 6 |
| Wt | 27 ± 4 | 11.9 ± 1.8 | 18 ± 5 | 10.3 ± 0.8 | – |
| $Z/\gamma^* + \text{jets}$ | 0.18 ± 0.07 | 2.1 ± 1.1 | 2.1 ± 0.5 | 0.81 ± 0.35 | – |
| $t\bar{t}Z$ | 1.32 ± 0.34 | 0.18 ± 0.09 | 0.52 ± 0.17 | 0.41 ± 0.16 | 0.120 ± 0.029 |
| Others | 2.41 ± 0.17 | 0.30 ± 0.26 | 1.34 ± 0.20 | 1.2 ± 0.2 | 0.095 ± 0.028 |
| Fake and non-prompt | 2.3 ± 2.1 | 20 ± 4 | 20.7 ± 3.4 | 28 ± 5 | 7.9 ± 1.1 |

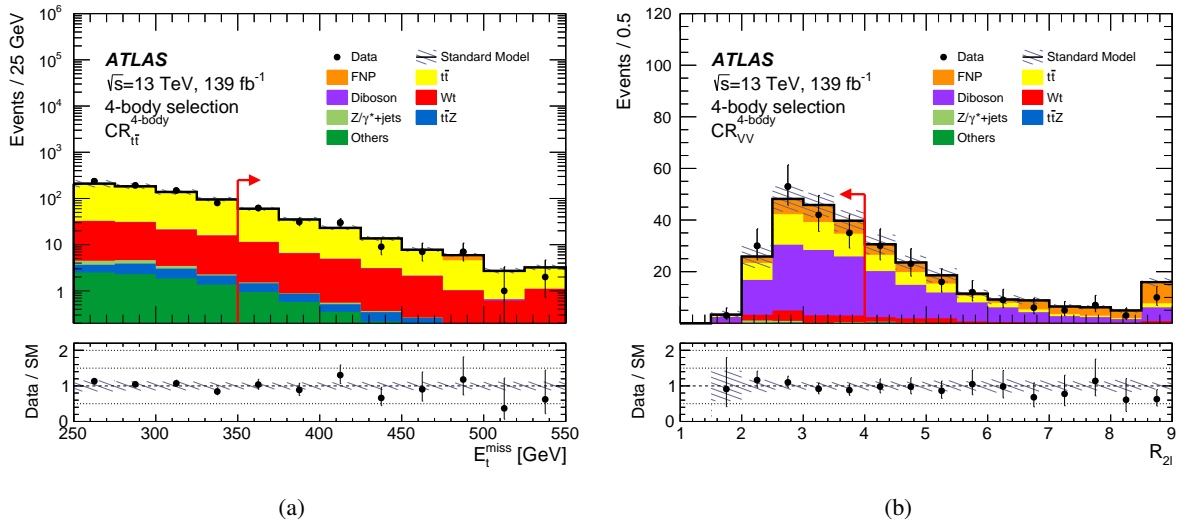


Figure 6: Four-body selection. Distributions of (a) E_T^{miss} in $\text{CR}_{t\bar{t}}^{4\text{-body}}$ and (b) $R_{2\ell}$ in $\text{CR}_{VV}^{4\text{-body}}$ after the background fit. The contributions from all SM backgrounds are shown as a histogram stack. “Others” includes contributions from VVV , $t\bar{t}t$, $t\bar{t}t\bar{t}$, $t\bar{t}W$, $t\bar{t}WW$, $t\bar{t}WZ$, $t\bar{t}H$, and $t\bar{t}Z$ processes. The hatched bands represent the total statistical and detector-related systematic uncertainty. The rightmost bin of each plot includes overflow events. In the upper panels, red arrows indicate the control region selection criteria. The bottom panels show the ratio of the observed data to the total SM background prediction, with hatched bands representing the total uncertainty in the background prediction.

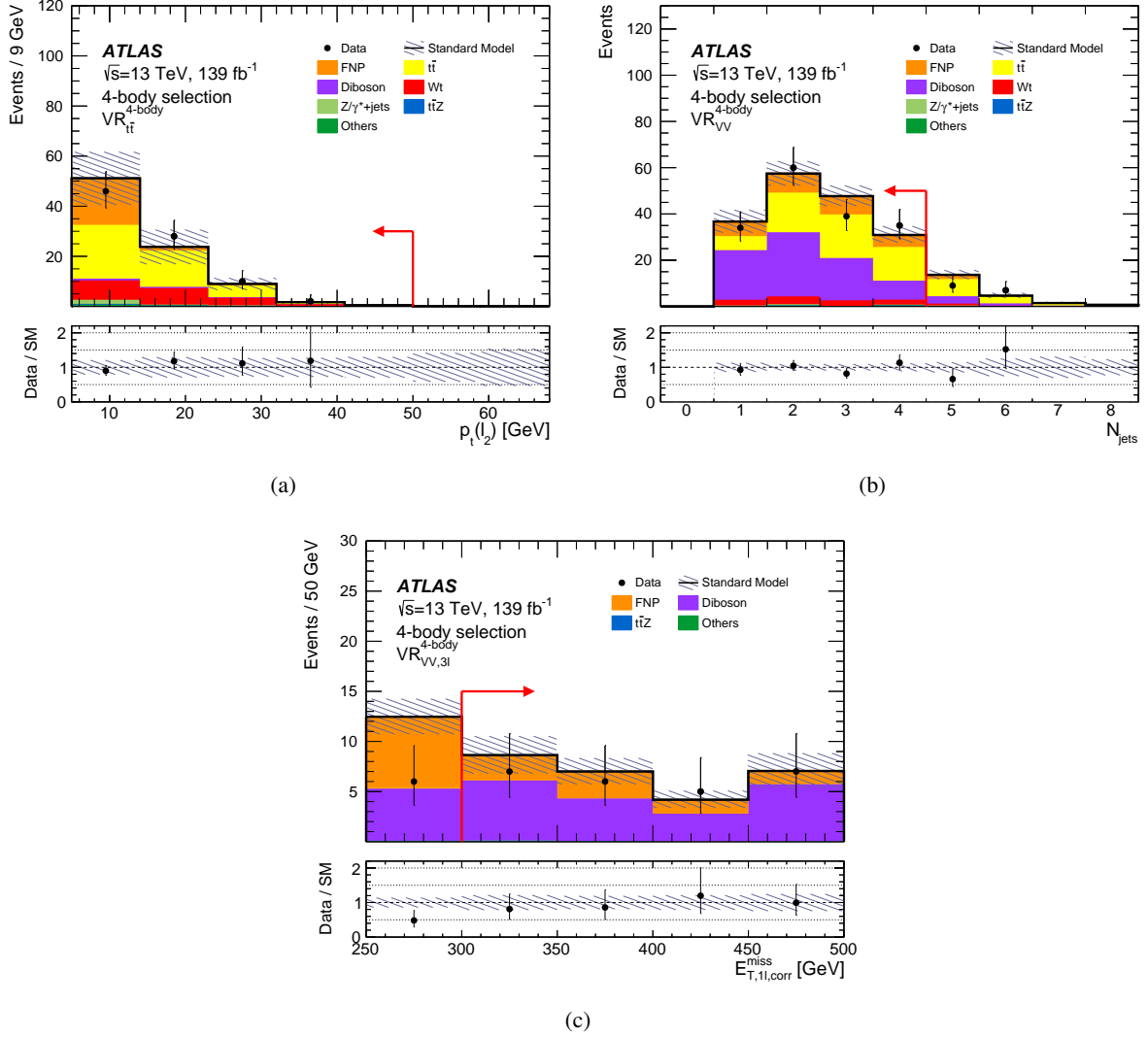


Figure 7: Four-body selection. Distributions of (a) $p_T(\ell_2)$ in $VR_{t\bar{t}}^{4\text{-body}}$, (b) n_{jets} in $VR_{VV}^{4\text{-body}}$ and (c) $E_{T,1\ell,corr}^{miss}$ in $VR_{VV,3\ell}^{4\text{-body}}$ after the background fit. The contributions from all SM backgrounds are shown as a histogram stack. “Others” includes contributions from VVV , $t\bar{t}t$, $t\bar{t}t\bar{t}$, $t\bar{t}W$, $t\bar{t}WW$, $t\bar{t}WZ$, $t\bar{t}H$, and tZ processes. The hatched bands represent the total statistical and detector-related systematic uncertainty. The rightmost bin of each plot includes overflow events. In the upper panels, red arrows indicate the validation region selection criteria. The bottom panels show the ratio of the observed data to the total SM background prediction, with hatched bands representing the total uncertainty in the background prediction.

7 Systematic uncertainties

Systematic uncertainties are evaluated for the signal and for the background predictions. The main experimental uncertainties in the yields of the reconstructed objects, the theoretical uncertainties in the processes' yields, and the uncertainties related to the MC modelling of the SM backgrounds are described in this section. The statistical uncertainties in the simulated event samples are also taken into account.

The main sources of experimental uncertainty are related to the jet energy scale (JES) and the jet energy resolution (JER). The JES and JER uncertainties are derived as a function of the p_T and η of the jet, as well as of the pile-up conditions and the jet-flavour composition of the selected jet sample [112]. Uncertainties associated with the modelling of the b -tagging efficiencies for b -jets, c -jets and light-flavour jets [113, 114] are also considered. The systematic uncertainties related to the modelling of E_T^{miss} in the simulation are estimated by propagating the uncertainties in the energy and momentum scales of electrons, muons and jets, as well as the uncertainties in the resolution and scale of the soft term [115]. Other detector-related systematic uncertainties, including those arising from lepton reconstruction efficiency, energy scale, energy resolution and in the modelling of the trigger efficiency [45, 51, 52, 116, 117], or the ones due to the pile-up reweighting and JVT are found to have a small impact on the results.

Systematic uncertainties in the theoretical modelling of the observed final states can be broadly divided into uncertainties in the description of the parton-level final states (uncertainties in the proton PDF, cross-section, and strong coupling constant) and further uncertainties arising from the parton showering and hadronisation processes that convert partons into the hadronic final states. The uncertainties in the modelling of the $t\bar{t}$ background are estimated by varying the renormalisation and factorisation scales, as well as the amount of initial- and final-state radiation produced when generating the samples [118, 119]. Comparison between the yields obtained with POWHEG and MADGRAPH5_aMC@NLO [118] is used to estimate uncertainties from the event generator choice. For $t\bar{t}Z$ production, in the two-body and three-body selections, the effects of QCD scale uncertainties are evaluated using seven-point variations of the factorisation and renormalisation scales [120]. Uncertainties for additional radiation contributions (ISR, FSR) are evaluated by comparing the nominal sample with one obtained with a PYTHIA tune enhancing the radiation [55]. In the four-body selection, since the $t\bar{t}Z$ background contribution is minor, a total theoretical error of 14%, coming from the cross-section uncertainty [121], is applied instead. For $t\bar{t}$ and $t\bar{t}Z$ production, the parton showering and hadronisation uncertainties are covered by the difference between samples obtained using the two different showering models implemented in PYTHIA and in HERWIG. Single top quark production via the Wt -channel is a minor background in all the selections. An uncertainty in the acceptance due to the interference between $t\bar{t}$ and Wt production is assigned by comparing dedicated samples produced with POWHEG and PYTHIA using the diagram removal (DR) and the diagram subtraction (DS) approaches [122]. The modelling uncertainties for the diboson background are estimated using the seven-point variations of the renormalisation and factorisation scales. Additional uncertainties in the resummation (QSF) and matching (CKKM) scales between the matrix element generator and parton shower are computed by varying the scale parameters in SHERPA [90]. For the other background processes which make minor contributions a conservative uncertainty is applied. These minor backgrounds are mainly $t\bar{t}WZ$ and ttW processes. A 30% uncertainty, driven by the DR versus DS difference for the $t\bar{t}WZ$ [123] process, is applied in the two-body and three-body selections. For the four-body selection a 22% uncertainty is applied for the uncertainty in the $t\bar{t}W$ cross-section [121]. For all the processes mentioned above the PDF uncertainties [65] were evaluated and found to be negligible.

Systematic uncertainties in the data-driven FNP background estimate are expected due to potential differences in the FNP composition (heavy flavour, light flavour or photon conversions) between the regions

defined in Section 6 and the CR^{FNP} used to extract the fake factor. A FNP systematic error is evaluated in each of the regions by varying the FNP composition in the CR^{FNP} to match that of the considered analysis region. The statistical error is also included by propagating the statistical uncertainty in the ratio used to compute the fake factor. For the four-body selection, where the FNP lepton background is dominant, a FNP closure uncertainty is also evaluated from the full difference between the data and the FNP predictions as observed in a validation region with two same-charge leptons with kinematics similar to the four-body selection. The closure uncertainty ranges between 13% and 33% in the regions where the FNP background is important.

A 1.7% uncertainty in the luminosity measurement is considered for all signal and background estimates that are derived directly from MC simulations [46].

Tables 12, 13 and 14 summarise the contributions from the different sources of systematic uncertainty in the total SM background predictions for the two-body, three-body and four-body signal regions. The total systematic uncertainty ranges between 14% and 26%, with the dominant sources being the MC statistical error, the JES and JER, the uncertainty in the background normalisation and the theoretical uncertainties.

The SUSY signal cross-section uncertainty is evaluated from an envelope of the cross-section predictions using different PDF sets and factorisation and renormalisation scales as described in Ref. [124]. The uncertainty in the DM production cross-section is derived from the scale variations and the PDF choices. The SUSY and DM theory signal uncertainties are computed from the variation of the radiation, renormalisation, factorisation and merging scales. These uncertainties are most relevant for the four-body selection, where the largest theory uncertainties are those resulting from radiation and are in the range 10% to 24% depending on the mass difference $m(\tilde{t}_1) - m(\tilde{\chi}_1^0)$. For the DM signals the total systematic uncertainty is between 5% and 20%.

Table 12: Two-body selection. Sources of systematic uncertainty in the SM background estimates, after the background fits, for the SF selection. The values are given as relative uncertainties in the total expected background event yields in the SRs. Entries marked ‘–’ indicate a contribution smaller than 1%. ‘MC statistical uncertainty’ refers to the statistical uncertainty from the simulated event samples. ‘Other theoretical uncertainties’ represent the theoretical uncertainty coming from VVV , $t\bar{t}t$, $t\bar{t}\bar{t}$, $t\bar{t}W$, $t\bar{t}WW$, $t\bar{t}WZ$, $t\bar{t}H$, and tZ contributions. The individual components can be correlated and therefore do not necessarily add up in quadrature to the total systematic uncertainty.

| Signal Region | SR-SF $_{[110,120]}^{2\text{-body}}$ | SR-SF $_{[120,140]}^{2\text{-body}}$ | SR-SF $_{[140,160]}^{2\text{-body}}$ | SR-SF $_{[160,180]}^{2\text{-body}}$ | SR-SF $_{[180,220]}^{2\text{-body}}$ | SR-SF $_{[220,\infty]}^{2\text{-body}}$ |
|---------------------------------------|--------------------------------------|--------------------------------------|--------------------------------------|--------------------------------------|--------------------------------------|---|
| Total SM background uncertainty | 19% | 20% | 17% | 15% | 15% | 20% |
| VV theoretical uncertainties | – | 2.4% | 3.5% | 4.9% | 4.4% | 7.1% |
| $t\bar{t}$ theoretical uncertainties | 10% | 11% | 6.2% | – | 1.7% | 2.7% |
| $t\bar{t}Z$ theoretical uncertainties | 1.0% | 2.2% | 4.2% | 5.2% | 5.0% | 11% |
| $t\bar{t}-Wt$ interference | – | – | – | – | 1.0% | 5.7% |
| Other theoretical uncertainties | 1.0% | 1.4% | 2.7% | 2.5% | 2.6% | 1.9% |
| MC statistical uncertainty | 5.1% | 5.4% | 7.0% | 7.7% | 9.9% | 8.7% |
| $t\bar{t}$ normalisation | 7.6% | 4.8% | 1.0% | – | – | – |
| $t\bar{t}Z$ normalisation | 1.1% | 3.2% | 5.6% | 7.2% | 6.4% | 4.8% |
| Jet energy scale | 11% | 6.7% | 9.6% | 2.0% | 3.4% | 2.0% |
| Jet energy resolution | 3.6% | 13% | 7.0% | 6.1% | 3.6% | 7.7% |
| E_T^{miss} modelling | 2.9% | 3.6% | 1.0% | 4.1% | 2.7% | 1.2% |
| Lepton modelling | 3.6% | 1.8% | 1.8% | 3.8% | 3.7% | 6.4% |
| Flavour tagging | 1.0% | 1.0% | 1.0% | 2.6% | 3.0% | 2.4% |
| Pile-up reweighting and JVT | – | 1.4% | 1.0% | 1.0% | 1.7% | – |
| Fake and non-prompt leptons | – | – | 1.1% | – | 2.8% | 4.3% |

Table 13: Two-body selection. Sources of systematic uncertainty in the SM background estimates, after the background fits, for the DF selection. The values are given as relative uncertainties in the total expected background event yields in the SRs. Entries marked ‘–’ indicate a contribution smaller than 1%. ‘MC statistical uncertainty’ refers to the statistical uncertainty from the simulated event samples. ‘Other theoretical uncertainties’ represent the theoretical uncertainty coming from VVV , $t\bar{t}t$, $t\bar{t}t\bar{t}$, $t\bar{t}W$, $t\bar{t}WW$, $t\bar{t}WZ$, $t\bar{t}H$, and tZ contributions. The individual components can be correlated and therefore do not necessarily add up in quadrature to the total systematic uncertainty.

| Signal Region | SR-DF $_{[110,120]}^{2\text{-body}}$ | SR-DF $_{[120,140]}^{2\text{-body}}$ | SR-DF $_{[140,160]}^{2\text{-body}}$ | SR-DF $_{[160,180]}^{2\text{-body}}$ | SR-DF $_{[180,220]}^{2\text{-body}}$ | SR-DF $_{[220,\infty)}^{2\text{-body}}$ |
|---------------------------------------|--------------------------------------|--------------------------------------|--------------------------------------|--------------------------------------|--------------------------------------|---|
| Total SM background uncertainty | 20% | 20% | 15% | 16% | 14% | 21% |
| VV theoretical uncertainties | 1.0% | 1.3% | 2.6% | 1.0% | 2.0% | 1.8% |
| $t\bar{t}$ theoretical uncertainties | 9.6% | 12% | 7.6% | – | 3.1% | – |
| $t\bar{t}Z$ theoretical uncertainties | 1.2% | 2.0% | 5.3% | 6.6% | 5.7% | 16% |
| $t\bar{t}\text{-}Wt$ interference | – | – | – | – | – | – |
| Other theoretical uncertainties | 1.0% | 1.2% | 2.8% | 3.2% | 2.7% | 3.3% |
| MC statistical uncertainty | 4.7% | 5.0% | 6.9% | 8.2% | 7.7% | 6.6% |
| $t\bar{t}$ normalisation | 7.2% | 5.6% | 1.2% | – | – | – |
| $t\bar{t}Z$ normalisation | 1.4% | 2.8% | 6.9% | 9.1% | 7.3% | 7.2% |
| Jet energy scale | 8.5% | 10% | 2.5% | 6.1% | 1.0% | 2.6% |
| Jet energy resolution | 13% | 6.6% | 6.2% | 4.3% | 5.3% | 2.0% |
| E_T^{miss} modelling | 3.5% | 6.1% | 1.0% | 2.2% | 2.2% | 1.0% |
| Lepton modelling | 1.5% | 1.1% | 1.6% | 1.3% | 1.3% | 1.0% |
| Flavour tagging | 1.0% | 1.0% | 1.3% | 2.0% | 1.0% | 1.0% |
| Pile-up reweighting and JVT | – | 1.6% | 1.0% | – | 1.0% | – |
| Fake and non-prompt leptons | – | 3.5% | – | – | 7.1% | 13% |

Table 14: Three-body and four-body selections. Sources of systematic uncertainty in the SM background estimates, after the background fits. The values are given as relative uncertainties in the total expected background event yields in the SRs. Entries marked ‘–’ indicate a contribution smaller than 1%. ‘MC statistical uncertainty’ refers to the statistical uncertainty from the simulated event samples. ‘Other theoretical uncertainties’ represent the theoretical uncertainty coming from VVV , $t\bar{t}t$, $t\bar{t}t\bar{t}$, $t\bar{t}W$, $t\bar{t}WW$, $t\bar{t}WZ$, $t\bar{t}H$, and tZ contributions. The individual components can be correlated and therefore do not necessarily add up in quadrature to the total systematic uncertainty.

| Signal Region | SR-DF _W ^{3-body} | SR-SF _W ^{3-body} | SR-DF _t ^{3-body} | SR-SF _t ^{3-body} | SR _{Small Δm} ^{4-body} | SR _{Large Δm} ^{4-body} |
|---------------------------------------|--------------------------------------|--------------------------------------|--------------------------------------|--------------------------------------|---|---|
| Total SM background uncertainty | 18% | 26% | 18% | 22% | 25% | 14% |
| VV theoretical uncertainties | 8.0% | 10% | 1.0% | 1.5% | 3.6% | 4.9% |
| $t\bar{t}$ theoretical uncertainties | 8.2% | 6.6% | 14% | 8.6% | 1.0% | 6.3% |
| $t\bar{t}Z$ theoretical uncertainties | – | – | 1.2% | 2.0% | – | – |
| $t\bar{t}-Wt$ interference | – | 1.0% | – | 1.1% | – | 2.4% |
| Other theoretical uncertainties | – | – | 1.4% | 1.6% | – | – |
| MC statistical uncertainty | 5.8% | 7.4% | 5.6% | 6.7% | 3.3% | 2.7% |
| VV normalisation | 15% | 20% | 1.0% | 2.0% | 2.8% | 8.6% |
| $t\bar{t}$ normalisation | 2.3% | 1.9% | 4.9% | 3.3% | 1.0% | 6.1% |
| $t\bar{t}Z$ normalisation | – | – | 4.1% | 4.5% | – | – |
| Jet energy scale | 5.5% | 3.7% | 3.8% | 4.1% | 1.0% | 3.2% |
| Jet energy resolution | 2.3% | 11% | 9.0% | 18% | 1.3% | 3.5% |
| Lepton modelling | 1.3% | 2.0% | 1.0% | 2.5% | 1.3% | 3.3% |
| E_T^{miss} modelling | 1.1% | 2.2% | 3.0% | 1.8% | – | 1.0% |
| Flavour tagging | 3.1% | 2.9% | 1.6% | 1.0% | – | 1.3% |
| Pile-up reweighting and JVT | 1.0% | 1.0% | – | – | 1.0% | – |
| Fake and non-prompt leptons | 1.7% | – | – | 4.6% | 25% | – |

8 Results

A set of simultaneous likelihood fits is performed, for each one of the three different selections, using standard minimisation software packages, HistFitter and pyhf [106, 107]. For the normalisation of the semi-data-driven backgrounds, only the CRs are considered in the background fit, while for the computation of the exclusion limits both the CRs and SRs are included as constraining channels. The likelihood is a product of Poisson probability density functions (pdf), describing the observed number of events in each CR/SR, and Gaussian pdf distributions that describe the nuisance parameters associated with all the systematic uncertainties. Systematic uncertainties that are correlated between different samples are accounted for in the fit configuration by using the same nuisance parameter. The uncertainties are applied in each of the CRs and SRs and their effect is correlated for events across all regions in the fit.

The results of the background fit are shown in Figures 8–10 for each of the three analysis selections. In general, good agreement, within about one standard deviation, is observed in all the SRs and VRs except in SR-DF_W^{3-body} where the data fluctuates well below the fit.

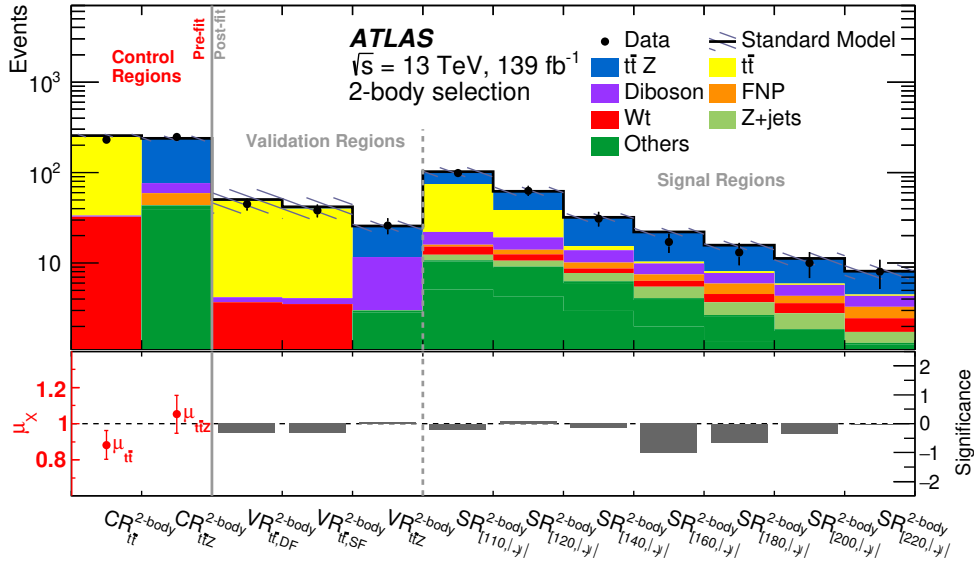


Figure 8: Two-body selection. Expected and observed yields are shown. The upper panel shows the observed number of events in each of the CRs, VRs and the inclusive SRs defined in the two-body selection, together with the expected SM backgrounds obtained before the fit in the CRs and after the fit in the VRs and SRs. “Others” includes contributions from VVV , $t\bar{t}$, $t\bar{t}t\bar{t}$, $t\bar{t}W$, $t\bar{t}WW$, $t\bar{t}WZ$, $t\bar{t}H$, and tZ processes. The shaded band represents the total uncertainty in the expected SM background. The lower panel shows the normalisation factors μ_X (left two bins) extracted in the CRs for the $t\bar{t}$ and $t\bar{t}Z$ processes, while, for the VRs and the inclusive SRs (right bins), the significance as defined in Ref. [125].

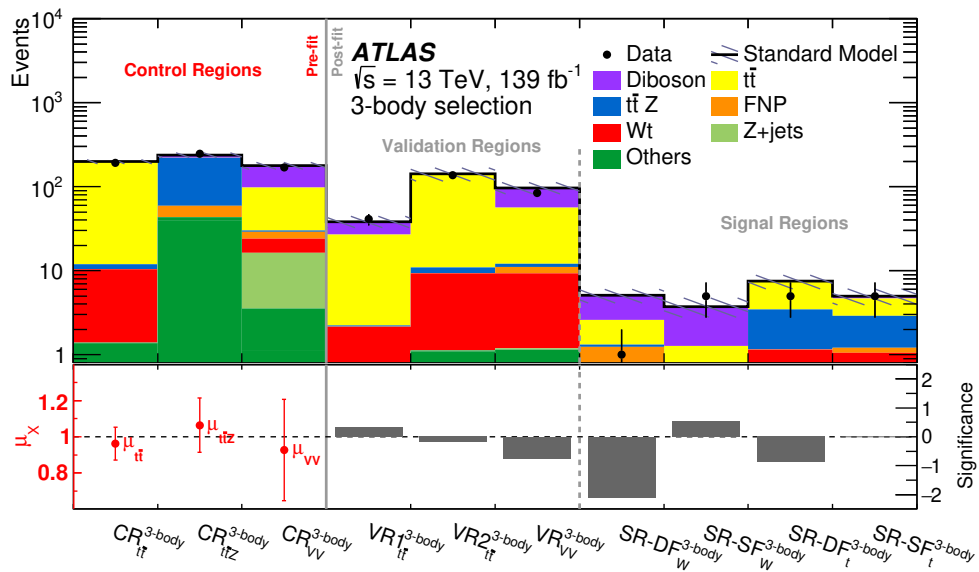


Figure 9: Three-body selection. Expected and observed yields are shown. The upper panel shows the observed number of events in each of the CRs, VRs and SRs defined in the three-body selection, together with the expected SM backgrounds obtained before the fit in the CRs and after the fit in the VRs and SRs. “Others” includes contributions from VVV , $t\bar{t}t$, $t\bar{t}t\bar{t}$, $t\bar{t}W$, $t\bar{t}WW$, $t\bar{t}WZ$, $t\bar{t}H$, and tZ processes. The shaded band represents the total uncertainty in the expected SM background. The lower panel shows the normalisation factors μ_X (left three bins) extracted in the CRs for the $t\bar{t}$, $t\bar{t}Z$ and diboson processes, while, for the VRs and the SRs (right bins), the significance as defined in Ref. [125].

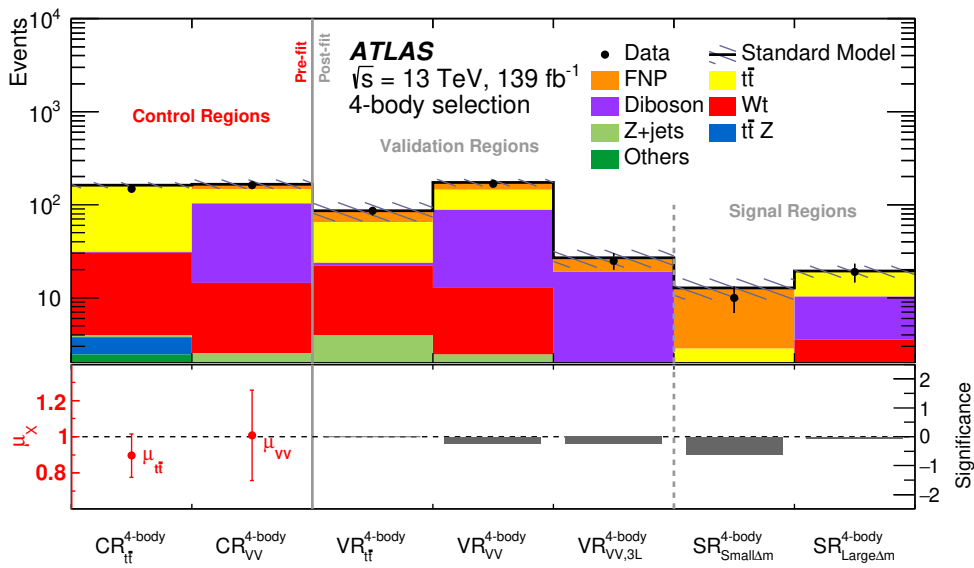


Figure 10: Four-body selection. Expected and observed yields are shown. The upper panel shows the observed number of events in each of the CRs, VRs and SRs defined in the four-body selection, together with the expected SM backgrounds obtained before the fit in the CRs and after the fit in the VRs and SRs. “Others” includes contributions from VVV , $t\bar{t}$, $t\bar{t}t\bar{t}$, $t\bar{t}W$, $t\bar{t}WW$, $t\bar{t}WZ$, $t\bar{t}H$, and tZ processes. The shaded band represents the total uncertainty in the expected SM background. The lower panel shows the normalisation factors μ_X (left two bins) extracted in the CRs for the $t\bar{t}$ and diboson processes, while, for the VRs and the SRs (right bins), the significance as defined in Ref. [125].

8.1 Two-body selection results

The estimated SM yields in the binned and inclusive SRs defined in the two-body selection are obtained with a background fit which simultaneously determines the normalisations of the background contributions from $t\bar{t}$ and $t\bar{t}Z$. Figure 11 shows the $m_{T2}^{\ell\ell}$ distribution for events satisfying all the selection criteria of the $\text{SR}_{110,\infty}^{2\text{-body}}$ (SF and DF) signal regions, after the background fit. Each bin corresponds to one of the binned SRs. No significant excess over the SM prediction is observed, as can be seen from results shown in Tables 15 and 16 for the binned SRs.

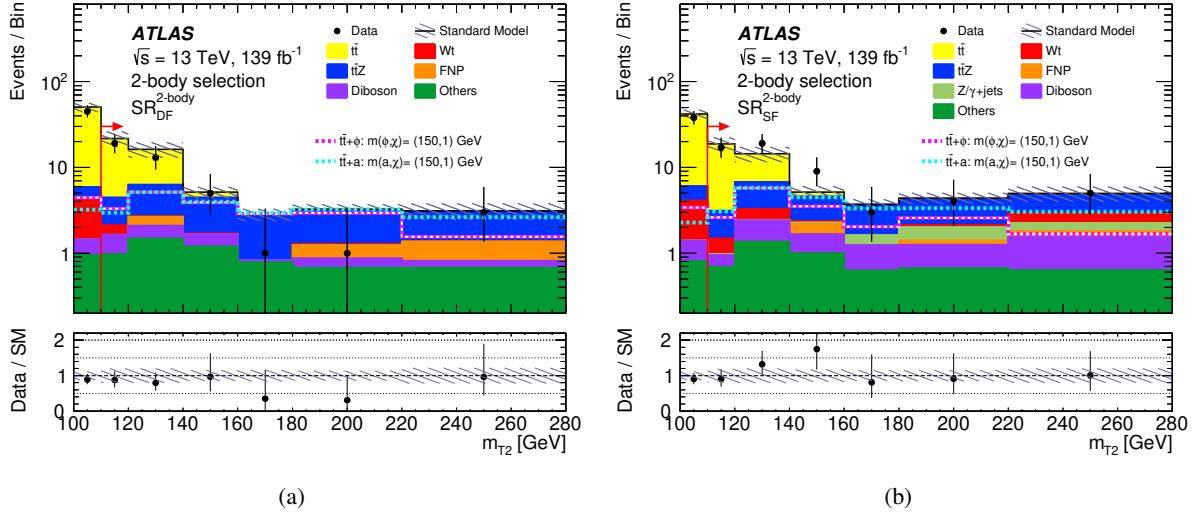


Figure 11: Two-body selection. Distributions of $m_{T2}^{\ell\ell}$ in $\text{SR}_{110,\infty}^{2\text{-body}}$ for (a) different-flavour and (b) same-flavour events satisfying the selection criteria of the given SR, except the one for the presented variable, after the background fit. The contributions from all SM backgrounds are shown as a histogram stack. “Others” includes contributions from VVV , $t\bar{t}t$, $t\bar{t}t\bar{t}$, $t\bar{t}W$, $t\bar{t}WW$, $t\bar{t}WZ$, $t\bar{t}H$, and tZ processes. The hatched bands represent the total statistical and systematic uncertainty. The rightmost bin of each plot includes overflow events. Reference dark-matter signal models are overlaid for comparison. Red arrows in the upper panels indicate the signal region selection criteria. The bottom panels show the ratio of the observed data to the total SM background prediction, with hatched bands representing the total uncertainty in the background prediction.

Table 15: Two-body selection. Background fit results for the different-flavour leptons binned SRs. The ‘Others’ category contains the contributions from VVV , $t\bar{t}$, $t\bar{t}t$, $t\bar{t}W$, $t\bar{t}WW$, $t\bar{t}WZ$, $t\bar{t}H$, and tZ . Combined statistical and systematic uncertainties are given. Entries marked ‘-’ indicate a negligible background contribution (less than 0.001 events). The individual uncertainties can be correlated, and do not necessarily add up in quadrature to the total background uncertainty.

| | SR-DF $_{[110,120]}^{2\text{-body}}$ | SR-DF $_{[120,140]}^{2\text{-body}}$ | SR-DF $_{[140,160]}^{2\text{-body}}$ | SR-DF $_{[160,180]}^{2\text{-body}}$ | SR-DF $_{[180,220]}^{2\text{-body}}$ | SR-DF $_{[220,\infty)}^{2\text{-body}}$ |
|----------------------------|--------------------------------------|--------------------------------------|--------------------------------------|--------------------------------------|--------------------------------------|---|
| Observed events | 19 | 13 | 5 | 1 | 1 | 3 |
| Fitted bkg. events | 22 ± 4 | 16.3 ± 3.2 | 5.1 ± 0.8 | 2.83 ± 0.45 | 3.25 ± 0.45 | 3.11 ± 0.67 |
| Post-fit, $t\bar{t}$ | 17 ± 4 | 10.0 ± 3.2 | 0.7 ± 0.5 | $0.01^{+0.10}_{-0.01}$ | 0.13 ± 0.11 | – |
| Post-fit, $t\bar{t} + Z$ | 2.3 ± 0.5 | 3.5 ± 0.7 | 2.7 ± 0.7 | 2.0 ± 0.4 | 1.9 ± 0.4 | 1.7 ± 0.6 |
| Wt | 0.47 ± 0.27 | $0.05^{+0.33}_{-0.05}$ | 0.025 ± 0.012 | – | 0.033 ± 0.013 | – |
| $Z/\gamma^* + \text{jets}$ | – | – | – | – | – | – |
| Diboson | 0.67 ± 0.27 | 0.61 ± 0.24 | 0.49 ± 0.16 | $0.05^{+0.07}_{-0.05}$ | 0.19 ± 0.13 | 0.14 ± 0.07 |
| Others | 0.97 ± 0.19 | 1.48 ± 0.28 | 1.19 ± 0.16 | 0.78 ± 0.12 | 0.68 ± 0.13 | 0.67 ± 0.11 |
| Fake and non-prompt | $0.0^{+0.5}_{-0.0}$ | 0.6 ± 0.6 | $0.0^{+0.5}_{-0.0}$ | $0.0^{+0.5}_{-0.0}$ | 0.37 ± 0.23 | 0.6 ± 0.4 |

Table 16: Two-body selection. Background fit results for the same-flavour leptons binned SRs. The ‘Others’ category contains the contributions from VVV , $t\bar{t}t$, $t\bar{t}t\bar{t}$, $t\bar{t}W$, $t\bar{t}WW$, $t\bar{t}WZ$, $t\bar{t}H$, and tZ . Combined statistical and systematic uncertainties are given. The individual uncertainties can be correlated, and do not necessarily add up in quadrature to the total background uncertainty.

| | SR-SF $_{[110,120]}^{2\text{-body}}$ | SR-SF $_{[120,140]}^{2\text{-body}}$ | SR-SF $_{[140,160]}^{2\text{-body}}$ | SR-SF $_{[160,180]}^{2\text{-body}}$ | SR-SF $_{[180,220]}^{2\text{-body}}$ | SR-SF $_{[220,\infty)}^{2\text{-body}}$ |
|----------------------------|--------------------------------------|--------------------------------------|--------------------------------------|--------------------------------------|--------------------------------------|---|
| Observed events | 17 | 19 | 9 | 3 | 4 | 5 |
| Fitted bkg. events | 18.8 ± 3.5 | 14.4 ± 2.9 | 5.1 ± 0.9 | 3.7 ± 0.6 | 4.4 ± 0.7 | 5 ± 1 |
| Post-fit, $t\bar{t}$ | 15.7 ± 3.4 | 7.6 ± 2.3 | 0.6 ± 0.4 | $0.007^{+0.020}_{-0.007}$ | 0.10 ± 0.08 | $0.16^{+0.18}_{-0.16}$ |
| Post-fit, $t\bar{t} + Z$ | 1.65 ± 0.35 | 3.5 ± 0.7 | 2.2 ± 0.5 | 2.1 ± 0.4 | 2.18 ± 0.45 | 1.9 ± 0.6 |
| Wt | 0.5 ± 0.5 | 0.8 ± 0.8 | 0.10 ± 0.04 | $0.018^{+0.019}_{-0.018}$ | 0.12 ± 0.06 | 0.71 ± 0.29 |
| $Z/\gamma^* + \text{jets}$ | 0.020 ± 0.014 | 0.044 ± 0.003 | $0.07^{+0.17}_{-0.07}$ | 0.38 ± 0.13 | 0.60 ± 0.33 | 0.4 ± 0.4 |
| Diboson | 0.27 ± 0.20 | 1.0 ± 0.6 | 0.65 ± 0.24 | 0.6 ± 0.4 | 0.59 ± 0.28 | 0.9 ± 0.5 |
| Others | 0.69 ± 0.13 | 1.37 ± 0.21 | 0.99 ± 0.16 | 0.63 ± 0.11 | 0.67 ± 0.14 | 0.64 ± 0.10 |
| Fake and non-prompt | $0.0^{+0.4}_{-0.0}$ | $0.0^{+0.4}_{-0.0}$ | 0.56 ± 0.06 | $0.0^{+0.7}_{-0.0}$ | 0.15 ± 0.12 | 0.28 ± 0.21 |

8.2 Three-body selection results

The dominant background processes in the three-body selection are diboson, $t\bar{t}$ and $t\bar{t}Z$ production, and the yields are determined with a simultaneous fit. Figure 12 shows the distributions of M_{Δ}^R in $\text{SR}_W^{3\text{-body}}$ (top) and in $\text{SR}_t^{3\text{-body}}$ (bottom), for events satisfying all the selection criteria except the one for the presented variable, after the background fit. Table 17 shows the observed events in each signal region and the SM background estimates. No excess over the SM prediction is observed while a fluctuation of about -2σ is observed in $\text{SR-DF}_W^{3\text{-body}}$ and is also visible in Figure 12(a).

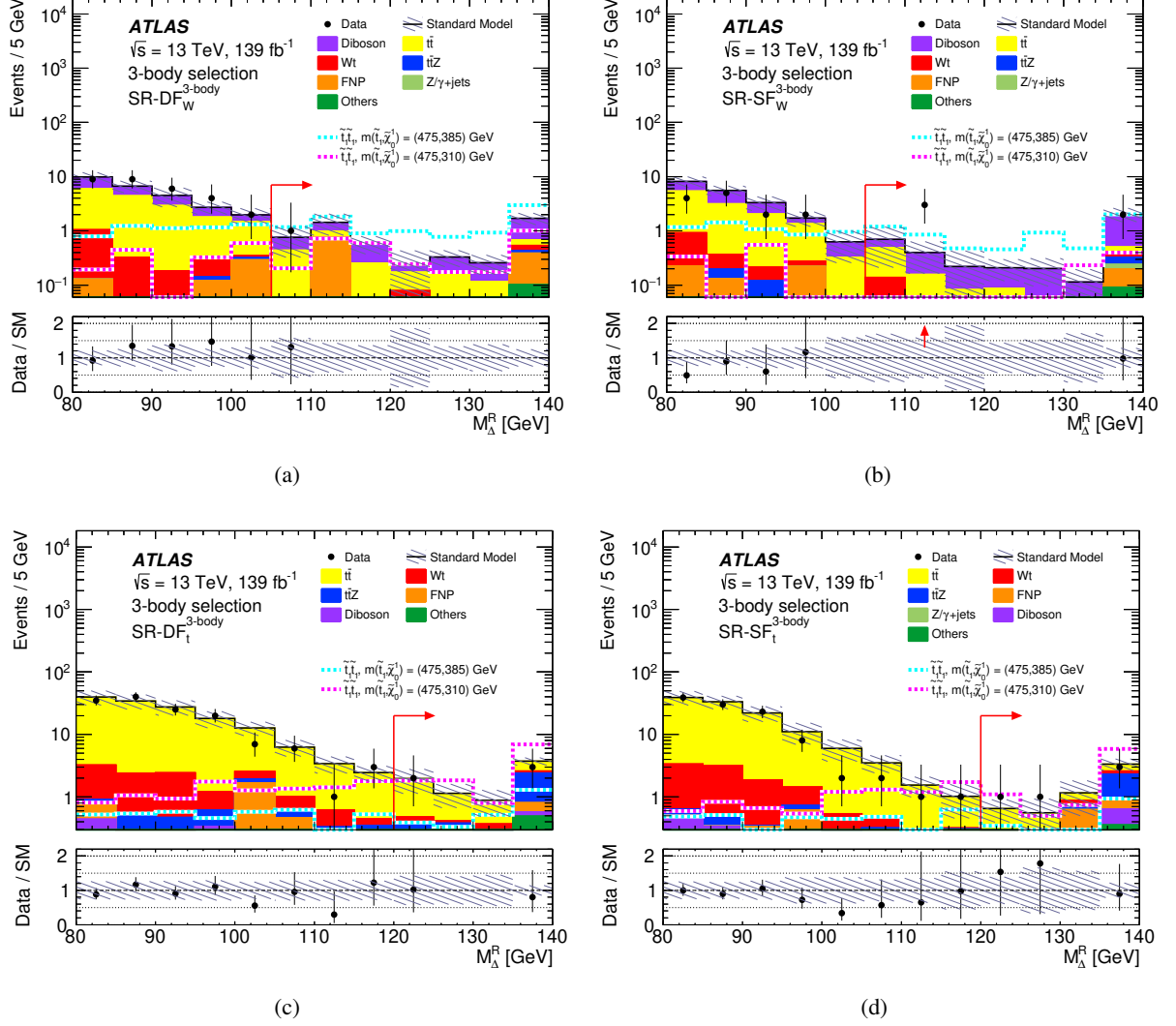


Figure 12: Three-body selection. Distributions of M_Δ^R in (a,b) $SR_W^{3\text{-body}}$ and (c,d) $SR_t^{3\text{-body}}$ for (left) same-flavour and (right) different-flavour events satisfying the selection criteria of the given SR, except the one for the presented variable, after the background fit. The contributions from all SM backgrounds are shown as a histogram stack. “Others” includes contributions from VVV , $t\bar{t}t$, $t\bar{t}t\bar{t}$, $t\bar{t}W$, $t\bar{t}WW$, $t\bar{t}WZ$, $t\bar{t}H$, and tZ processes. The hatched bands represent the total statistical and systematic uncertainty. The rightmost bin of each plot includes overflow events. Reference top squark pair production signal models are overlaid for comparison. Red arrows in the upper panels indicate the signal region selection criteria. The bottom panels show the ratio of the observed data to the total SM background prediction, with hatched bands representing the total uncertainty in the background prediction; red arrows show data outside the vertical-axis range.

Table 17: Three-body selection. Observed event yields and background fit results for the three-body selection SRs. The ‘Others’ category contains contributions from VVV , $t\bar{t}$, $t\bar{t}\bar{t}$, $t\bar{t}W$, $t\bar{t}WW$, $t\bar{t}WZ$, $t\bar{t}H$, and tZ . Combined statistical and systematic uncertainties are given. Entries marked ‘–’ indicate a negligible background contribution (less than 0.001 events). The individual uncertainties can be correlated, and do not necessarily add up in quadrature to the total background uncertainty.

| | $\text{SR-DF}_W^{3\text{-body}}$ | $\text{SR-SF}_W^{3\text{-body}}$ | $\text{SR-DF}_t^{3\text{-body}}$ | $\text{SR-SF}_t^{3\text{-body}}$ |
|----------------------------|----------------------------------|----------------------------------|----------------------------------|----------------------------------|
| Observed events | 1 | 5 | 5 | 5 |
| Total (post-fit) SM events | 5.1 ± 1.0 | 4.0 ± 1.0 | 7.5 ± 1.4 | 5.0 ± 1.1 |
| Post-fit, $t\bar{t}$ | 1.3 ± 0.5 | 0.76 ± 0.32 | 3.9 ± 1.1 | 1.8 ± 0.7 |
| Post-fit, $t\bar{t} + Z$ | 0.085 ± 0.034 | 0.08 ± 0.05 | 2.3 ± 0.4 | 1.69 ± 0.35 |
| Post-fit, diboson | 2.5 ± 1.0 | 2.5 ± 1.0 | 0.17 ± 0.09 | 0.34 ± 0.14 |
| Wt | 0.30 ± 0.05 | 0.211 ± 0.030 | $0.4^{+0.5}_{-0.4}$ | 0.54 ± 0.19 |
| $Z/\gamma^* + \text{jets}$ | – | 0.044 ± 0.019 | – | $0.015^{+0.027}_{-0.015}$ |
| Others | 0.232 ± 0.020 | 0.25 ± 0.05 | 0.70 ± 0.12 | 0.49 ± 0.08 |
| Fake and non-prompt | 0.70 ± 0.09 | $0.00^{+0.25}_{-0.00}$ | $0.00^{+0.23}_{-0.00}$ | $0.16^{+0.23}_{-0.16}$ |

8.3 Four-body selection results

The estimated SM yields in $\text{SR}_{\text{Small } \Delta m}^{4\text{-body}}$ and $\text{SR}_{\text{Large } \Delta m}^{4\text{-body}}$ are determined with a background fit that provides the normalisation factors for $t\bar{t}$ and diboson production. Figure 13 shows the distributions of (a) E_T^{miss} in $\text{SR}_{\text{Small } \Delta m}^{4\text{-body}}$ and (b) $R_{2\ell 4j}$ in $\text{SR}_{\text{Large } \Delta m}^{4\text{-body}}$ for events satisfying the selection criteria of the given SR, except the one for the presented variable, after the background fit. The background fit results are shown in Table 18. The observed yield in the SR is within one standard deviation of the background prediction.

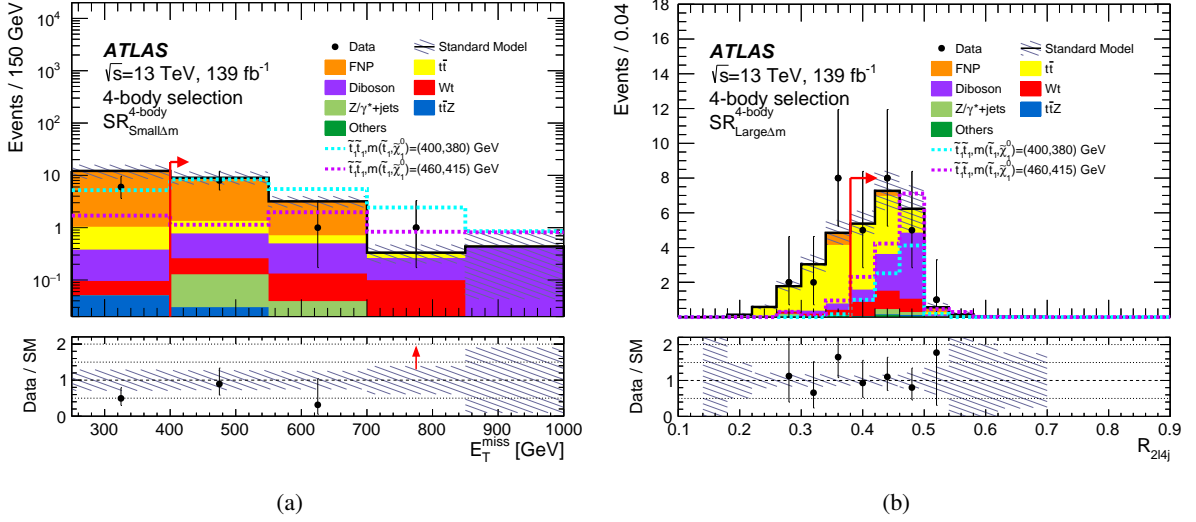


Figure 13: Four-body selection. (a) distributions of E_T^{miss} in $\text{SR}_{\text{Small } \Delta m}^{4\text{-body}}$ and (b) distribution of $R_{2\ell 4j}$ in $\text{SR}_{\text{Large } \Delta m}^{4\text{-body}}$ for events satisfying the selection criteria of the given SR, except the one for the presented variable, after the background fit. The contributions from all SM backgrounds are shown as a histogram stack. “Others” includes contributions from VVV , $t\bar{t}t$, $t\bar{t}t\bar{t}$, $t\bar{t}W$, $t\bar{t}WW$, $t\bar{t}WZ$, $t\bar{t}H$, and tZ processes. The hatched bands represent the total statistical and systematic uncertainty. The rightmost bin of each plot includes overflow events. Reference top squark pair production signal models are overlaid for comparison. Red arrows in the upper panel indicate the signal region selection criteria. The bottom panels show the ratio of the observed data to the total SM background prediction, with hatched bands representing the total uncertainty in the background prediction; red arrows show data outside the vertical-axis range.

Table 18: Four-body selection. Observed event yields and background fit results for $\text{SR}_{\text{Small } \Delta m}^{4\text{-body}}$ and $\text{SR}_{\text{Large } \Delta m}^{4\text{-body}}$. The ‘Others’ category contains the contributions from VVV , $t\bar{t}$, $t\bar{t}\bar{t}$, $t\bar{t}W$, $t\bar{t}WW$, $t\bar{t}WZ$, $t\bar{t}H$, and tZ . Combined statistical and systematic uncertainties are given. The individual uncertainties can be correlated, and do not necessarily add up in quadrature to the total background uncertainty.

| | $\text{SR}_{\text{Small } \Delta m}^{4\text{-body}}$ | $\text{SR}_{\text{Large } \Delta m}^{4\text{-body}}$ |
|----------------------------|--|--|
| Observed events | 10 | 19 |
| Total (post-fit) SM events | 12.8 ± 3.2 | 19.3 ± 2.7 |
| Post-fit, $t\bar{t}$ | 0.87 ± 0.26 | 8.7 ± 1.5 |
| Post-fit, diboson | 1.5 ± 0.5 | 6.8 ± 2.3 |
| Wt | 0.32 ± 0.08 | 2.7 ± 0.5 |
| $Z/\gamma^* + \text{jets}$ | 0.128 ± 0.023 | 0.46 ± 0.19 |
| $t\bar{t}Z$ | 0.047 ± 0.010 | 0.126 ± 0.033 |
| Others | $0.019^{+0.021}_{-0.019}$ | 0.26 ± 0.07 |
| Fake and non-prompt | 10.0 ± 3.1 | 0.24 ± 0.09 |

9 Interpretation

No excess is observed in the data relative to the expected background. The analysis results are therefore interpreted in terms of model-independent upper limits on the visible cross-section (σ_{vis}) of new physics, defined as the 95% confidence level (CL) upper limit on the number of signal events (S^{95}) divided by the integrated luminosity, and in terms of exclusion limits in the plane of the masses parameters of our simplified models. For the two-body selection the upper limits are derived using the inclusive SRs.

The upper limits on σ_{vis} are derived, in each SR, by performing a model-independent hypothesis test, which introduces a free signal as an additional process to be constrained by the observed yield. The CL_s method [126] is used to derive all the exclusion confidence levels. Model-independent upper limits are presented in Table 19. These limits assume negligible signal contamination in the CRs, resulting in a more conservative result than from the model-dependent limits, where a small signal contamination is allowed in the CRs.

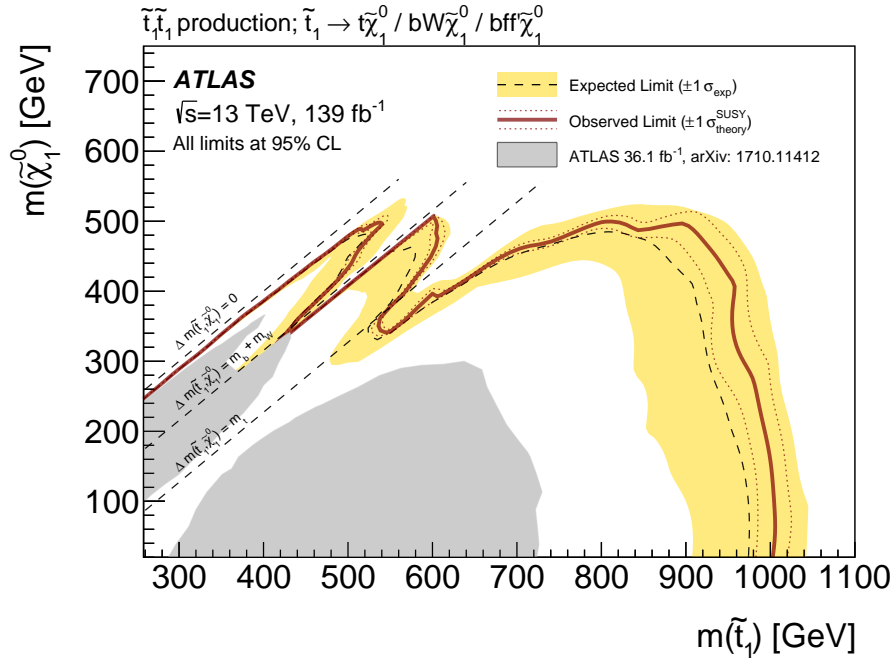
Model-dependent limits are computed for the various signal scenarios considered in the analysis. The hypothesis tests are performed including the expected signal yield and its associated uncertainties in the CRs and SRs. All limits are quoted at 95% CL with the CL_s method. When setting limits, the two-body selection binned SRs $\text{SR} - \text{DF}_{[x,y]}^{2\text{-body}}$ and $\text{SR} - \text{SF}_{[x,y]}^{2\text{-body}}$ regions are combined. Similarly, the $\text{SR} - \text{DF}_W^{3\text{-body}}$, $\text{SR} - \text{SF}_W^{3\text{-body}}$, $\text{SR} - \text{DF}_t^{3\text{-body}}$, and $\text{SR} - \text{SF}_t^{3\text{-body}}$ signal regions are combined for the three-body selection, and so are $\text{SR}_{\text{Small } \Delta m}^{4\text{-body}}$ and $\text{SR}_{\text{Large } \Delta m}^{4\text{-body}}$ for the four-body selection.

Limits for simplified models in which pair-produced \tilde{t}_1 decay with 100% branching ratio into a top quark and $\tilde{\chi}_1^0$ are shown in the $\tilde{t}_1 - \tilde{\chi}_1^0$ mass plane in Figure 14(a) and in the $m(\tilde{t}_1) - \Delta m(\tilde{t}_1, \tilde{\chi}_1^0)$ plane in Figure 14(b). The exclusion contour is the envelope of the exclusion regions obtained separately for the three selections. Top squark masses up to 1 TeV are excluded for a massless lightest neutralino. Neutralino masses up to 500 GeV are excluded for $m(\tilde{t}_1)$ above the top quark production kinematic limit. In the three-body

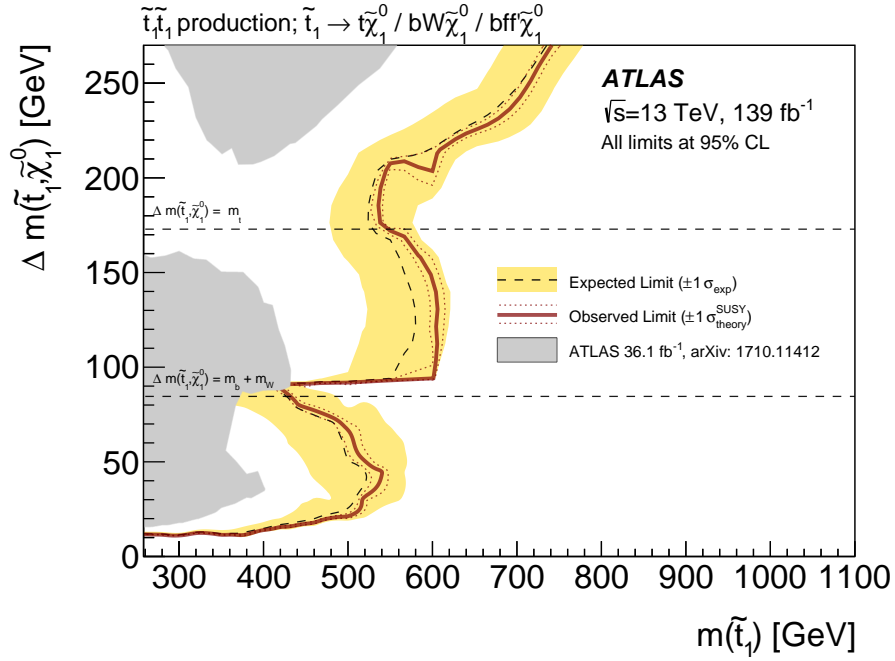
decay region, top squark masses are excluded up to 600 GeV for $\Delta m(\tilde{t}_1, \tilde{\chi}_1^0) = 120$ GeV, up to 550 GeV for $\Delta m(\tilde{t}_1, \tilde{\chi}_1^0)$ close to the top quark mass and up to 430 GeV for $\Delta m(\tilde{t}_1, \tilde{\chi}_1^0)$ close to the W boson mass. In the four-body decay region, top squark masses are excluded up to 540 GeV for $\Delta m(\tilde{t}_1, \tilde{\chi}_1^0) = 40$ GeV. Top squark decay around the W boson production kinematic limit is not fully excluded for $m(\tilde{t}_1)$ above 400 GeV because there the four-body and three-body decay exclusion regions do not overlap. The four-body selection loses sensitivity for $\Delta m(\tilde{t}, \tilde{\chi}_1^0) \gtrsim m(W)$ due to the upper bound of the sub-leading lepton p_T while, for the three body selection, the M_Δ^R requirement suppresses the sensitivity for $\Delta m(\tilde{t}, \tilde{\chi}_1^0) \lesssim m(W)$ because of the smaller mass splitting. The three-body and two-body overlap in the sensitivity provides exclusion coverage around the top quark production kinematic limit up to $m(\tilde{t}_1)$ of 540 GeV.

Table 19: Model-independent 95% CL upper limits on the visible cross-section (σ_{vis}) of new physics, on the visible number of signal events (S_{obs}^{95}), on the visible number of signal events (S_{exp}^{95}) given the expected number of background events (and $\pm 1\sigma$ excursions of the expected number), and the discovery p -value ($p(s=0)$), all calculated with pseudo-experiments, are shown for each of the SRs. The p -value is reported as 0.5 if the observed yield is smaller than that predicted.

| Selection | Signal Region | σ_{vis} [fb] | S_{obs}^{95} | S_{exp}^{95} | $p(s=0)$ |
|----------------------------------|--|----------------------------------|-----------------------|-----------------------|---------------------|
| Two-body | $\text{SR}_{[110, \infty)}^{2\text{-body}}$ | 0.21 | 29.3 | 31^{+11}_{-8} | 0.5 |
| | $\text{SR}_{[120, \infty)}^{2\text{-body}}$ | 0.15 | 21.4 | 21^{+8}_{-6} | 0.4 |
| | $\text{SR}_{[140, \infty)}^{2\text{-body}}$ | 0.10 | 13.2 | 14^{+5}_{-4} | 0.5 |
| | $\text{SR}_{[160, \infty)}^{2\text{-body}}$ | 0.06 | 8.2 | $11^{+5}_{-3.0}$ | 0.5 |
| | $\text{SR}_{[180, \infty)}^{2\text{-body}}$ | 0.06 | 7.9 | $9.6^{+3.8}_{-2.8}$ | 0.5 |
| | $\text{SR}_{[200, \infty)}^{2\text{-body}}$ | 0.06 | 7.6 | $8.4^{+3.6}_{-2.3}$ | 0.5 |
| | $\text{SR}_{[220, \infty)}^{2\text{-body}}$ | 0.05 | 7.6 | $7.5^{+3.1}_{-2.0}$ | 0.5 |
| | Three-body | $\text{SR-DF}_W^{3\text{-body}}$ | 0.023 | 3.2 | $5.7^{+2.3}_{-1.5}$ |
| $\text{SR-SF}_W^{3\text{-body}}$ | | 0.05 | 7.0 | $5.6^{+2.3}_{-1.5}$ | 0.27 |
| $\text{SR-DF}_t^{3\text{-body}}$ | | 0.04 | 5.5 | $6.9^{+2.9}_{-1.9}$ | 0.5 |
| $\text{SR-SF}_t^{3\text{-body}}$ | | 0.04 | 6.3 | $6.1^{+2.6}_{-1.6}$ | 0.5 |
| Four-body | $\text{SR}_{\text{Small } \Delta m}^{4\text{-body}}$ | 0.06 | 8.2 | $9.6^{+3.8}_{-2.5}$ | 0.5 |
| | $\text{SR}_{\text{Large } \Delta m}^{4\text{-body}}$ | 0.08 | 11.1 | $11.1^{+4.5}_{-3.0}$ | 0.5 |



(a)



(b)

Figure 14: Exclusion limit contour (95% CL) for a simplified model assuming \tilde{t}_1 pair production, decaying via $\tilde{t}_1 \rightarrow t^{(*)} \tilde{\chi}_1^0$ with 100% branching ratio, in the (a) $m(\tilde{t}_1) - m(\tilde{\chi}_1^0)$ and (b) $m(\tilde{t}_1) - \Delta m(\tilde{t}_1, \tilde{\chi}_1^0)$ planes. The dashed lines and the shaded bands are the expected limits and their $\pm 1\sigma$ uncertainties. The thick solid lines are the observed limits for the central value of the signal cross-section. The expected and observed limits do not include the effect of the theoretical uncertainties in the signal cross-section. The dotted lines show the effect on the observed limit when varying the signal cross-section by $\pm 1\sigma$ of the theoretical uncertainty.

For the DM mediator models, Figure 15 shows upper limits at 95% CL on the observed signal cross-section scaled to the theoretical signal cross-section for a coupling $g = g_q = g_\chi = 1$, denoted by $\sigma_{\text{obs}}/\sigma_{\text{Th}}(g = 1.0)$. These limits are obtained as a function of the mediator mass, assuming a specific DM particle mass of 1 GeV. Both the scalar and pseudoscalar mediator cases are considered. The sensitivity is approximately constant for mediator masses below 100 GeV and the models are excluded for scalar (pseudoscalar) mediator masses up to 250 (300) GeV when assuming $g = 1$.

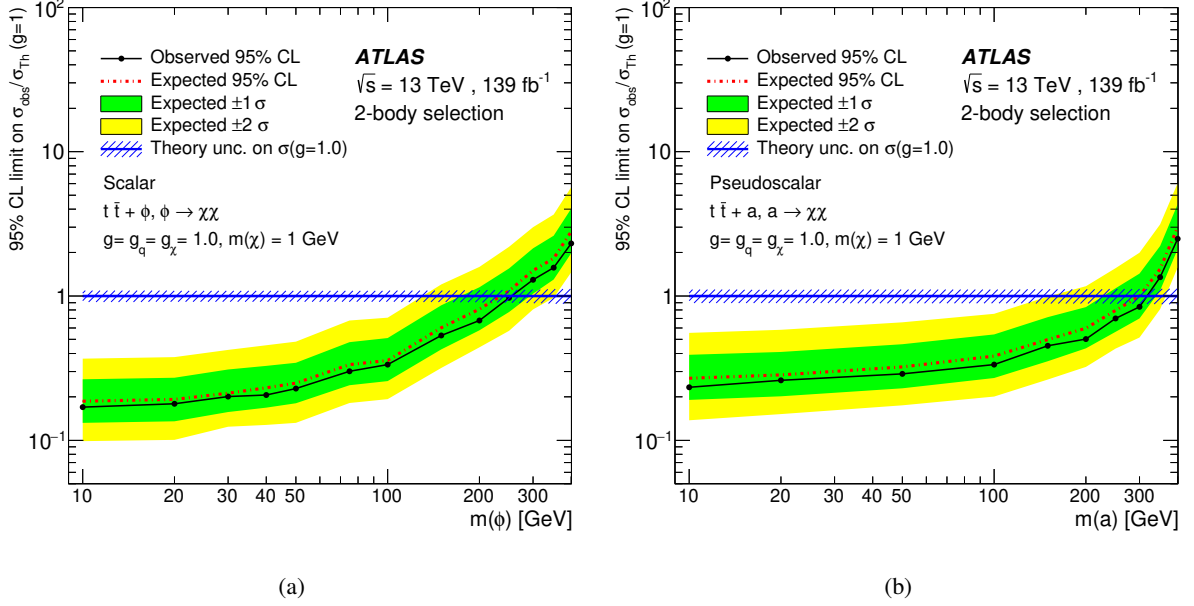


Figure 15: Exclusion limits for (a) $t\bar{t} + \phi$ scalar and (b) $t\bar{t} + a$ pseudoscalar models as a function of the mediator mass for a DM particle mass of $m(\chi) = 1$ GeV. The limits are calculated at 95% CL and are expressed in terms of the ratio of the excluded cross-section to the nominal cross-section for a coupling assumption of $g = g_q = g_\chi = 1$. The solid (dashed) lines shows the observed (expected) exclusion limits.

10 Conclusion

This paper reports the results of a search for direct top squark pair production and for dark matter in a final state containing two leptons with opposite electric charge, jets and missing transverse momentum. The search uses an integrated luminosity of 139 fb^{-1} of proton–proton collisions at $\sqrt{s} = 13$ TeV, as collected by the ATLAS experiment at the Large Hadron Collider during Run 2 (2015–2018).

Compared to previous searches a significant improvement in sensitivity is obtained by using additional integrated luminosity and a new discriminating variable, the object-based E_T^{miss} significance. Moreover, in the small- $\Delta m(\tilde{t}_1, \tilde{\chi}_1^0)$ region, an important gain in sensitivity is also achieved by lowering the p_T threshold for lepton selection.

The data are found to be consistent with the Standard Model predictions. Assuming direct \tilde{t}_1 pair production with both top squarks decaying in either the two-body channel $\tilde{t}_1 \rightarrow t\tilde{\chi}_1^0$, the three-body channel $\tilde{t}_1 \rightarrow bW\tilde{\chi}_1^0$, or the four-body channel $\tilde{t}_1 \rightarrow b\ell\nu\tilde{\chi}_1^0$, constraints at 95% confidence level are placed on

the minimum \tilde{t}_1 and $\tilde{\chi}_1^0$ masses up to about 1 TeV and 500 GeV respectively. The results improve on the previous ATLAS limits obtained in a two-lepton final state and provide unique sensitivity among the ATLAS searches in the mass region where the decay $\tilde{t}_1 \rightarrow t\tilde{\chi}_1^0$ becomes kinematically allowed. For the dark-matter model, assuming spin-0 mediator production in association with a pair of top quarks and decay with 100% branching ratio into a pair of dark-matter particles, scalar (pseudoscalar) mediator masses up to about 250 (300) GeV are excluded at 95% confidence level for mediator couplings $g_q = g_\chi = 1$ to Standard Model and dark-matter particles.

Acknowledgements

We thank CERN for the very successful operation of the LHC, as well as the support staff from our institutions without whom ATLAS could not be operated efficiently.

We acknowledge the support of ANPCyT, Argentina; YerPhI, Armenia; ARC, Australia; BMWFW and FWF, Austria; ANAS, Azerbaijan; SSTC, Belarus; CNPq and FAPESP, Brazil; NSERC, NRC and CFI, Canada; CERN; ANID, Chile; CAS, MOST and NSFC, China; COLCIENCIAS, Colombia; MSMT CR, MPO CR and VSC CR, Czech Republic; DNRF and DNSRC, Denmark; IN2P3-CNRS and CEA-DRF/IRFU, France; SRNSFG, Georgia; BMBF, HGF and MPG, Germany; GSRT, Greece; RGC and Hong Kong SAR, China; ISF and Benozio Center, Israel; INFN, Italy; MEXT and JSPS, Japan; CNRST, Morocco; NWO, Netherlands; RCN, Norway; MNiSW and NCN, Poland; FCT, Portugal; MNE/IFA, Romania; JINR; MES of Russia and NRC KI, Russian Federation; MESTD, Serbia; MSSR, Slovakia; ARRS and MIZŠ, Slovenia; DST/NRF, South Africa; MICINN, Spain; SRC and Wallenberg Foundation, Sweden; SERI, SNSF and Cantons of Bern and Geneva, Switzerland; MOST, Taiwan; TAEK, Turkey; STFC, United Kingdom; DOE and NSF, United States of America. In addition, individual groups and members have received support from BCKDF, CANARIE, Compute Canada, CRC and IVADO, Canada; Beijing Municipal Science & Technology Commission, China; COST, ERC, ERDF, Horizon 2020 and Marie Skłodowska-Curie Actions, European Union; Investissements d'Avenir Labex, Investissements d'Avenir Idex and ANR, France; DFG and AvH Foundation, Germany; Herakleitos, Thales and Aristeia programmes co-financed by EU-ESF and the Greek NSRF, Greece; BSF-NSF and GIF, Israel; La Caixa Banking Foundation, CERCA Programme Generalitat de Catalunya and PROMETEO and GenT Programmes Generalitat Valenciana, Spain; Göran Gustafssons Stiftelse, Sweden; The Royal Society and Leverhulme Trust, United Kingdom.

The crucial computing support from all WLCG partners is acknowledged gratefully, in particular from CERN, the ATLAS Tier-1 facilities at TRIUMF (Canada), NDGF (Denmark, Norway, Sweden), CC-IN2P3 (France), KIT/GridKA (Germany), INFN-CNAF (Italy), NL-T1 (Netherlands), PIC (Spain), ASGC (Taiwan), RAL (UK) and BNL (USA), the Tier-2 facilities worldwide and large non-WLCG resource providers. Major contributors of computing resources are listed in Ref. [127].

References

- [1] F. Zwicky, *Die Rotverschiebung von extragalaktischen Nebeln*, [Helv. Phys. Acta](#) **6** (1933) 110.
- [2] G. Bertone, D. Hooper and J. Silk, *Particle dark matter: evidence, candidates and constraints*, [Phys. Rept.](#) **405** (2005) 279, arXiv: [hep-ph/0404175](#).
- [3] L. Evans and P. Bryant, *LHC Machine*, [JINST](#) **3** (2008) S08001.
- [4] Y. Golfand and E. Likhtman, *Extension of the Algebra of Poincare Group Generators and Violation of P Invariance*, [JETP Lett.](#) **13** (1971) 323, [[Pisma Zh. Eksp. Teor. Fiz.](#) **13** (1971) 452].
- [5] D. Volkov and V. Akulov, *Is the neutrino a goldstone particle?*, [Phys. Lett. B](#) **46** (1973) 109.
- [6] J. Wess and B. Zumino, *Supergauge transformations in four dimensions*, [Nucl. Phys. B](#) **70** (1974) 39.
- [7] J. Wess and B. Zumino, *Supergauge invariant extension of quantum electrodynamics*, [Nucl. Phys. B](#) **78** (1974) 1.
- [8] S. Ferrara and B. Zumino, *Supergauge invariant Yang-Mills theories*, [Nucl. Phys. B](#) **79** (1974) 413.
- [9] A. Salam and J. Strathdee, *Super-symmetry and non-Abelian gauges*, [Phys. Lett. B](#) **51** (1974) 353.
- [10] ATLAS Collaboration, *Search for a scalar partner of the top quark in the all-hadronic $t\bar{t}$ plus missing transverse momentum final state at $\sqrt{s} = 13$ TeV with the ATLAS detector*, [Eur. Phys. J. C](#) **80** (2020) 737, arXiv: [2004.14060 \[hep-ex\]](#).
- [11] ATLAS Collaboration, *ATLAS Run 1 searches for direct pair production of third-generation squarks at the Large Hadron Collider*, [Eur. Phys. J. C](#) **75** (2015) 510, arXiv: [1506.08616 \[hep-ex\]](#).
- [12] ATLAS Collaboration, *Search for a scalar partner of the top quark in the jets plus missing transverse momentum final state at $\sqrt{s} = 13$ TeV with the ATLAS detector*, [JHEP](#) **12** (2017) 085, arXiv: [1709.04183 \[hep-ex\]](#).
- [13] ATLAS Collaboration, *Search for top-squark pair production in final states with one lepton, jets, and missing transverse momentum using 36fb^{-1} of $\sqrt{s} = 13$ TeV pp collision data with the ATLAS detector*, [JHEP](#) **06** (2018) 108, arXiv: [1711.11520 \[hep-ex\]](#).
- [14] ATLAS Collaboration, *Search for supersymmetry in final states with charm jets and missing transverse momentum in 13 TeV pp collisions with the ATLAS detector*, [JHEP](#) **09** (2018) 050, arXiv: [1805.01649 \[hep-ex\]](#).
- [15] ATLAS Collaboration, *Search for dark matter and other new phenomena in events with an energetic jet and large missing transverse momentum using the ATLAS detector*, [JHEP](#) **01** (2018) 126, arXiv: [1711.03301 \[hep-ex\]](#).
- [16] ATLAS Collaboration, *Measurements of top-quark pair spin correlations in the $e\mu$ channel at $\sqrt{s} = 13$ TeV using pp collisions in the ATLAS detector*, [Eur. Phys. J. C](#) **80** (2020) 754, arXiv: [1903.07570 \[hep-ex\]](#).
- [17] CMS Collaboration, *Inclusive search for supersymmetry using razor variables in pp collisions at $\sqrt{s} = 13$ TeV*, [Phys. Rev. D](#) **95** (2017) 012003, arXiv: [1609.07658 \[hep-ex\]](#).
- [18] CMS Collaboration, *A search for new phenomena in pp collisions at $\sqrt{s} = 13$ TeV in final states with missing transverse momentum and at least one jet using the α_T variable*, [Eur. Phys. J. C](#) **77** (2017) 294, arXiv: [1611.00338 \[hep-ex\]](#).
- [19] CMS Collaboration, *Searches for pair production of third-generation squarks in $\sqrt{s} = 13$ TeV pp collisions*, [Eur. Phys. J. C](#) **77** (2017) 327, arXiv: [1612.03877 \[hep-ex\]](#).

- [20] CMS Collaboration, *Search for direct production of supersymmetric partners of the top quark in the all-jets final state in proton–proton collisions at $\sqrt{s} = 13$ TeV*, *JHEP* **10** (2017) 005, arXiv: [1707.03316 \[hep-ex\]](#).
- [21] CMS Collaboration, *Search for top squark pair production in pp collisions at $\sqrt{s} = 13$ TeV using single lepton events*, *JHEP* **10** (2017) 019, arXiv: [1706.04402 \[hep-ex\]](#).
- [22] CMS Collaboration, *Search for top squarks and dark matter particles in opposite-charge dilepton final states at $\sqrt{s} = 13$ TeV*, *Phys. Rev. D* **97** (2018) 032009, arXiv: [1711.00752 \[hep-ex\]](#).
- [23] CMS Collaboration, *Searches for physics beyond the standard model with the M_{T2} variable in hadronic final states with and without disappearing tracks in proton–proton collisions at $\sqrt{s} = 13$ TeV*, *Eur. Phys. J. C* **80** (2020) 3, arXiv: [1909.03460 \[hep-ex\]](#).
- [24] CMS Collaboration, *Search for supersymmetry in proton–proton collisions at 13 TeV in final states with jets and missing transverse momentum*, *JHEP* **10** (2019) 244, arXiv: [1908.04722 \[hep-ex\]](#).
- [25] CMS Collaboration, *Search for direct top squark pair production in events with one lepton, jets, and missing transverse momentum at 13 TeV with the CMS experiment*, *JHEP* **05** (2020) 032, arXiv: [1912.08887 \[hep-ex\]](#).
- [26] CMS Collaboration, *Search for Dark Matter Particles Produced in Association with a Top Quark Pair at $\sqrt{s} = 13$ TeV*, *Phys. Rev. Lett.* **122** (2019) 011803, arXiv: [1807.06522 \[hep-ex\]](#).
- [27] ATLAS Collaboration, *Search for direct top squark pair production in final states with two leptons in $\sqrt{s} = 13$ TeV pp collisions with the ATLAS detector*, *Eur. Phys. J. C* **77** (2017) 898, arXiv: [1708.03247 \[hep-ex\]](#).
- [28] ATLAS Collaboration, *Search for dark matter produced in association with bottom or top quarks in $\sqrt{s} = 13$ TeV pp collisions with the ATLAS detector*, *Eur. Phys. J. C* **78** (2018) 18, arXiv: [1710.11412 \[hep-ex\]](#).
- [29] ATLAS Collaboration, *Object-based missing transverse momentum significance in the ATLAS Detector*, ATLAS-CONF-2018-038, 2018, URL: <https://cds.cern.ch/record/2630948>.
- [30] J. Goodman and W. Shepherd, *LHC Bounds on UV-Complete Models of Dark Matter*, 2011, arXiv: [1111.2359 \[hep-ph\]](#).
- [31] J. Alwall, P. Schuster and N. Toro, *Simplified models for a first characterization of new physics at the LHC*, *Phys. Rev. D* **79** (2009) 075020, arXiv: [0810.3921 \[hep-ph\]](#).
- [32] D. Alves et al., *Simplified models for LHC new physics searches*, *J. Phys. G* **39** (2012) 105005, arXiv: [1105.2838 \[hep-ph\]](#).
- [33] D. Abercrombie et al., *Dark Matter benchmark models for early LHC Run-2 Searches: Report of the ATLAS/CMS Dark Matter Forum*, *Phys. Dark Univ.* **26** (2019) 100371, arXiv: [1507.00966 \[hep-ex\]](#).
- [34] M. R. Buckley, D. Feld and D. Goncalves, *Scalar simplified models for dark matter*, *Phys. Rev. D* **91** (2015), arXiv: [1410.6497 \[hep-ph\]](#).
- [35] U. Haisch and E. Re, *Simplified dark matter top-quark interactions at the LHC*, *JHEP* **06** (2015) 078, arXiv: [1503.00691 \[hep-ph\]](#).
- [36] G. D’Ambrosio, G. Giudice, G. Isidori and A. Strumia, *Minimal Flavour Violation: an effective field theory approach*, *Nucl. Phys. B* **645** (2002) 155, arXiv: [hep-ph/0207036](#).
- [37] G. R. Farrar and P. Fayet, *Phenomenology of the production, decay, and detection of new hadronic states associated with supersymmetry*, *Phys. Lett. B* **76** (1978) 575.

- [38] H. Goldberg, *Constraint on the Photino Mass from Cosmology*, *Phys. Rev. Lett.* **50** (1983) 1419, Erratum: *Phys. Rev. Lett.* **103** (2009) 099905.
- [39] J. Ellis, J. Hagelin, D. V. Nanopoulos, K. A. Olive and M. Srednicki, *Supersymmetric relics from the big bang*, *Nucl. Phys. B* **238** (1984) 453.
- [40] P. Fayet, *Supersymmetry and weak, electromagnetic and strong interactions*, *Phys. Lett. B* **64** (1976) 159.
- [41] P. Fayet, *Spontaneously broken supersymmetric theories of weak, electromagnetic and strong interactions*, *Phys. Lett. B* **69** (1977) 489.
- [42] ATLAS Collaboration, *The ATLAS Experiment at the CERN Large Hadron Collider*, *JINST* **3** (2008) S08003.
- [43] ATLAS Collaboration, *ATLAS Insertable B-Layer Technical Design Report*, ATLAS-TDR-19, 2010, URL: <https://cds.cern.ch/record/1291633>, *ATLAS Insertable B-Layer Technical Design Report Addendum*, ATLAS-TDR-19-ADD-1, 2012, URL: <https://cds.cern.ch/record/1451888>.
- [44] B. Abbott et al., *Production and integration of the ATLAS Insertable B-Layer*, *JINST* **13** (2018) T05008, arXiv: [1803.00844](https://arxiv.org/abs/1803.00844) [[physics.ins-det](https://arxiv.org/archive/physics)].
- [45] ATLAS Collaboration, *Performance of the ATLAS trigger system in 2015*, *Eur. Phys. J. C* **77** (2017) 317, arXiv: [1611.09661](https://arxiv.org/abs/1611.09661) [[hep-ex](https://arxiv.org/archive/hep)].
- [46] ATLAS Collaboration, *Luminosity determination in pp collisions at $\sqrt{s} = 13$ TeV using the ATLAS detector at the LHC*, ATLAS-CONF-2019-021, 2019, URL: <https://cds.cern.ch/record/2677054>.
- [47] G. Avoni et al., *The new LUCID-2 detector for luminosity measurement and monitoring in ATLAS*, *JINST* **13** (2018) P07017.
- [48] ATLAS Collaboration, *Performance of the missing transverse momentum triggers for the ATLAS detector during Run-2 data taking*, *JHEP* **08** (2020) 080, arXiv: [2005.09554](https://arxiv.org/abs/2005.09554) [[hep-ex](https://arxiv.org/archive/hep)].
- [49] S. Agostinelli et al., *GEANT4 – a simulation toolkit*, *Nucl. Instrum. Meth. A* **506** (2003) 250.
- [50] ATLAS Collaboration, *The ATLAS Simulation Infrastructure*, *Eur. Phys. J. C* **70** (2010) 823, arXiv: [1005.4568](https://arxiv.org/abs/1005.4568) [[physics.ins-det](https://arxiv.org/archive/physics)].
- [51] ATLAS Collaboration, *Electron and photon performance measurements with the ATLAS detector using the 2015–2017 LHC proton–proton collision data*, *JINST* **14** (2019) P12006, arXiv: [1908.00005](https://arxiv.org/abs/1908.00005) [[hep-ex](https://arxiv.org/archive/hep)].
- [52] ATLAS Collaboration, *Muon reconstruction performance of the ATLAS detector in proton–proton collision data at $\sqrt{s} = 13$ TeV*, *Eur. Phys. J. C* **76** (2016) 292, arXiv: [1603.05598](https://arxiv.org/abs/1603.05598) [[hep-ex](https://arxiv.org/archive/hep)].
- [53] ATLAS Collaboration, *ATLAS b-jet identification performance and efficiency measurement with $t\bar{t}$ events in pp collisions at $\sqrt{s} = 13$ TeV*, *Eur. Phys. J. C* **79** (2019) 970, arXiv: [1907.05120](https://arxiv.org/abs/1907.05120) [[hep-ex](https://arxiv.org/archive/hep)].
- [54] J. Alwall et al., *The automated computation of tree-level and next-to-leading order differential cross sections, and their matching to parton shower simulations*, *JHEP* **07** (2014) 079, arXiv: [1405.0301](https://arxiv.org/abs/1405.0301) [[hep-ph](https://arxiv.org/archive/hep)].
- [55] T. Sjöstrand et al., *An introduction to PYTHIA 8.2*, *Comput. Phys. Commun.* **191** (2015) 159, arXiv: [1410.3012](https://arxiv.org/abs/1410.3012) [[hep-ph](https://arxiv.org/archive/hep)].

- [56] P. Artoisenet, R. Frederix, O. Mattelaer and R. Rietkerk, *Automatic spin-entangled decays of heavy resonances in Monte Carlo simulations*, *JHEP* **03** (2013) 015, arXiv: [1212.3460 \[hep-ph\]](#).
- [57] W. Beenakker, C. Borschensky, M. Krämer, A. Kulesza and E. Laenen, *NNLL-fast: predictions for coloured supersymmetric particle production at the LHC with threshold and Coulomb resummation*, *JHEP* **12** (2016) 133, arXiv: [1607.07741 \[hep-ph\]](#).
- [58] W. Beenakker et al., *NNLL Resummation for Squark-Antisquark and Gluino-Pair Production at the LHC*, *JHEP* **12** (2014) 023, arXiv: [1404.3134 \[hep-ph\]](#).
- [59] W. Beenakker et al., *Towards NNLL resummation: hard matching coefficients for squark and gluino hadroproduction*, *JHEP* **10** (2013) 120, arXiv: [1304.6354 \[hep-ph\]](#).
- [60] W. Beenakker et al., *NNLL resummation for squark-antisquark pair production at the LHC*, *JHEP* **01** (2012) 076, arXiv: [1110.2446 \[hep-ph\]](#).
- [61] W. Beenakker et al., *Soft-gluon resummation for squark and gluino hadroproduction*, *JHEP* **12** (2009) 041, arXiv: [0909.4418 \[hep-ph\]](#).
- [62] A. Kulesza and L. Motyka, *Soft gluon resummation for the production of gluino-gluino and squark-antisquark pairs at the LHC*, *Phys. Rev. D* **80** (2009) 095004, arXiv: [0905.4749 \[hep-ph\]](#).
- [63] A. Kulesza and L. Motyka, *Threshold Resummation for Squark-Antisquark and Gluino-Pair Production at the LHC*, *Phys. Rev. Lett.* **102** (2009) 111802, arXiv: [0807.2405 \[hep-ph\]](#).
- [64] W. Beenakker, R. Höpker, M. Spira and P. Zerwas, *Squark and gluino production at hadron colliders*, *Nucl. Phys. B* **492** (1997) 51, arXiv: [hep-ph/9610490](#).
- [65] J. Butterworth et al., *PDF4LHC recommendations for LHC Run II*, *J. Phys. G* **43** (2016) 023001, arXiv: [1510.03865 \[hep-ph\]](#).
- [66] L. Lönnblad and S. Prestel, *Merging multi-leg NLO matrix elements with parton showers*, *JHEP* **03** (2013) 166, arXiv: [1211.7278 \[hep-ph\]](#).
- [67] ATLAS Collaboration, *ATLAS Pythia 8 tunes to 7 TeV data*, ATL-PHYS-PUB-2014-021, 2014, URL: <https://cds.cern.ch/record/1966419>.
- [68] R. D. Ball et al., *Parton distributions with LHC data*, *Nucl. Phys. B* **867** (2013) 244, arXiv: [1207.1303 \[hep-ph\]](#).
- [69] O. Mattelaer and E. Vryonidou, *Dark matter production through loop-induced processes at the LHC: the s-channel mediator case*, *Eur. Phys. J. C* **75** (2015) 436, arXiv: [1508.00564 \[hep-ph\]](#).
- [70] M. Backović et al., *Higher-order QCD predictions for dark matter production at the LHC in simplified models with s-channel mediators*, *Eur. Phys. J. C* **75** (2015) 482, arXiv: [1508.05327 \[hep-ph\]](#).
- [71] T. Sjöstrand, S. Mrenna and P. Z. Skands, *A brief introduction to PYTHIA 8.1*, *Comput. Phys. Commun.* **178** (2008) 852, arXiv: [0710.3820 \[hep-ph\]](#).
- [72] D. J. Lange, *The EvtGen particle decay simulation package*, *Nucl. Instrum. Meth. A* **462** (2001) 152.
- [73] ATLAS Collaboration, *The Pythia 8 A3 tune description of ATLAS minimum bias and inelastic measurements incorporating the Donnachie–Landshoff diffractive model*, ATL-PHYS-PUB-2016-017, 2016, URL: <https://cds.cern.ch/record/2206965>.
- [74] S. Frixione, P. Nason and C. Oleari, *Matching NLO QCD computations with parton shower simulations: the POWHEG method*, *JHEP* **11** (2007) 070, arXiv: [0709.2092 \[hep-ph\]](#).

- [75] S. Alioli, P. Nason, C. Oleari and E. Re, *A general framework for implementing NLO calculations in shower Monte Carlo programs: the POWHEG BOX*, *JHEP* **06** (2010) 043, arXiv: [1002.2581 \[hep-ph\]](#).
- [76] P. Nason, *A new method for combining NLO QCD with shower Monte Carlo algorithms*, *JHEP* **11** (2004) 040, arXiv: [hep-ph/0409146](#).
- [77] M. Czakon and A. Mitov, *Top++: A program for the calculation of the top-pair cross-section at hadron colliders*, *Comput. Phys. Commun.* **185** (2014) 2930, arXiv: [1112.5675 \[hep-ph\]](#).
- [78] R. D. Ball et al., *Parton distributions for the LHC run II*, *JHEP* **04** (2015) 040, arXiv: [1410.8849 \[hep-ph\]](#).
- [79] ATLAS Collaboration, *Modelling of the $t\bar{t}H$ and $t\bar{t}V$ ($V = W, Z$) processes for $\sqrt{s} = 13$ TeV ATLAS analyses*, ATL-PHYS-PUB-2016-005, 2016, URL: <https://cds.cern.ch/record/2120826>.
- [80] R. Frederix, E. Re and P. Torrielli, *Single-top t -channel hadroproduction in the four-flavour scheme with POWHEG and aMC@NLO*, *JHEP* **09** (2012) 130, arXiv: [1207.5391 \[hep-ph\]](#).
- [81] S. Alioli, P. Nason, C. Oleari and E. Re, *NLO single-top production matched with shower in POWHEG: s - and t -channel contributions*, *JHEP* **09** (2009) 111, arXiv: [0907.4076 \[hep-ph\]](#).
- [82] M. Aliev et al., *HATHOR - HAdronic Top and Heavy quarks crOss section calculatoR*, *Comput. Phys. Commun.* **182** (2011) 1034, arXiv: [1007.1327 \[hep-ph\]](#).
- [83] P. Kant et al., *HATHOR for single top-quark production: Updated predictions and uncertainty estimates for single top-quark production in hadronic collisions*, *Comput. Phys. Commun.* **191** (2015) 74, arXiv: [1406.4403 \[hep-ph\]](#).
- [84] N. Kidonakis, *Next-to-next-to-leading-order collinear and soft gluon corrections for t -channel single top quark production*, *Phys. Rev. D* **83** (2011) 091503, arXiv: [1103.2792 \[hep-ph\]](#).
- [85] N. Kidonakis, *Two-loop soft anomalous dimensions for single top quark associated production with a W - or H -*, *Phys. Rev. D* **82** (2010) 054018, arXiv: [1005.4451 \[hep-ph\]](#).
- [86] N. Kidonakis, *NNLL resummation for s -channel single top quark production*, *Phys. Rev. D* **81** (2010) 054028, arXiv: [1001.5034 \[hep-ph\]](#).
- [87] T. Gleisberg et al., *Event generation with SHERPA 1.1*, *JHEP* **02** (2009) 007, arXiv: [0811.4622 \[hep-ph\]](#).
- [88] ATLAS Collaboration, *Monte Carlo Generators for the Production of a W or Z/γ^* Boson in Association with Jets at ATLAS in Run 2*, ATL-PHYS-PUB-2016-003, 2016, URL: <https://cds.cern.ch/record/2120133>.
- [89] R. Gavin, Y. Li, F. Petriello and S. Quackenbush, *FEWZ 2.0: A code for hadronic Z production at next-to-next-to-leading order*, *Comput. Phys. Commun.* **182** (2011) 2388.
- [90] ATLAS Collaboration, *Multi-Boson Simulation for 13 TeV ATLAS Analyses*, ATL-PHYS-PUB-2017-005, 2017, URL: <https://cds.cern.ch/record/2261933>.
- [91] H. B. Hartanto, B. Jager, L. Reina and D. Wackerroth, *Higgs boson production in association with top quarks in the POWHEG BOX*, *Phys. Rev. D* **91** (2015) 094003, arXiv: [1501.04498 \[hep-ph\]](#).
- [92] ATLAS Collaboration, *Topological cell clustering in the ATLAS calorimeters and its performance in LHC Run 1*, *Eur. Phys. J. C* **77** (2017) 490, arXiv: [1603.02934 \[hep-ex\]](#).
- [93] M. Cacciari, G. P. Salam and G. Soyez, *The anti- k_t jet clustering algorithm*, *JHEP* **04** (2008) 063, arXiv: [0802.1189 \[hep-ph\]](#).

- [94] M. Cacciari, G. P. Salam and G. Soyez, *FastJet user manual*, *Eur. Phys. J. C* **72** (2012) 1896, arXiv: [1111.6097 \[hep-ph\]](#).
- [95] ATLAS Collaboration, *Jet energy scale measurements and their systematic uncertainties in proton–proton collisions at $\sqrt{s} = 13$ TeV with the ATLAS detector*, *Phys. Rev. D* **96** (2017) 072002, arXiv: [1703.09665 \[hep-ex\]](#).
- [96] ATLAS Collaboration, *Tagging and suppression of pileup jets with the ATLAS detector*, ATLAS-CONF-2014-018, 2014, URL: <https://cds.cern.ch/record/1700870>.
- [97] ATLAS Collaboration, *Selection of jets produced in 13 TeV proton–proton collisions with the ATLAS detector*, ATLAS-CONF-2015-029, 2015, URL: <https://cds.cern.ch/record/2037702>.
- [98] ATLAS Collaboration, *Performance of pile-up mitigation techniques for jets in pp collisions at $\sqrt{s} = 8$ TeV using the ATLAS detector*, *Eur. Phys. J. C* **76** (2016) 581, arXiv: [1510.03823 \[hep-ex\]](#).
- [99] ATLAS Collaboration, *Performance of missing transverse momentum reconstruction with the ATLAS detector using proton–proton collisions at $\sqrt{s} = 13$ TeV*, *Eur. Phys. J. C* **78** (2018) 903, arXiv: [1802.08168 \[hep-ex\]](#).
- [100] C. G. Lester and D. J. Summers, *Measuring masses of semi-invisibly decaying particles pair produced at hadron colliders*, *Phys. Lett. B* **463** (1999) 99, arXiv: [hep-ph/9906349](#).
- [101] A. Barr, C. G. Lester and P. Stephens, *A variable for measuring masses at hadron colliders when missing energy is expected; m_{T2} : the truth behind the glamour*, *J. Phys. G* **29** (2003) 2343, arXiv: [hep-ph/0304226](#).
- [102] W. S. Cho, K. Choi, Y. G. Kim and C. B. Park, *Measuring superparticle masses at hadron collider using the transverse mass kink*, *JHEP* **02** (2008) 035, arXiv: [0711.4526 \[hep-ph\]](#).
- [103] M. Burns, K. Kong, K. T. Matchev and M. Park, *Using subsystem M_{T2} for complete mass determinations in decay chains with missing energy at hadron colliders*, *JHEP* **03** (2009) 143, arXiv: [0810.5576 \[hep-ph\]](#).
- [104] M. R. Buckley, J. D. Lykken, C. Rogan and M. Spiropulu, *Super-razor and searches for sleptons and charginos at the LHC*, *Phys. Rev. D* **89** (2014) 055020, arXiv: [1310.4827 \[hep-ph\]](#).
- [105] G. Cowan, K. Cranmer, E. Gross and O. Vitells, *Asymptotic formulae for likelihood-based tests of new physics*, *Eur. Phys. J. C* **71** (2011) 1554, arXiv: [1007.1727 \[physics.data-an\]](#), Erratum: *Eur. Phys. J. C* **73** (2013) 2501.
- [106] M. Baak et al., *HistFitter software framework for statistical data analysis*, *Eur. Phys. J. C* **75** (2015) 153, arXiv: [1410.1280 \[hep-ex\]](#).
- [107] L. Heinrich, M. Feickert and G. Stark, *pyhf*, version 0.4.4, URL: <https://github.com/scikit-hep/pyhf>.
- [108] ATLAS Collaboration, *Measurement of the WW cross section in $\sqrt{s} = 7$ TeV pp collisions with ATLAS*, *Phys. Rev. Lett.* **107** (2011) 041802, arXiv: [1104.5225 \[hep-ex\]](#).
- [109] ATLAS Collaboration, *Search for anomalous production of prompt same-sign lepton pairs and pair-produced doubly charged Higgs bosons with $\sqrt{s} = 8$ TeV pp collisions using the ATLAS detector*, *JHEP* **03** (2015) 041, arXiv: [1412.0237 \[hep-ex\]](#).
- [110] CMS Collaboration, *Search for charged Higgs bosons with the $H^\pm \rightarrow \tau^\pm \nu_\tau$ decay channel in proton-proton collisions at $\sqrt{s} = 13$ TeV*, *JHEP* **07** (2019) 142, arXiv: [1903.04560 \[hep-ex\]](#).

- [111] CMS Collaboration, *Search for singly produced third-generation leptoquarks decaying to a τ lepton and a b quark in proton-proton collisions at $\sqrt{s} = 13$ TeV*, *JHEP* **07** (2018) 115, arXiv: [1806.03472 \[hep-ex\]](#).
- [112] ATLAS Collaboration, *Jet Calibration and Systematic Uncertainties for Jets Reconstructed in the ATLAS Detector at $\sqrt{s} = 13$ TeV*, ATL-PHYS-PUB-2015-015, 2015, URL: <https://cds.cern.ch/record/2037613>.
- [113] ATLAS Collaboration, *Calibration of b -tagging using dileptonic top pair events in a combinatorial likelihood approach with the ATLAS experiment*, ATLAS-CONF-2014-004, 2014, URL: <https://cds.cern.ch/record/1664335>.
- [114] ATLAS Collaboration, *Calibration of the performance of b -tagging for c and light-flavour jets in the 2012 ATLAS data*, ATLAS-CONF-2014-046, 2014, URL: <https://cds.cern.ch/record/1741020>.
- [115] ATLAS Collaboration, *Expected performance of missing transverse momentum reconstruction for the ATLAS detector at $\sqrt{s} = 13$ TeV*, ATL-PHYS-PUB-2015-023, 2015, URL: <https://cds.cern.ch/record/2037700>.
- [116] ATLAS Collaboration, *Performance of electron and photon triggers in ATLAS during LHC Run 2*, *Eur. Phys. J. C* **80** (2020) 47, arXiv: [1909.00761 \[hep-ex\]](#).
- [117] ATLAS Collaboration, *Performance of the ATLAS muon triggers in Run 2*, arXiv e-prints, arXiv:2004.13447 (2020) arXiv:2004.13447, arXiv: [2004.13447 \[hep-ex\]](#).
- [118] ATLAS Collaboration, *Simulation of top-quark production for the ATLAS experiment at $\sqrt{s} = 13$ TeV*, ATL-PHYS-PUB-2016-004, 2016, URL: <https://cds.cern.ch/record/2120417>.
- [119] ATLAS Collaboration, *Improvements in $t\bar{t}$ modelling using NLO+PS Monte Carlo generators for Run 2*, ATL-PHYS-PUB-2018-009, 2018, URL: <https://cds.cern.ch/record/2630327>.
- [120] ATLAS Collaboration, *Modelling of the $t\bar{t}H$ and $t\bar{t}V$ ($V = W, Z$) processes for $\sqrt{s} = 13$ TeV ATLAS analyses*, ATL-PHYS-PUB-2015-022, 2016, URL: <http://cds.cern.ch/record/2120826>.
- [121] ATLAS Collaboration, *Measurement of the $t\bar{t}Z$ and $t\bar{t}W$ cross sections in proton-proton collisions at $\sqrt{s} = 13$ TeV with the ATLAS detector*, *Phys. Rev. D* **99** (2019) 072009, arXiv: [1901.03584 \[hep-ex\]](#).
- [122] S. Frixione, E. Laenen, P. Motylinski, C. White and B. R. Webber, *Single-top hadroproduction in association with a W boson*, *JHEP* **07** (2008) 029, arXiv: [0805.3067 \[hep-ph\]](#).
- [123] O. Bessidskaia Bylund, ‘Modelling Wt and tWZ production at NLO for ATLAS analyses’, *9th International Workshop on Top Quark Physics*, 2016, arXiv: [1612.00440 \[hep-ph\]](#).
- [124] C. Borschensky et al., *Squark and gluino production cross sections in pp collisions at $\sqrt{s} = 13, 14, 33$ and 100 TeV*, *Eur. Phys. J. C* **74** (2014) 3174, arXiv: [1407.5066 \[hep-ph\]](#).
- [125] R. D. Cousins, J. T. Linnemann and J. Tucker, *Evaluation of three methods for calculating statistical significance when incorporating a systematic uncertainty into a test of the background-only hypothesis for a Poisson process*, *Nucl. Instrum. Meth. A* **595** (2008) 480, arXiv: [physics/0702156 \[physics.data-an\]](#).
- [126] A. L. Read, *Presentation of search results: the CL_s technique*, *J. Phys. G* **28** (2002) 2693.
- [127] ATLAS Collaboration, *ATLAS Computing Acknowledgements*, ATL-SOFT-PUB-2020-001, URL: <https://cds.cern.ch/record/2717821>.

The ATLAS Collaboration

G. Aad¹⁰², B. Abbott¹²⁸, D.C. Abbott¹⁰³, A. Abed Abud³⁶, K. Abeling⁵³, D.K. Abhayasinghe⁹⁴, S.H. Abidi¹⁶⁷, O.S. AbouZeid⁴⁰, N.L. Abraham¹⁵⁶, H. Abramowicz¹⁶¹, H. Abreu¹⁶⁰, Y. Abulaiti⁶, B.S. Acharya^{67a,67b,o}, B. Achkar⁵³, L. Adam¹⁰⁰, C. Adam Bourdarios⁵, L. Adamczyk^{84a}, L. Adamek¹⁶⁷, J. Adelman¹²¹, A. Adiguzel^{12c,ad}, S. Adorni⁵⁴, T. Adye¹⁴³, A.A. Affolder¹⁴⁵, Y. Afik¹⁶⁰, C. Agapopoulou⁶⁵, M.N. Agaras³⁸, A. Aggarwal¹¹⁹, C. Agheorghiesei^{27c}, J.A. Aguilar-Saavedra^{139f,139a,ac}, A. Ahmad³⁶, F. Ahmadov⁸⁰, W.S. Ahmed¹⁰⁴, X. Ai¹⁸, G. Aielli^{74a,74b}, S. Akatsuka⁸⁶, M. Akbiyik¹⁰⁰, T.P.A. Åkesson⁹⁷, E. Akilli⁵⁴, A.V. Akimov¹¹¹, K. Al Houry⁶⁵, G.L. Alberghi^{23b,23a}, J. Albert¹⁷⁶, M.J. Alconada Verzini¹⁶¹, S. Alderweireldt³⁶, M. Aleksa³⁶, I.N. Aleksandrov⁸⁰, C. Alexa^{27b}, T. Alexopoulos¹⁰, A. Alfonsi¹²⁰, F. Alfonsi^{23b,23a}, M. Alhroob¹²⁸, B. Ali¹⁴¹, S. Ali¹⁵⁸, M. Aliev¹⁶⁶, G. Alimonti^{69a}, C. Allaire³⁶, B.M.M. Allbrooke¹⁵⁶, B.W. Allen¹³¹, P.P. Allport²¹, A. Aloisio^{70a,70b}, F. Alonso⁸⁹, C. Alpigiani¹⁴⁸, E. Alunno Camelia^{74a,74b}, M. Alvarez Estevez⁹⁹, M.G. Alvigi^{70a,70b}, Y. Amaral Coutinho^{81b}, A. Ambler¹⁰⁴, L. Ambroz¹³⁴, C. Amelung³⁶, D. Amidei¹⁰⁶, S.P. Amor Dos Santos^{139a}, S. Amoroso⁴⁶, C.S. Amrouche⁵⁴, F. An⁷⁹, C. Anastopoulos¹⁴⁹, N. Andari¹⁴⁴, T. Andeen¹¹, J.K. Anders²⁰, S.Y. Andreev^{45a,45b}, A. Andreazza^{69a,69b}, V. Andrei^{61a}, C.R. Anelli¹⁷⁶, S. Angelidakis⁹, A. Angerami³⁹, A.V. Anisenkov^{122b,122a}, A. Annovi^{72a}, C. Antel⁵⁴, M.T. Anthony¹⁴⁹, E. Antipov¹²⁹, M. Antonelli⁵¹, D.J.A. Antrim¹⁸, F. Anulli^{73a}, M. Aoki⁸², J.A. Aparisi Pozo¹⁷⁴, M.A. Aparo¹⁵⁶, L. Aperio Bella⁴⁶, N. Aranzabal³⁶, V. Araujo Ferraz^{81a}, R. Araujo Pereira^{81b}, C. Arcangeletti⁵¹, A.T.H. Arce⁴⁹, J-F. Arguin¹¹⁰, S. Argyropoulos⁵², J.-H. Arling⁴⁶, A.J. Armbruster³⁶, A. Armstrong¹⁷¹, O. Arnaez¹⁶⁷, H. Arnold¹²⁰, Z.P. Arrubarrena Tame¹¹⁴, G. Artoni¹³⁴, H. Asada¹¹⁷, K. Asai¹²⁶, S. Asai¹⁶³, T. Asawatavonvanich¹⁶⁵, N. Asbah⁵⁹, E.M. Asimakopoulou¹⁷², L. Asquith¹⁵⁶, J. Assahsah^{35e}, K. Assamagan²⁹, R. Astalos^{28a}, R.J. Atkin^{33a}, M. Atkinson¹⁷³, N.B. Atlay¹⁹, H. Atmani⁶⁵, P.A. Atmasiddha¹⁰⁶, K. Augsten¹⁴¹, V.A. Austrup¹⁸², G. Avolio³⁶, M.K. Ayoub^{15a}, G. Azuelos^{110,ak}, D. Babal^{28a}, H. Bachacou¹⁴⁴, K. Bachas¹⁶², F. Backman^{45a,45b}, P. Bagnaia^{73a,73b}, M. Bahmani⁸⁵, H. Bahrasemani¹⁵², A.J. Bailey¹⁷⁴, V.R. Bailey¹⁷³, J.T. Baines¹⁴³, C. Bakalis¹⁰, O.K. Baker¹⁸³, P.J. Bakker¹²⁰, E. Bakos¹⁶, D. Bakshi Gupta⁸, S. Balaji¹⁵⁷, R. Balasubramanian¹²⁰, E.M. Baldin^{122b,122a}, P. Balek¹⁸⁰, F. Balli¹⁴⁴, W.K. Balunas¹³⁴, J. Balz¹⁰⁰, E. Banas⁸⁵, M. Bandieramonte¹³⁸, A. Bandyopadhyay¹⁹, Sw. Banerjee^{181j}, L. Barak¹⁶¹, W.M. Barbe³⁸, E.L. Barberio¹⁰⁵, D. Barberis^{55b,55a}, M. Barbero¹⁰², G. Barbour⁹⁵, T. Barillari¹¹⁵, M-S. Barisits³⁶, J. Barkeloo¹³¹, T. Barklow¹⁵³, R. Barnea¹⁶⁰, B.M. Barnett¹⁴³, R.M. Barnett¹⁸, Z. Barnovska-Blenessy^{60a}, A. Baroncelli^{60a}, G. Barone²⁹, A.J. Barr¹³⁴, L. Barranco Navarro^{45a,45b}, F. Barreiro⁹⁹, J. Barreiro Guimarães da Costa^{15a}, U. Barron¹⁶¹, S. Barsov¹³⁷, F. Bartels^{61a}, R. Bartoldus¹⁵³, G. Bartolini¹⁰², A.E. Barton⁹⁰, P. Bartos^{28a}, A. Basalae⁴⁶, A. Basan¹⁰⁰, A. Bassalat^{65,ah}, M.J. Basso¹⁶⁷, R.L. Bates⁵⁷, S. Batlamous^{35f}, J.R. Batley³², B. Batool¹⁵¹, M. Battaglia¹⁴⁵, M. Baue^{73a,73b}, F. Bauer^{144,*}, P. Bauer²⁴, H.S. Bawa³¹, A. Bayirli^{12c}, J.B. Beacham⁴⁹, T. Beau¹³⁵, P.H. Beauchemin¹⁷⁰, F. Becherer⁵², P. Bechtel²⁴, H.C. Beck⁵³, H.P. Beck^{20,q}, K. Becker¹⁷⁸, C. Becot⁴⁶, A. Beddall^{12d}, A.J. Beddall^{12a}, V.A. Bednyakov⁸⁰, M. Bedognetti¹²⁰, C.P. Bee¹⁵⁵, T.A. Beermann¹⁸², M. Begalli^{81b}, M. Begel²⁹, A. Behera¹⁵⁵, J.K. Behr⁴⁶, F. Beisiegel²⁴, M. Belfkir⁵, A.S. Bell⁹⁵, G. Bella¹⁶¹, L. Bellagamba^{23b}, A. Bellerive³⁴, P. Bellos⁹, K. Beloborodov^{122b,122a}, K. Belotskiy¹¹², N.L. Belyaev¹¹², D. Benchekroun^{35a}, N. Benekos¹⁰, Y. Benhammou¹⁶¹, D.P. Benjamin⁶, M. Benoit²⁹, J.R. Bensinger²⁶, S. Bentvelsen¹²⁰, L. Beresford¹³⁴, M. Beretta⁵¹, D. Berge¹⁹, E. Bergeaas Kuutmann¹⁷², N. Berger⁵, B. Bergmann¹⁴¹, L.J. Bergsten²⁶, J. Beringer¹⁸, S. Berlendis⁷, G. Bernardi¹³⁵, C. Bernius¹⁵³, F.U. Bernlochner²⁴, T. Berry⁹⁴, P. Berta¹⁰⁰, A. Berthold⁴⁸, I.A. Bertram⁹⁰, O. Bessidskaia Bylund¹⁸², N. Besson¹⁴⁴, S. Bethke¹¹⁵, A. Betti⁴², A.J. Bevan⁹³, J. Beyer¹¹⁵, S. Bhatta¹⁵⁵, D.S. Bhattacharya¹⁷⁷, P. Bhattarai²⁶, V.S. Bhopatkar⁶, R. Bi¹³⁸, R.M. Bianchi¹³⁸, O. Biebel¹¹⁴, D. Biedermann¹⁹, R. Bielski³⁶, K. Bierwagen¹⁰⁰, N.V. Biesuz^{72a,72b}, M. Biglietti^{75a}, T.R.V. Billoud¹⁴¹, M. Bindi⁵³, A. Bingul^{12d},

C. Bini^{73a,73b}, S. Biondi^{23b,23a}, C.J. Birch-sykes¹⁰¹, M. Birman¹⁸⁰, T. Bisanz³⁶, J.P. Biswal³, D. Biswas^{181j}, A. Bitadze¹⁰¹, C. Bittrich⁴⁸, K. Bjørke¹³³, T. Blazek^{28a}, I. Bloch⁴⁶, C. Blocker²⁶, A. Blue⁵⁷, U. Blumenschein⁹³, G.J. Bobbink¹²⁰, V.S. Bobrovnikov^{122b,122a}, S.S. Bocchetta⁹⁷, D. Bogavac¹⁴, A.G. Bogdanchikov^{122b,122a}, C. Bohm^{45a}, V. Boisvert⁹⁴, P. Bokan^{172,53}, T. Bold^{84a}, A.E. Bolz^{61b}, M. Bomben¹³⁵, M. Bona⁹³, J.S. Bonilla¹³¹, M. Boonekamp¹⁴⁴, C.D. Booth⁹⁴, A.G. Borbély⁵⁷, H.M. Borecka-Bielska⁹¹, L.S. Borgna⁹⁵, A. Borisov¹²³, G. Borissov⁹⁰, D. Bortoletto¹³⁴, D. Boscherini^{23b}, M. Bosman¹⁴, J.D. Bossio Sola¹⁰⁴, K. Bouaouda^{35a}, J. Boudreau¹³⁸, E.V. Bouhova-Thacker⁹⁰, D. Boumediene³⁸, A. Boveia¹²⁷, J. Boyd³⁶, D. Boye^{33c}, I.R. Boyko⁸⁰, A.J. Bozson⁹⁴, J. Bracnik²¹, N. Brahim^{60d,60c}, G. Brandt¹⁸², O. Brandt³², F. Braren⁴⁶, B. Brau¹⁰³, J.E. Brau¹³¹, W.D. Breaden Madden⁵⁷, K. Brendlinger⁴⁶, R. Brenner¹⁶⁰, L. Brenner³⁶, R. Brenner¹⁷², S. Bressler¹⁸⁰, B. Brickwedde¹⁰⁰, D.L. Briglin²¹, D. Britton⁵⁷, D. Britzger¹¹⁵, I. Brock²⁴, R. Brock¹⁰⁷, G. Brooijmans³⁹, W.K. Brooks^{146d}, E. Brost²⁹, P.A. Bruckman de Renstrom⁸⁵, B. Brüers⁴⁶, D. Bruncko^{28b}, A. Bruni^{23b}, G. Bruni^{23b}, M. Bruschi^{23b}, N. Brusino^{73a,73b}, L. Bryngemark¹⁵³, T. Buanes¹⁷, Q. Buat¹⁵⁵, P. Buchholz¹⁵¹, A.G. Buckley⁵⁷, I.A. Budagov⁸⁰, M.K. Bugge¹³³, O. Bulekov¹¹², B.A. Bullard⁵⁹, T.J. Burch¹²¹, S. Burdin⁹¹, C.D. Burgard¹²⁰, A.M. Burger¹²⁹, B. Burghgrave⁸, J.T.P. Burr⁴⁶, C.D. Burton¹¹, J.C. Burzynski¹⁰³, V. Büscher¹⁰⁰, E. Buschmann⁵³, P.J. Bussey⁵⁷, J.M. Butler²⁵, C.M. Buttar⁵⁷, J.M. Butterworth⁹⁵, P. Butti³⁶, W. Buttinger¹⁴³, C.J. Buxo Vazquez¹⁰⁷, A. Buzatu¹⁵⁸, A.R. Buzykaev^{122b,122a}, G. Cabras^{23b,23a}, S. Cabrera Urbán¹⁷⁴, D. Caforio⁵⁶, H. Cai¹³⁸, V.M.M. Cairo¹⁵³, O. Cakir^{4a}, N. Calace³⁶, P. Calafiura¹⁸, G. Calderini¹³⁵, P. Calfayan⁶⁶, G. Callea⁵⁷, L.P. Caloba^{81b}, A. Caltabiano^{74a,74b}, S. Calvente Lopez⁹⁹, D. Calvet³⁸, S. Calvet³⁸, T.P. Calvet¹⁰², M. Calvetti^{72a,72b}, R. Camacho Toro¹³⁵, S. Camarda³⁶, D. Camarero Munoz⁹⁹, P. Camarri^{74a,74b}, M.T. Camerlingo^{75a,75b}, D. Cameron¹³³, C. Camincher³⁶, S. Campana³⁶, M. Campanelli⁹⁵, A. Camplani⁴⁰, V. Canale^{70a,70b}, A. Canesse¹⁰⁴, M. Cano Bret⁷⁸, J. Cantero¹²⁹, T. Cao¹⁶¹, Y. Cao¹⁷³, M. Capua^{41b,41a}, R. Cardarelli^{74a}, F. Cardillo¹⁷⁴, G. Carducci^{41b,41a}, I. Carli¹⁴², T. Carli³⁶, G. Carlino^{70a}, B.T. Carlson¹³⁸, E.M. Carlson^{176,168a}, L. Carminati^{69a,69b}, R.M.D. Carney¹⁵³, S. Caron¹¹⁹, E. Carquin^{146d}, S. Carrá⁴⁶, G. Carratta^{23b,23a}, J.W.S. Carter¹⁶⁷, T.M. Carter⁵⁰, M.P. Casado^{14g}, A.F. Casha¹⁶⁷, E.G. Castiglia¹⁸³, F.L. Castillo¹⁷⁴, L. Castillo Garcia¹⁴, V. Castillo Gimenez¹⁷⁴, N.F. Castro^{139a,139e}, A. Catinaccio³⁶, J.R. Catmore¹³³, A. Cattai³⁶, V. Cavaliere²⁹, V. Cavasinni^{72a,72b}, E. Celebi^{12b}, F. Celli¹³⁴, K. Cerny¹³⁰, A.S. Cerqueira^{81a}, A. Cerri¹⁵⁶, L. Cerrito^{74a,74b}, F. Cerutti¹⁸, A. Cervelli^{23b,23a}, S.A. Cetin^{12b}, Z. Chadi^{35a}, D. Chakraborty¹²¹, J. Chan¹⁸¹, W.S. Chan¹²⁰, W.Y. Chan⁹¹, J.D. Chapman³², B. Chargeishvili^{159b}, D.G. Charlton²¹, T.P. Charman⁹³, M. Chatterjee²⁰, C.C. Chau³⁴, S. Che¹²⁷, S. Chekanov⁶, S.V. Chekulaev^{168a}, G.A. Chelkov^{80,af}, B. Chen⁷⁹, C. Chen^{60a}, C.H. Chen⁷⁹, H. Chen^{15c}, H. Chen²⁹, J. Chen^{60a}, J. Chen³⁹, J. Chen²⁶, S. Chen¹³⁶, S.J. Chen^{15c}, X. Chen^{15b}, Y. Chen^{60a}, Y-H. Chen⁴⁶, H.C. Cheng^{63a}, H.J. Cheng^{15a}, A. Cheplakov⁸⁰, E. Cheremushkina¹²³, R. Cherkaoui El Moursli^{35f}, E. Cheu⁷, K. Cheung⁶⁴, T.J.A. Chevalérias¹⁴⁴, L. Chevalier¹⁴⁴, V. Chiarella⁵¹, G. Chiarelli^{72a}, G. Chiodini^{68a}, A.S. Chisholm²¹, A. Chitan^{27b}, I. Chiu¹⁶³, Y.H. Chiu¹⁷⁶, M.V. Chizhov⁸⁰, K. Choi¹¹, A.R. Chomont^{73a,73b}, Y. Chou¹⁰³, Y.S. Chow¹²⁰, L.D. Christopher^{33e}, M.C. Chu^{63a}, X. Chu^{15a,15d}, J. Chudoba¹⁴⁰, J.J. Chwastowski⁸⁵, L. Chytka¹³⁰, D. Cieri¹¹⁵, K.M. Ciesla⁸⁵, V. Cindro⁹², I.A. Cioară^{27b}, A. Ciocio¹⁸, F. Ciroto^{70a,70b}, Z.H. Citron^{180,k}, M. Citterio^{69a}, D.A. Ciubotaru^{27b}, B.M. Ciungu¹⁶⁷, A. Clark⁵⁴, P.J. Clark⁵⁰, S.E. Clawson¹⁰¹, C. Clement^{45a,45b}, L. Clissa^{23b,23a}, Y. Coadou¹⁰², M. Cobal^{67a,67c}, A. Coccaro^{55b}, J. Cochran⁷⁹, R. Coelho Lopes De Sa¹⁰³, H. Cohen¹⁶¹, A.E.C. Coimbra³⁶, B. Cole³⁹, A.P. Colijn¹²⁰, J. Collot⁵⁸, P. Conde Muiño^{139a,139h}, S.H. Connell^{33c}, I.A. Connelly⁵⁷, S. Constantinescu^{27b}, F. Conventi^{70a,al}, A.M. Cooper-Sarkar¹³⁴, F. Cormier¹⁷⁵, K.J.R. Cormier¹⁶⁷, L.D. Corpe⁹⁵, M. Corradi^{73a,73b}, E.E. Corrigan⁹⁷, F. Corriveau^{104,aa}, M.J. Costa¹⁷⁴, F. Costanza⁵, D. Costanzo¹⁴⁹, G. Cowan⁹⁴, J.W. Cowley³², J. Crane¹⁰¹, K. Cranmer¹²⁵, R.A. Creager¹³⁶, S. Crépe-Renaudin⁵⁸, F. Crescioli¹³⁵, M. Cristinziani²⁴, V. Croft¹⁷⁰, G. Crosetti^{41b,41a}, A. Cueto⁵, T. Cuhadar Donszelmann¹⁷¹, H. Cui^{15a,15d}, A.R. Cukierman¹⁵³, W.R. Cunningham⁵⁷, S. Czekierda⁸⁵,

P. Czodrowski³⁶, M.M. Czurylo^{61b}, M.J. Da Cunha Sargedas De Sousa^{60b}, J.V. Da Fonseca Pinto^{81b},
 C. Da Via¹⁰¹, W. Dabrowski^{84a}, F. Dachs³⁶, T. Dado⁴⁷, S. Dahbi^{33e}, T. Dai¹⁰⁶, C. Dallapiccola¹⁰³,
 M. Dam⁴⁰, G. D'amen²⁹, V. D'Amico^{75a,75b}, J. Damp¹⁰⁰, J.R. Dandoy¹³⁶, M.F. Daneri³⁰, M. Danninger¹⁵²,
 V. Dao³⁶, G. Darbo^{55b}, O. Dartsis⁵, A. Dattagupta¹³¹, T. Daubney⁴⁶, S. D'Auria^{69a,69b}, C. David^{168b},
 T. Davidek¹⁴², D.R. Davis⁴⁹, I. Dawson¹⁴⁹, K. De⁸, R. De Asmundis^{70a}, M. De Beurs¹²⁰,
 S. De Castro^{23b,23a}, N. De Groot¹¹⁹, P. de Jong¹²⁰, H. De la Torre¹⁰⁷, A. De Maria^{15c}, D. De Pedis^{73a},
 A. De Salvo^{73a}, U. De Sanctis^{74a,74b}, M. De Santis^{74a,74b}, A. De Santo¹⁵⁶, J.B. De Vivie De Regie⁶⁵,
 D.V. Dedovich⁸⁰, A.M. Deiana⁴², J. Del Peso⁹⁹, Y. Delabat Diaz⁴⁶, D. Delgove⁶⁵, F. Deliot¹⁴⁴,
 C.M. Delitzsch⁷, M. Della Pietra^{70a,70b}, D. Della Volpe⁵⁴, A. Dell'Acqua³⁶, L. Dell'Asta^{74a,74b},
 M. Delmastro⁵, C. Delporte⁶⁵, P.A. Delsart⁵⁸, S. Demers¹⁸³, M. Demichev⁸⁰, G. Demontigny¹¹⁰,
 S.P. Denisov¹²³, L. D'Eramo¹²¹, D. Derendarz⁸⁵, J.E. Derkaoui^{35e}, F. Derue¹³⁵, P. Dervan⁹¹, K. Desch²⁴,
 K. Dette¹⁶⁷, C. Deutsch²⁴, M.R. Devesa³⁰, P.O. Deviveiros³⁶, F.A. Di Bello^{73a,73b}, A. Di Ciaccio^{74a,74b},
 L. Di Ciaccio⁵, C. Di Donato^{70a,70b}, A. Di Girolamo³⁶, G. Di Gregorio^{72a,72b}, A. Di Luca^{76a,76b},
 B. Di Micco^{75a,75b}, R. Di Nardo^{75a,75b}, K.F. Di Petrillo⁵⁹, R. Di Sipio¹⁶⁷, C. Diaconu¹⁰², F.A. Dias¹²⁰,
 T. Dias Do Vale^{139a}, M.A. Diaz^{146a}, F.G. Diaz Capriles²⁴, J. Dickinson¹⁸, M. Didenko¹⁶⁶, E.B. Diehl¹⁰⁶,
 J. Dietrich¹⁹, S. Díez Cornell⁴⁶, C. Diez Pardos¹⁵¹, A. Dimitrievska¹⁸, W. Ding^{15b}, J. Dingfelder²⁴,
 S.J. Dittmeier^{61b}, F. Dittus³⁶, F. Djama¹⁰², T. Djobava^{159b}, J.I. Djuvslund¹⁷, M.A.B. Do Vale¹⁴⁷,
 M. Dobre^{27b}, D. Dodsworth²⁶, C. Doglioni⁹⁷, J. Dolejsi¹⁴², Z. Dolezal¹⁴², M. Donadelli^{81c}, B. Dong^{60c},
 J. Donini³⁸, A. D'onofrio^{15c}, M. D'Onofrio⁹¹, J. Dopke¹⁴³, A. Doria^{70a}, M.T. Dova⁸⁹, A.T. Doyle⁵⁷,
 E. Drechsler¹⁵², E. Dreyer¹⁵², T. Dreyer⁵³, A.S. Drobac¹⁷⁰, D. Du^{60b}, T.A. du Pree¹²⁰, Y. Duan^{60d},
 F. Dubinin¹¹¹, M. Dubovsky^{28a}, A. Dubreuil⁵⁴, E. Duchovni¹⁸⁰, G. Duckeck¹¹⁴, O.A. Ducu^{36,27b},
 D. Duda¹¹⁵, A. Dudarev³⁶, A.C. Dudder¹⁰⁰, E.M. Duffield¹⁸, M. D'uffizi¹⁰¹, L. Dufflot⁶⁵, M. Dührssen³⁶,
 C. Dülsen¹⁸², M. Dumancic¹⁸⁰, A.E. Dumitriu^{27b}, M. Dunford^{61a}, S. Dungs⁴⁷, A. Duperrin¹⁰²,
 H. Duran Yildiz^{4a}, M. Düren⁵⁶, A. Durglishvili^{159b}, D. Duschinger⁴⁸, B. Dutta⁴⁶, D. Duvnjak¹,
 G.I. Dyckes¹³⁶, M. Dyndal³⁶, S. Dysch¹⁰¹, B.S. Dziedzic⁸⁵, M.G. Eggleston⁴⁹, T. Eifert⁸, G. Eigen¹⁷,
 K. Einsweiler¹⁸, T. Ekelof¹⁷², H. El Jarrari^{35f}, V. Ellajosyula¹⁷², M. Ellert¹⁷², F. Ellinghaus¹⁸²,
 A.A. Elliot⁹³, N. Ellis³⁶, J. Elmsheuser²⁹, M. Elsing³⁶, D. Emeliyanov¹⁴³, A. Emerman³⁹, Y. Enari¹⁶³,
 M.B. Epland⁴⁹, J. Erdmann⁴⁷, A. Ereditato²⁰, P.A. Erland⁸⁵, M. Errenst¹⁸², M. Escalier⁶⁵, C. Escobar¹⁷⁴,
 O. Estrada Pastor¹⁷⁴, E. Etzion¹⁶¹, G. Evans^{139a}, H. Evans⁶⁶, M.O. Evans¹⁵⁶, A. Ezhilov¹³⁷, F. Fabbri⁵⁷,
 L. Fabbri^{23b,23a}, V. Fabiani¹¹⁹, G. Facini¹⁷⁸, R.M. Fakhrutdinov¹²³, S. Falciano^{73a}, P.J. Falke²⁴, S. Falke³⁶,
 J. Faltova¹⁴², Y. Fang^{15a}, Y. Fang^{15a}, G. Fanourakis⁴⁴, M. Fanti^{69a,69b}, M. Faraj^{67a,67c}, A. Farbin⁸,
 A. Farilla^{75a}, E.M. Farina^{71a,71b}, T. Farooque¹⁰⁷, S.M. Farrington⁵⁰, P. Farthouat³⁶, F. Fassi^{35f},
 P. Fassnacht³⁶, D. Fassouliotis⁹, M. Fauci Giannelli⁵⁰, W.J. Fawcett³², L. Fayard⁶⁵, O.L. Fedin^{137,p},
 W. Fedorko¹⁷⁵, A. Fehr²⁰, M. Feickert¹⁷³, L. Feligioni¹⁰², A. Fell¹⁴⁹, C. Feng^{60b}, M. Feng⁴⁹,
 M.J. Fenton¹⁷¹, A.B. Fenyuk¹²³, S.W. Ferguson⁴³, J. Ferrando⁴⁶, A. Ferrari¹⁷², P. Ferrari¹²⁰, R. Ferrari^{71a},
 D.E. Ferreira de Lima^{61b}, A. Ferrer¹⁷⁴, D. Ferrere⁵⁴, C. Ferretti¹⁰⁶, F. Fiedler¹⁰⁰, A. Filipčić⁹²,
 F. Filthaut¹¹⁹, K.D. Finelli²⁵, M.C.N. Fiolhais^{139a,139c,a}, L. Fiorini¹⁷⁴, F. Fischer¹¹⁴, J. Fischer¹⁰⁰,
 W.C. Fisher¹⁰⁷, T. Fitschen²¹, I. Fleck¹⁵¹, P. Fleischmann¹⁰⁶, T. Flick¹⁸², B.M. Flierl¹¹⁴, L. Flores¹³⁶,
 L.R. Flores Castillo^{63a}, F.M. Follega^{76a,76b}, N. Fomin¹⁷, J.H. Foo¹⁶⁷, G.T. Forcolin^{76a,76b}, B.C. Forland⁶⁶,
 A. Formica¹⁴⁴, F.A. Förster¹⁴, A.C. Forti¹⁰¹, E. Fortin¹⁰², M.G. Foti¹³⁴, D. Fournier⁶⁵, H. Fox⁹⁰,
 P. Francavilla^{72a,72b}, S. Francescato^{73a,73b}, M. Franchini^{23b,23a}, S. Franchino^{61a}, D. Francis³⁶, L. Franco⁵,
 L. Franconi²⁰, M. Franklin⁵⁹, G. Frattari^{73a,73b}, A.N. Fray⁹³, P.M. Freeman²¹, B. Freund¹¹⁰,
 W.S. Freund^{81b}, E.M. Freundlich⁴⁷, D.C. Frizzell¹²⁸, D. Froidevaux³⁶, J.A. Frost¹³⁴, M. Fujimoto¹²⁶,
 C. Fukunaga¹⁶⁴, E. Fullana Torregrosa¹⁷⁴, T. Fusayasu¹¹⁶, J. Fuster¹⁷⁴, A. Gabrielli^{23b,23a}, A. Gabrielli³⁶,
 S. Gadatsch⁵⁴, P. Gadow¹¹⁵, G. Gagliardi^{55b,55a}, L.G. Gagnon¹¹⁰, G.E. Gallardo¹³⁴, E.J. Gallas¹³⁴,
 B.J. Gallop¹⁴³, R. Gamboa Goni⁹³, K.K. Gan¹²⁷, S. Ganguly¹⁸⁰, J. Gao^{60a}, Y. Gao⁵⁰, Y.S. Gao^{31,m},
 F.M. Garay Walls^{146a}, C. García¹⁷⁴, J.E. García Navarro¹⁷⁴, J.A. García Pascual^{15a}, C. Garcia-Argos⁵²,

M. Garcia-Sciveres¹⁸, R.W. Gardner³⁷, N. Garelli¹⁵³, S. Gargiulo⁵², C.A. Garner¹⁶⁷, V. Garonne¹³³,
S.J. Gasiorowski¹⁴⁸, P. Gaspar^{81b}, A. Gaudiello^{55b,55a}, G. Gaudio^{71a}, P. Gauzzi^{73a,73b}, I.L. Gavrilenko¹¹¹,
A. Gavriluk¹²⁴, C. Gay¹⁷⁵, G. Gaycken⁴⁶, E.N. Gazis¹⁰, A.A. Geanta^{27b}, C.M. Gee¹⁴⁵, C.N.P. Gee¹⁴³,
J. Geisen⁹⁷, M. Geisen¹⁰⁰, C. Gemme^{55b}, M.H. Genest⁵⁸, C. Geng¹⁰⁶, S. Gentile^{73a,73b}, S. George⁹⁴,
T. Geralis⁴⁴, L.O. Gerlach⁵³, P. Gessinger-Befurt¹⁰⁰, G. Gessner⁴⁷, M. Ghasemi Bostanabad¹⁷⁶,
M. Ghneimat¹⁵¹, A. Ghosh⁶⁵, A. Ghosh⁷⁸, B. Giacobbe^{23b}, S. Giagu^{73a,73b}, N. Giangiacomi¹⁶⁷,
P. Giannetti^{72a}, A. Giannini^{70a,70b}, G. Giannini¹⁴, S.M. Gibson⁹⁴, M. Gignac¹⁴⁵, D.T. Gil^{84b}, B.J. Gilbert³⁹,
D. Gillberg³⁴, G. Gilles¹⁸², N.E.K. Gillwald⁴⁶, D.M. Gingrich^{3,ak}, M.P. Giordani^{67a,67c}, P.F. Giraud¹⁴⁴,
G. Giugliarelli^{67a,67c}, D. Giugni^{69a}, F. Giuli^{74a,74b}, S. Gkaitatzis¹⁶², I. Gkialas^{9,h}, E.L. Gkoukousis¹⁴,
P. Gkoutoumis¹⁰, L.K. Gladilin¹¹³, C. Glasman⁹⁹, J. Glatzer¹⁴, P.C.F. Glaysher⁴⁶, A. Glazov⁴⁶,
G.R. Gledhill¹³¹, I. Gnesi^{41b,c}, M. Goblirsch-Kolb²⁶, D. Godin¹¹⁰, S. Goldfarb¹⁰⁵, T. Golling⁵⁴,
D. Golubkov¹²³, A. Gomes^{139a,139b}, R. Goncalves Gama⁵³, R. Gonçalo^{139a,139c}, G. Gonella¹³¹,
L. Gonella²¹, A. Gongadze⁸⁰, F. Gonnella²¹, J.L. Gonski³⁹, S. González de la Hoz¹⁷⁴,
S. Gonzalez Fernandez¹⁴, R. Gonzalez Lopez⁹¹, C. Gonzalez Renteria¹⁸, R. Gonzalez Suarez¹⁷²,
S. Gonzalez-Sevilla⁵⁴, G.R. Gonzalvo Rodriguez¹⁷⁴, L. Goossens³⁶, N.A. Gorasia²¹, P.A. Gorbounov¹²⁴,
H.A. Gordon²⁹, B. Gorini³⁶, E. Gorini^{68a,68b}, A. Gorišek⁹², A.T. Goshaw⁴⁹, M.I. Gostkin⁸⁰,
C.A. Gottardo¹¹⁹, M. Gouighri^{35b}, A.G. Goussiou¹⁴⁸, N. Govender^{33c}, C. Goy⁵, I. Grabowska-Bold^{84a},
E.C. Graham⁹¹, J. Gramling¹⁷¹, E. Gramstad¹³³, S. Grancagnolo¹⁹, M. Grandi¹⁵⁶, V. Gratchev¹³⁷,
P.M. Gravila^{27f}, F.G. Gravili^{68a,68b}, C. Gray⁵⁷, H.M. Gray¹⁸, C. Grefe²⁴, K. Gregersen⁹⁷, I.M. Gregor⁴⁶,
P. Grenier¹⁵³, K. Grevtsov⁴⁶, C. Grieco¹⁴, N.A. Grieser¹²⁸, A.A. Grillo¹⁴⁵, K. Grimm^{31,l}, S. Grinstein^{14,w},
J.-F. Grivaz⁶⁵, S. Groh¹⁰⁰, E. Gross¹⁸⁰, J. Grosse-Knetter⁵³, Z.J. Grout⁹⁵, C. Grud¹⁰⁶, A. Grummer¹¹⁸,
J.C. Grundy¹³⁴, L. Guan¹⁰⁶, W. Guan¹⁸¹, C. Gubbels¹⁷⁵, J. Guenther⁷⁷, A. Guerguichon⁶⁵,
J.G.R. Guerrero Rojas¹⁷⁴, F. Guescini¹¹⁵, D. Guest⁷⁷, R. Gugel¹⁰⁰, A. Guida⁴⁶, T. Guillemin⁵,
S. Guindon³⁶, J. Guo^{60c}, W. Guo¹⁰⁶, Y. Guo^{60a}, Z. Guo¹⁰², R. Gupta⁴⁶, S. Gurbuz^{12c}, G. Gustavino¹²⁸,
M. Guth⁵², P. Gutierrez¹²⁸, C. Gutschow⁹⁵, C. Guyot¹⁴⁴, C. Gwenlan¹³⁴, C.B. Gwilliam⁹¹,
E.S. Haaland¹³³, A. Haas¹²⁵, C. Haber¹⁸, H.K. Hadavand⁸, A. Hadei¹⁰⁰, M. Haleem¹⁷⁷, J. Haley¹²⁹,
J.J. Hall¹⁴⁹, G. Halladjian¹⁰⁷, G.D. Hallewell¹⁰², K. Hamano¹⁷⁶, H. Hamdaoui^{35f}, M. Hamer²⁴,
G.N. Hamity⁵⁰, K. Han^{60a}, L. Han^{15c}, L. Han^{60a}, S. Han¹⁸, Y.F. Han¹⁶⁷, K. Hanagaki^{82,u}, M. Hance¹⁴⁵,
D.M. Handl¹¹⁴, M.D. Hank³⁷, R. Hankache¹³⁵, E. Hansen⁹⁷, J.B. Hansen⁴⁰, J.D. Hansen⁴⁰,
M.C. Hansen²⁴, P.H. Hansen⁴⁰, E.C. Hanson¹⁰¹, K. Hara¹⁶⁹, T. Harenberg¹⁸², S. Harkusha¹⁰⁸,
P.F. Harrison¹⁷⁸, N.M. Hartman¹⁵³, N.M. Hartmann¹¹⁴, Y. Hasegawa¹⁵⁰, A. Hasib⁵⁰, S. Hassani¹⁴⁴,
S. Haug²⁰, R. Hauser¹⁰⁷, M. Havranek¹⁴¹, C.M. Hawkes²¹, R.J. Hawkings³⁶, S. Hayashida¹¹⁷,
D. Hayden¹⁰⁷, C. Hayes¹⁰⁶, R.L. Hayes¹⁷⁵, C.P. Hays¹³⁴, J.M. Hays⁹³, H.S. Hayward⁹¹, S.J. Haywood¹⁴³,
F. He^{60a}, Y. He¹⁶⁵, M.P. Heath⁵⁰, V. Hedberg⁹⁷, A.L. Heggelund¹³³, N.D. Hehir⁹³, C. Heidegger⁵²,
K.K. Heidegger⁵², W.D. Heidorn⁷⁹, J. Heilman³⁴, S. Heim⁴⁶, T. Heim¹⁸, B. Heinemann^{46,ai},
J.G. Heinlein¹³⁶, J.J. Heinrich¹³¹, L. Heinrich³⁶, J. Hejbal¹⁴⁰, L. Helary⁴⁶, A. Held¹²⁵, S. Hellesund¹³³,
C.M. Helling¹⁴⁵, S. Hellman^{45a,45b}, C. Helsens³⁶, R.C.W. Henderson⁹⁰, L. Henkelmann³²,
A.M. Henriques Correia³⁶, H. Herde²⁶, Y. Hernández Jiménez^{33e}, H. Herr¹⁰⁰, M.G. Herrmann¹¹⁴,
T. Herrmann⁴⁸, G. Herten⁵², R. Hertenberger¹¹⁴, L. Hervas³⁶, G.G. Hesketh⁹⁵, N.P. Hessey^{168a}, H. Hibi⁸³,
S. Higashino⁸², E. Higón-Rodríguez¹⁷⁴, K. Hildebrand³⁷, J.C. Hill³², K.K. Hill²⁹, K.H. Hiller⁴⁶,
S.J. Hillier²¹, M. Hils⁴⁸, I. Hinchliffe¹⁸, F. Hinterkeuser²⁴, M. Hirose¹³², S. Hirose¹⁶⁹, D. Hirschbuehl¹⁸²,
B. Hiti⁹², O. Hladik¹⁴⁰, J. Hobbs¹⁵⁵, R. Hobincu^{27e}, N. Hod¹⁸⁰, M.C. Hodgkinson¹⁴⁹, A. Hoecker³⁶,
D. Hohn⁵², D. Hohov⁶⁵, T. Holm²⁴, T.R. Holmes³⁷, M. Holzbock¹¹⁵, L.B.A.H. Hommels³², T.M. Hong¹³⁸,
J.C. Honig⁵², A. Hönle¹¹⁵, B.H. Hooberman¹⁷³, W.H. Hopkins⁶, Y. Horii¹¹⁷, P. Horn⁴⁸, L.A. Horyn³⁷,
S. Hou¹⁵⁸, A. Hoummada^{35a}, J. Howarth⁵⁷, J. Hoya⁸⁹, M. Hrabovsky¹³⁰, J. Hrivnac⁶⁵, A. Hrynevich¹⁰⁹,
T. Hryn'ova⁵, P.J. Hsu⁶⁴, S.-C. Hsu¹⁴⁸, Q. Hu³⁹, S. Hu^{60c}, Y.F. Hu^{15a,15d,am}, D.P. Huang⁹⁵, X. Huang^{15c},
Y. Huang^{60a}, Y. Huang^{15a}, Z. Hubacek¹⁴¹, F. Hubaut¹⁰², M. Huebner²⁴, F. Huegging²⁴, T.B. Huffman¹³⁴,

M. Huhtinen³⁶, R. Hulsken⁵⁸, R.F.H. Hunter³⁴, N. Huseynov^{80,ab}, J. Huston¹⁰⁷, J. Huth⁵⁹, R. Hyneman¹⁵³,
S. Hyrych^{28a}, G. Iacobucci⁵⁴, G. Iakovidis²⁹, I. Ibragimov¹⁵¹, L. Iconomidou-Fayard⁶⁵, P. Iengo³⁶,
R. Ignazzi⁴⁰, R. Iguchi¹⁶³, T. Iizawa⁵⁴, Y. Ikegami⁸², M. Ikeno⁸², N. Ilic^{119,167,aa}, F. Iltzsche⁴⁸, H. Imam^{35a},
G. Introzzi^{71a,71b}, M. Iodice^{75a}, K. Iordanidou^{168a}, V. Ippolito^{73a,73b}, M.F. Isacson¹⁷², M. Ishino¹⁶³,
W. Islam¹²⁹, C. Issever^{19,46}, S. Istin¹⁶⁰, J.M. Iturbe Ponce^{63a}, R. Iuppa^{76a,76b}, A. Ivina¹⁸⁰, J.M. Izen⁴³,
V. Izzo^{70a}, P. Jacka¹⁴⁰, P. Jackson¹, R.M. Jacobs⁴⁶, B.P. Jaeger¹⁵², V. Jain², G. Jäkel¹⁸², K.B. Jakobi¹⁰⁰,
K. Jakobs⁵², T. Jakoubek¹⁸⁰, J. Jamieson⁵⁷, K.W. Janas^{84a}, R. Jansky⁵⁴, M. Janus⁵³, P.A. Janus^{84a},
G. Jarlskog⁹⁷, A.E. Jaspán⁹¹, N. Javadov^{80,ab}, T. Javûrek³⁶, M. Javurkova¹⁰³, F. Jeanneau¹⁴⁴, L. Jeanty¹³¹,
J. Jejelava^{159a}, P. Jenni^{52,d}, N. Jeong⁴⁶, S. Jézéquel⁵, J. Jia¹⁵⁵, Z. Jia^{15c}, H. Jiang⁷⁹, Y. Jiang^{60a}, Z. Jiang¹⁵³,
S. Jiggins⁵², F.A. Jimenez Morales³⁸, J. Jimenez Pena¹¹⁵, S. Jin^{15c}, A. Jinaru^{27b}, O. Jinnouchi¹⁶⁵,
H. Jivan^{33e}, P. Johansson¹⁴⁹, K.A. Johns⁷, C.A. Johnson⁶⁶, E. Jones¹⁷⁸, R.W.L. Jones⁹⁰, S.D. Jones¹⁵⁶,
T.J. Jones⁹¹, J. Jovicevic³⁶, X. Ju¹⁸, J.J. Junggeburch¹¹⁵, A. Juste Rozas^{14,w}, A. Kaczmarska⁸⁵,
M. Kado^{73a,73b}, H. Kagan¹²⁷, M. Kagan¹⁵³, A. Kahn³⁹, C. Kahra¹⁰⁰, T. Kaji¹⁷⁹, E. Kajomovitz¹⁶⁰,
C.W. Kalderon²⁹, A. Kaluza¹⁰⁰, A. Kamenshchikov¹²³, M. Kaneda¹⁶³, N.J. Kang¹⁴⁵, S. Kang⁷⁹,
Y. Kano¹¹⁷, J. Kanzaki⁸², L.S. Kaplan¹⁸¹, D. Kar^{33e}, K. Karava¹³⁴, M.J. Kareem^{168b}, I. Karkanas¹⁶²,
S.N. Karpov⁸⁰, Z.M. Karpova⁸⁰, V. Kartvelishvili⁹⁰, A.N. Karyukhin¹²³, E. Kasimi¹⁶², A. Kastanas^{45a,45b},
C. Kato^{60d}, J. Katzy⁴⁶, K. Kawade¹⁵⁰, K. Kawagoe⁸⁸, T. Kawaguchi¹¹⁷, T. Kawamoto¹⁴⁴, G. Kawamura⁵³,
E.F. Kay¹⁷⁶, F.I. Kaya¹⁷⁰, S. Kazakos¹⁴, V.F. Kazanin^{122b,122a}, J.M. Keaveney^{33a}, R. Keeler¹⁷⁶,
J.S. Keller³⁴, E. Kellermann⁹⁷, D. Kelsey¹⁵⁶, J.J. Kempster²¹, J. Kendrick²¹, K.E. Kennedy³⁹, O. Kepka¹⁴⁰,
S. Kersten¹⁸², B.P. Kerševan⁹², S. Ketabchi Haghghat¹⁶⁷, F. Khalil-Zada¹³, M. Khandoga¹⁴⁴,
A. Khanov¹²⁹, A.G. Kharlamov^{122b,122a}, T. Kharlamova^{122b,122a}, E.E. Khoda¹⁷⁵, T.J. Khoo⁷⁷,
G. Khorauli¹⁷⁷, E. Khramov⁸⁰, J. Khubua^{159b}, S. Kido⁸³, M. Kiehn³⁶, E. Kim¹⁶⁵, Y.K. Kim³⁷,
N. Kimura⁹⁵, A. Kirchhoff⁵³, D. Kirchmeier⁴⁸, J. Kirk¹⁴³, A.E. Kiryunin¹¹⁵, T. Kishimoto¹⁶³,
D.P. Kisliuk¹⁶⁷, V. Kitali⁴⁶, C. Kitsaki¹⁰, O. Kivernyk²⁴, T. Klapdor-Kleingrothaus⁵², M. Klassen^{61a},
C. Klein³⁴, M.H. Klein¹⁰⁶, M. Klein⁹¹, U. Klein⁹¹, K. Kleinknecht¹⁰⁰, P. Klimek³⁶, A. Klimentov²⁹,
F. Klimpel³⁶, T. Klingl²⁴, T. Klioutchnikova³⁶, F.F. Klitzner¹¹⁴, P. Kluit¹²⁰, S. Kluth¹¹⁵, E. Kneringer⁷⁷,
E.B.F.G. Knoop¹⁰², A. Knue⁵², D. Kobayashi⁸⁸, M. Kobel⁴⁸, M. Kocian¹⁵³, T. Kodama¹⁶³, P. Kodys¹⁴²,
D.M. Koeck¹⁵⁶, P.T. Koenig²⁴, T. Koffas³⁴, N.M. Köhler³⁶, M. Kolb¹⁴⁴, I. Koletsou⁵, T. Komarek¹³⁰,
T. Kondo⁸², K. Köneke⁵², A.X.Y. Kong¹, A.C. König¹¹⁹, T. Kono¹²⁶, V. Konstantinides⁹⁵,
N. Konstantinidis⁹⁵, B. Konya⁹⁷, R. Kopeliansky⁶⁶, S. Koperny^{84a}, K. Korcyl⁸⁵, K. Kordas¹⁶²,
G. Koren¹⁶¹, A. Korn⁹⁵, I. Korolkov¹⁴, E.V. Korolkova¹⁴⁹, N. Korotkova¹¹³, O. Kortner¹¹⁵, S. Kortner¹¹⁵,
V.V. Kostyukhin^{149,166}, A. Kotsokchagia⁶⁵, A. Kotwal⁴⁹, A. Koulouris¹⁰,
A. Kourkoumeli-Charalampidi^{71a,71b}, C. Kourkoumelis⁹, E. Kourlitis⁶, V. Kouskoura²⁹, R. Kowalewski¹⁷⁶,
W. Kozanecki¹⁰¹, A.S. Kozhin¹²³, V.A. Kramarenko¹¹³, G. Kramberger⁹², D. Krasnopevtsev^{60a},
M.W. Krasny¹³⁵, A. Krasznahorkay³⁶, D. Krauss¹¹⁵, J.A. Kremer¹⁰⁰, J. Kretschmar⁹¹, K. Kreul¹⁹,
P. Krieger¹⁶⁷, F. Krieter¹¹⁴, S. Krishnamurthy¹⁰³, A. Krishnan^{61b}, M. Krivos¹⁴², K. Krizka¹⁸,
K. Kroeninger⁴⁷, H. Kroha¹¹⁵, J. Kroll¹⁴⁰, J. Kroll¹³⁶, K.S. Krowpman¹⁰⁷, U. Kruchonak⁸⁰, H. Krüger²⁴,
N. Krumnack⁷⁹, M.C. Kruse⁴⁹, J.A. Krzysiak⁸⁵, A. Kubota¹⁶⁵, O. Kuchinskaia¹⁶⁶, S. Kuday^{4b},
D. Kuechler⁴⁶, J.T. Kuechler⁴⁶, S. Kuehn³⁶, T. Kuhl⁴⁶, V. Kukhtin⁸⁰, Y. Kulchitsky^{108,ae}, S. Kuleshov^{146b},
Y.P. Kulinich¹⁷³, M. Kuna⁵⁸, A. Kupco¹⁴⁰, T. Kupfer⁴⁷, O. Kuprash⁵², H. Kurashige⁸³,
L.L. Kurchaninov^{168a}, Y.A. Kurochkin¹⁰⁸, A. Kurova¹¹², M.G. Kurth^{15a,15d}, E.S. Kuwertz³⁶, M. Kuze¹⁶⁵,
A.K. Kvam¹⁴⁸, J. Kvita¹³⁰, T. Kwan¹⁰⁴, C. Lacasta¹⁷⁴, F. Lacava^{73a,73b}, D.P.J. Lack¹⁰¹, H. Lacker¹⁹,
D. Lacour¹³⁵, E. Ladygin⁸⁰, R. Lafaye⁵, B. Laforge¹³⁵, T. Lagouri^{146c}, S. Lai⁵³, I.K. Lakomic^{84a},
J.E. Lambert¹²⁸, S. Lammers⁶⁶, W. Lampl⁷, C. Lampoudis¹⁶², E. Lançon²⁹, U. Landgraf⁵²,
M.P.J. Landon⁹³, V.S. Lang⁵², J.C. Lange⁵³, R.J. Langenberg¹⁰³, A.J. Lankford¹⁷¹, F. Lanni²⁹,
K. Lantzsche²⁴, A. Lanza^{71a}, A. Lapertosa^{55b,55a}, J.F. Laporte¹⁴⁴, T. Lari^{69a}, F. Lasagni Manghi^{23b,23a},
M. Lassnig³⁶, V. Latonova¹⁴⁰, T.S. Lau^{63a}, A. Laudrain¹⁰⁰, A. Laurier³⁴, M. Lavorgna^{70a,70b},

S.D. Lawlor⁹⁴, M. Lazzaroni^{69a,69b}, B. Le¹⁰¹, E. Le Guirriec¹⁰², A. Lebedev⁷⁹, M. LeBlanc⁷, T. LeCompte⁶, F. Ledroit-Guillon⁵⁸, A.C.A. Lee⁹⁵, C.A. Lee²⁹, G.R. Lee¹⁷, L. Lee⁵⁹, S.C. Lee¹⁵⁸, S. Lee⁷⁹, B. Lefebvre^{168a}, H.P. Lefebvre⁹⁴, M. Lefebvre¹⁷⁶, C. Leggett¹⁸, K. Lehmann¹⁵², N. Lehmann²⁰, G. Lehmann Miotto³⁶, W.A. Leight⁴⁶, A. Leisos^{162,v}, M.A.L. Leite^{81c}, C.E. Leitgeb¹¹⁴, R. Leitner¹⁴², K.J.C. Leney⁴², T. Lenz²⁴, S. Leone^{72a}, C. Leonidopoulos⁵⁰, A. Leopold¹³⁵, C. Leroy¹¹⁰, R. Les¹⁰⁷, C.G. Lester³², M. Levchenko¹³⁷, J. Levêque⁵, D. Levin¹⁰⁶, L.J. Levinson¹⁸⁰, D.J. Lewis²¹, B. Li^{15b}, B. Li¹⁰⁶, C-Q. Li^{60c,60d}, F. Li^{60c}, H. Li^{60a}, H. Li^{60b}, J. Li^{60c}, K. Li¹⁴⁸, L. Li^{60c}, M. Li^{15a,15d}, Q.Y. Li^{60a}, S. Li^{60d,60c,b}, X. Li⁴⁶, Y. Li⁴⁶, Z. Li^{60b}, Z. Li¹³⁴, Z. Li¹⁰⁴, Z. Li⁹¹, Z. Liang^{15a}, M. Liberatore⁴⁶, B. Liberti^{74a}, K. Lie^{63c}, S. Lim²⁹, C.Y. Lin³², K. Lin¹⁰⁷, R.A. Linck⁶⁶, R.E. Lindley⁷, J.H. Lindon²¹, A. Linss⁴⁶, A.L. Lioni⁵⁴, E. Lipeles¹³⁶, A. Lipniacka¹⁷, T.M. Liss^{173,aj}, A. Lister¹⁷⁵, J.D. Little⁸, B. Liu⁷⁹, B.X. Liu¹⁵², H.B. Liu²⁹, J.B. Liu^{60a}, J.K.K. Liu³⁷, K. Liu^{60d,60c}, M. Liu^{60a}, M.Y. Liu^{60a}, P. Liu^{15a}, X. Liu^{60a}, Y. Liu⁴⁶, Y. Liu^{15a,15d}, Y.L. Liu¹⁰⁶, Y.W. Liu^{60a}, M. Livan^{71a,71b}, A. Lleres⁵⁸, J. Llorente Merino¹⁵², S.L. Lloyd⁹³, C.Y. Lo^{63b}, E.M. Lobodzinska⁴⁶, P. Loch⁷, S. Loffredo^{74a,74b}, T. Lohse¹⁹, K. Lohwasser¹⁴⁹, M. Lokajicek¹⁴⁰, J.D. Long¹⁷³, R.E. Long⁹⁰, I. Longarini^{73a,73b}, L. Longo³⁶, I. Lopez Paz¹⁰¹, A. Lopez Solis¹⁴⁹, J. Lorenz¹¹⁴, N. Lorenzo Martinez⁵, A.M. Lory¹¹⁴, A. Lösle⁵², X. Lou^{45a,45b}, X. Lou^{15a}, A. Lounis⁶⁵, J. Love⁶, P.A. Love⁹⁰, J.J. Lozano Bahilo¹⁷⁴, M. Lu^{60a}, Y.J. Lu⁶⁴, H.J. Lubatti¹⁴⁸, C. Luci^{73a,73b}, F.L. Lucio Alves^{15c}, A. Lucotte⁵⁸, F. Luehring⁶⁶, I. Luise¹⁵⁵, L. Luminari^{73a}, B. Lund-Jensen¹⁵⁴, N.A. Luongo¹³¹, M.S. Lutz¹⁶¹, D. Lynn²⁹, H. Lyons⁹¹, R. Lysak¹⁴⁰, E. Lytken⁹⁷, F. Lyu^{15a}, V. Lyubushkin⁸⁰, T. Lyubushkina⁸⁰, H. Ma²⁹, L.L. Ma^{60b}, Y. Ma⁹⁵, D.M. Mac Donell¹⁷⁶, G. Maccarrone⁵¹, C.M. Macdonald¹⁴⁹, J.C. MacDonald¹⁴⁹, J. Machado Miguens¹³⁶, R. Madar³⁸, W.F. Mader⁴⁸, M. Madugoda Ralalage Don¹²⁹, N. Madysa⁴⁸, J. Maeda⁸³, T. Maeno²⁹, M. Maerker⁴⁸, V. Magerl⁵², N. Magini⁷⁹, J. Magro^{67a,67c,r}, D.J. Mahon³⁹, C. Maidantchik^{81b}, A. Maio^{139a,139b,139d}, K. Maj^{84a}, O. Majersky^{28a}, S. Majewski¹³¹, Y. Makida⁸², N. Makovec⁶⁵, B. Malaescu¹³⁵, Pa. Malecki⁸⁵, V.P. Maleev¹³⁷, F. Malek⁵⁸, D. Malito^{41b,41a}, U. Mallik⁷⁸, C. Malone³², S. Maltezos¹⁰, S. Malyukov⁸⁰, J. Mamuzic¹⁷⁴, G. Mancini⁵¹, J.P. Mandalia⁹³, I. Mandić⁹², L. Manhaes de Andrade Filho^{81a}, I.M. Maniatis¹⁶², J. Manjarres Ramos⁴⁸, K.H. Mankinen⁹⁷, A. Mann¹¹⁴, A. Manousos⁷⁷, B. Mansoulie¹⁴⁴, I. Manthos¹⁶², S. Manzoni¹²⁰, A. Marantis¹⁶², G. Marceca³⁰, L. Marchese¹³⁴, G. Marchiori¹³⁵, M. Marcisovsky¹⁴⁰, L. Maccoccia^{74a,74b}, C. Marcon⁹⁷, M. Marjanovic¹²⁸, Z. Marshall¹⁸, M.U.F. Martensson¹⁷², S. Marti-Garcia¹⁷⁴, C.B. Martin¹²⁷, T.A. Martin¹⁷⁸, V.J. Martin⁵⁰, B. Martin dit Latour¹⁷, L. Martinelli^{75a,75b}, M. Martinez^{14,w}, P. Martinez Agullo¹⁷⁴, V.I. Martinez Outschoorn¹⁰³, S. Martin-Haugh¹⁴³, V.S. Martoiu^{27b}, A.C. Martyniuk⁹⁵, A. Marzin³⁶, S.R. Maschek¹¹⁵, L. Masetti¹⁰⁰, T. Mashimo¹⁶³, R. Mashinistov¹¹¹, J. Masik¹⁰¹, A.L. Maslennikov^{122b,122a}, L. Massa^{23b,23a}, P. Massarotti^{70a,70b}, P. Mastrandrea^{72a,72b}, A. Mastroberardino^{41b,41a}, T. Masubuchi¹⁶³, D. Matakias²⁹, A. Matic¹¹⁴, N. Matsuzawa¹⁶³, P. Mättig²⁴, J. Maurer^{27b}, B. Maček⁹², D.A. Maximov^{122b,122a}, R. Mazini¹⁵⁸, I. Maznas¹⁶², S.M. Mazza¹⁴⁵, J.P. Mc Gowan¹⁰⁴, S.P. Mc Kee¹⁰⁶, T.G. McCarthy¹¹⁵, W.P. McCormack¹⁸, E.F. McDonald¹⁰⁵, A.E. McDougall¹²⁰, J.A. Mcfayden¹⁸, G. Mchedlidze^{159b}, M.A. McKay⁴², K.D. McLean¹⁷⁶, S.J. McMahon¹⁴³, P.C. McNamara¹⁰⁵, C.J. McNicol¹⁷⁸, R.A. McPherson^{176,aa}, J.E. Mdhului^{33e}, Z.A. Meadows¹⁰³, S. Meehan³⁶, T. Megy³⁸, S. Mehlhase¹¹⁴, A. Mehta⁹¹, B. Meirose⁴³, D. Melini¹⁶⁰, B.R. Mellado Garcia^{33e}, J.D. Mellenthin⁵³, M. Melo^{28a}, F. Meloni⁴⁶, A. Melzer²⁴, E.D. Mendes Gouveia^{139a,139e}, A.M. Mendes Jacques Da Costa²¹, H.Y. Meng¹⁶⁷, L. Meng³⁶, X.T. Meng¹⁰⁶, S. Menke¹¹⁵, E. Meoni^{41b,41a}, S. Mergelmeyer¹⁹, S.A.M. Merkt¹³⁸, C. Merlassino¹³⁴, P. Mermod⁵⁴, L. Merola^{70a,70b}, C. Meroni^{69a}, G. Merz¹⁰⁶, O. Meshkov^{113,111}, J.K.R. Meshreki¹⁵¹, J. Metcalfe⁶, A.S. Mete⁶, C. Meyer⁶⁶, J-P. Meyer¹⁴⁴, M. Michetti¹⁹, R.P. Middleton¹⁴³, L. Mijović⁵⁰, G. Mikenberg¹⁸⁰, M. Mikestikova¹⁴⁰, M. Mikuš⁹², H. Mildner¹⁴⁹, A. Milic¹⁶⁷, C.D. Milke⁴², D.W. Miller³⁷, L.S. Miller³⁴, A. Milov¹⁸⁰, D.A. Milstead^{45a,45b}, A.A. Minaenko¹²³, I.A. Minashvili^{159b}, L. Mince⁵⁷, A.I. Mincer¹²⁵, B. Mindur^{84a}, M. Mineev⁸⁰, Y. Minegishi¹⁶³, Y. Mino⁸⁶, L.M. Mir¹⁴, M. Mironova¹³⁴, T. Mitani¹⁷⁹, J. Mitrevski¹¹⁴, V.A. Mitsou¹⁷⁴,

M. Mittal^{60c}, O. Miu¹⁶⁷, A. Miucci²⁰, P.S. Miyagawa⁹³, A. Mizukami⁸², J.U. Mjörnmark⁹⁷,
T. Mkrtchyan^{61a}, M. Mlynarikova¹²¹, T. Moa^{45a,45b}, S. Mobius⁵³, K. Mochizuki¹¹⁰, P. Moder⁴⁶,
P. Mogg¹¹⁴, S. Mohapatra³⁹, R. Moles-Valls²⁴, K. Mönig⁴⁶, E. Monnier¹⁰², A. Montalbano¹⁵²,
J. Montejo Berlingen³⁶, M. Montella⁹⁵, F. Monticelli⁸⁹, S. Monzani^{69a}, N. Morange⁶⁵,
A.L. Moreira De Carvalho^{139a}, D. Moreno^{22a}, M. Moreno Llácer¹⁷⁴, C. Moreno Martinez¹⁴,
P. Morettini^{55b}, M. Morgenstern¹⁶⁰, S. Morgenstern⁴⁸, D. Mori¹⁵², M. Morii⁵⁹, M. Morinaga¹⁷⁹,
V. Morisbak¹³³, A.K. Morley³⁶, G. Mornacchi³⁶, A.P. Morris⁹⁵, L. Morvaj³⁶, P. Moschovakos³⁶,
B. Moser¹²⁰, M. Mosidze^{159b}, T. Moskalets¹⁴⁴, P. Moskvitina¹¹⁹, J. Moss^{31,n}, E.J.W. Moyse¹⁰³,
S. Muanza¹⁰², J. Mueller¹³⁸, R.S.P. Mueller¹¹⁴, D. Muenstermann⁹⁰, G.A. Mullier⁹⁷, J.J. Mullin¹³⁶,
D.P. Mungo^{69a,69b}, J.L. Munoz Martinez¹⁴, F.J. Munoz Sanchez¹⁰¹, P. Murin^{28b}, W.J. Murray^{178,143},
A. Murrone^{69a,69b}, J.M. Muse¹²⁸, M. Muškinja¹⁸, C. Mwewa^{33a}, A.G. Myagkov^{123,af}, A.A. Myers¹³⁸,
G. Myers⁶⁶, J. Myers¹³¹, M. Myska¹⁴¹, B.P. Nachman¹⁸, O. Nackenhorst⁴⁷, A.Nag Nag⁴⁸, K. Nagai¹³⁴,
K. Nagano⁸², Y. Nagasaka⁶², J.L. Nagle²⁹, E. Nagy¹⁰², A.M. Nairz³⁶, Y. Nakahama¹¹⁷, K. Nakamura⁸²,
T. Nakamura¹⁶³, H. Nanjo¹³², F. Napolitano^{61a}, R.F. Naranjo Garcia⁴⁶, R. Narayan⁴², I. Naryshkin¹³⁷,
M. Naseri³⁴, T. Naumann⁴⁶, G. Navarro^{22a}, P.Y. Nechaeva¹¹¹, F. Nechansky⁴⁶, T.J. Neep²¹, A. Negri^{71a,71b},
M. Negrini^{23b}, C. Nellist¹¹⁹, C. Nelson¹⁰⁴, M.E. Nelson^{45a,45b}, S. Nemecek¹⁴⁰, M. Nessi^{36,f},
M.S. Neubauer¹⁷³, F. Neuhaus¹⁰⁰, M. Neumann¹⁸², R. Newhouse¹⁷⁵, P.R. Newman²¹, C.W. Ng¹³⁸,
Y.S. Ng¹⁹, Y.W.Y. Ng¹⁷¹, B. Ngair^{35f}, H.D.N. Nguyen¹⁰², T. Nguyen Manh¹¹⁰, E. Nibigira³⁸,
R.B. Nickerson¹³⁴, R. Nicolaidou¹⁴⁴, D.S. Nielsen⁴⁰, J. Nielsen¹⁴⁵, M. Niemeyer⁵³, N. Nikiforou¹¹,
V. Nikolaenko^{123,af}, I. Nikolic-Audit¹³⁵, K. Nikolopoulos²¹, P. Nilsson²⁹, H.R. Nindhito⁵⁴, A. Nisati^{73a},
N. Nishu^{60c}, R. Nisius¹¹⁵, I. Nitsche⁴⁷, T. Nitta¹⁷⁹, T. Nobe¹⁶³, D.L. Noel³², Y. Noguchi⁸⁶, I. Nomidis¹³⁵,
M.A. Nomura²⁹, M. Nordberg³⁶, J. Novak⁹², T. Novak⁹², O. Novgorodova⁴⁸, R. Novotny¹¹⁸, L. Nozka¹³⁰,
K. Ntekas¹⁷¹, E. Nurse⁹⁵, F.G. Oakham^{34,ak}, J. Ocariz¹³⁵, A. Ochi⁸³, I. Ochoa^{139a}, J.P. Ochoa-Ricoux^{146a},
K. O'Connor²⁶, S. Oda⁸⁸, S. Odaka⁸², S. Oerdek⁵³, A. Ogrodnik^{84a}, A. Oh¹⁰¹, C.C. Ohm¹⁵⁴, H. Oide¹⁶⁵,
R. Oishi¹⁶³, M.L. Ojeda¹⁶⁷, H. Okawa¹⁶⁹, Y. Okazaki⁸⁶, M.W. O'Keefe⁹¹, Y. Okumura¹⁶³, A. Olariu^{27b},
L.F. Oleiro Seabra^{139a}, S.A. Olivares Pino^{146a}, D. Oliveira Damazio²⁹, J.L. Oliver¹, M.J.R. Olsson¹⁷¹,
A. Olszewski⁸⁵, J. Olszowska⁸⁵, Ö.O. Öncel²⁴, D.C. O'Neil¹⁵², A.P. O'Neill¹³⁴, A. Onofre^{139a,139e},
P.U.E. Onyisi¹¹, H. Oppen¹³³, R.G. Oreamuno Madriz¹²¹, M.J. Oreglia³⁷, G.E. Orellana⁸⁹,
D. Orestano^{75a,75b}, N. Orlando¹⁴, R.S. Orr¹⁶⁷, V. O'Shea⁵⁷, R. Ospanov^{60a}, G. Otero y Garzon³⁰,
H. Otono⁸⁸, P.S. Ott^{61a}, G.J. Ottino¹⁸, M. Ouchrif^{35c}, J. Ouellette²⁹, F. Ould-Saada¹³³, A. Ouraou^{144,*},
Q. Ouyang^{15a}, M. Owen⁵⁷, R.E. Owen¹⁴³, V.E. Ozcan^{12c}, N. Ozturk⁸, J. Pacalt¹³⁰, H.A. Pacey³²,
K. Pachal⁴⁹, A. Pacheco Pages¹⁴, C. Padilla Aranda¹⁴, S. Pagan Griso¹⁸, G. Palacino⁶⁶, S. Palazzo⁵⁰,
S. Palestini³⁶, M. Palka^{84b}, P. Palni^{84a}, C.E. Pandini⁵⁴, J.G. Panduro Vazquez⁹⁴, P. Pani⁴⁶, G. Panizzo^{67a,67c},
L. Paolozzi⁵⁴, C. Papadatos¹¹⁰, K. Papageorgiou^{9,h}, S. Parajuli⁴², A. Paramonov⁶, C. Paraskevopoulos¹⁰,
D. Paredes Hernandez^{63b}, S.R. Paredes Saenz¹³⁴, B. Parida¹⁸⁰, T.H. Park¹⁶⁷, A.J. Parker³¹, M.A. Parker³²,
F. Parodi^{55b,55a}, E.W. Parrish¹²¹, J.A. Parsons³⁹, U. Parzefall⁵², L. Pascual Dominguez¹³⁵, V.R. Pascuzzi¹⁸,
J.M.P. Pasner¹⁴⁵, F. Pasquali¹²⁰, E. Pasqualucci^{73a}, S. Passaggio^{55b}, F. Pastore⁹⁴, P. Pasuwan^{45a,45b},
S. Pataria¹⁰⁰, J.R. Pater¹⁰¹, A. Pathak^{181,j}, J. Patton⁹¹, T. Pauly³⁶, J. Parkes¹⁵³, M. Pedersen¹³³,
L. Pedraza Diaz¹¹⁹, R. Pedro^{139a}, T. Peiffer⁵³, S.V. Peleganchuk^{122b,122a}, O. Penc¹⁴⁰, C. Peng^{63b},
H. Peng^{60a}, B.S. Peralva^{81a}, M.M. Perego⁶⁵, A.P. Pereira Peixoto^{139a}, L. Pereira Sanchez^{45a,45b},
D.V. Perepelitsa²⁹, E. Perez Codina^{168a}, L. Perini^{69a,69b}, H. Pernegger³⁶, S. Perrella³⁶, A. Perrevoort¹²⁰,
K. Peters⁴⁶, R.F.Y. Peters¹⁰¹, B.A. Petersen³⁶, T.C. Petersen⁴⁰, E. Petit¹⁰², V. Petousis¹⁴¹, C. Petridou¹⁶²,
F. Petrucci^{75a,75b}, M. Pettee¹⁸³, N.E. Pettersson¹⁰³, K. Petukhova¹⁴², A. Peyaud¹⁴⁴, R. Pezoa^{146d},
L. Pezzotti^{71a,71b}, T. Pham¹⁰⁵, P.W. Phillips¹⁴³, M.W. Phipps¹⁷³, G. Piacquadio¹⁵⁵, E. Pianori¹⁸,
A. Picazio¹⁰³, R.H. Pickles¹⁰¹, R. Piegaia³⁰, D. Pietreanu^{27b}, J.E. Pilcher³⁷, A.D. Pilkington¹⁰¹,
M. Pinamonti^{67a,67c}, J.L. Pinfold³, C. Pitman Donaldson⁹⁵, M. Pitt¹⁶¹, L. Pizzimento^{74a,74b}, A. Pizzini¹²⁰,
M.-A. Pleier²⁹, V. Plesanovs⁵², V. Pleskot¹⁴², E. Plotnikova⁸⁰, P. Podberezko^{122b,122a}, R. Poettgen⁹⁷,

R. Poggi⁵⁴, L. Poggioli¹³⁵, I. Pogrebnyak¹⁰⁷, D. Pohl²⁴, I. Pokharel⁵³, G. Polesello^{71a}, A. Poley^{152,168a}, A. Policicchio^{73a,73b}, R. Polifka¹⁴², A. Polini^{23b}, C.S. Pollard⁴⁶, V. Polychronakos²⁹, D. Ponomarenko¹¹², L. Pontecorvo³⁶, S. Popa^{27a}, G.A. Popeneciu^{27d}, L. Portales⁵, D.M. Portillo Quintero⁵⁸, S. Pospisil¹⁴¹, K. Potamianos⁴⁶, I.N. Potrap⁸⁰, C.J. Potter³², H. Potti¹¹, T. Poulsen⁹⁷, J. Poveda¹⁷⁴, T.D. Powell¹⁴⁹, G. Pownall⁴⁶, M.E. Pozo Astigarraga³⁶, A. Prades Ibanez¹⁷⁴, P. Pralavorio¹⁰², M.M. Prapa⁴⁴, S. Prell⁷⁹, D. Price¹⁰¹, M. Primavera^{68a}, M.L. Proffitt¹⁴⁸, N. Proklova¹¹², K. Prokofiev^{63c}, F. Prokoshin⁸⁰, S. Protopopescu²⁹, J. Proudfoot⁶, M. Przybycien^{84a}, D. Pudzha¹³⁷, A. Puri¹⁷³, P. Puzo⁶⁵, D. Pyatiizbyantseva¹¹², J. Qian¹⁰⁶, Y. Qin¹⁰¹, A. Quadt⁵³, M. Queitsch-Maitland³⁶, G. Rabanal Bolanos⁵⁹, M. Racko^{28a}, F. Ragusa^{69a,69b}, G. Rahal⁹⁸, J.A. Raine⁵⁴, S. Rajagopalan²⁹, A. Ramirez Morales⁹³, K. Ran^{15a,15d}, D.F. Rassloff^{61a}, D.M. Rauch⁴⁶, F. Rauscher¹¹⁴, S. Rave¹⁰⁰, B. Ravina⁵⁷, I. Ravinovich¹⁸⁰, M. Raymond³⁶, A.L. Read¹³³, N.P. Readioff¹⁴⁹, M. Reale^{68a,68b}, D.M. Rebuffi^{71a,71b}, G. Redlinger²⁹, K. Reeves⁴³, D. Reikher¹⁶¹, A. Reiss¹⁰⁰, A. Rej¹⁵¹, C. Rembser³⁶, A. Renardi⁴⁶, M. Renda^{27b}, M.B. Rendel¹¹⁵, A.G. Rennie⁵⁷, S. Resconi^{69a}, E.D. Resseguie¹⁸, S. Rettie⁹⁵, B. Reynolds¹²⁷, E. Reynolds²¹, O.L. Rezanova^{122b,122a}, P. Reznicek¹⁴², E. Ricci^{76a,76b}, R. Richter¹¹⁵, S. Richter⁴⁶, E. Richter-Was^{84b}, M. Ridel¹³⁵, P. Rieck¹¹⁵, O. Rifki⁴⁶, M. Rijssenbeek¹⁵⁵, A. Rimoldi^{71a,71b}, M. Rimoldi⁴⁶, L. Rinaldi^{23b}, T.T. Rinn¹⁷³, G. Ripellino¹⁵⁴, I. Riu¹⁴, P. Rivadeneira⁴⁶, J.C. Rivera Vergara¹⁷⁶, F. Rizatdinova¹²⁹, E. Rizvi⁹³, C. Rizzi³⁶, S.H. Robertson^{104,aa}, M. Robin⁴⁶, D. Robinson³², C.M. Robles Gajardo^{146d}, M. Robles Manzano¹⁰⁰, A. Robson⁵⁷, A. Rocchi^{74a,74b}, C. Roda^{72a,72b}, S. Rodriguez Bosca¹⁷⁴, A. Rodriguez Rodriguez⁵², A.M. Rodríguez Vera^{168b}, S. Roe³⁶, J. Roggel¹⁸², O. Røhne¹³³, R. Röhrig¹¹⁵, R.A. Rojas^{146d}, B. Roland⁵², C.P.A. Roland⁶⁶, J. Roloff²⁹, A. Romaniouk¹¹², M. Romano^{23b,23a}, N. Rompotis⁹¹, M. Ronzani¹²⁵, L. Roos¹³⁵, S. Rosati^{73a}, G. Rosin¹⁰³, B.J. Rosser¹³⁶, E. Rossi⁴⁶, E. Rossi^{75a,75b}, E. Rossi^{70a,70b}, L.P. Rossi^{55b}, L. Rossini⁴⁶, R. Rosten¹⁴, M. Rotaru^{27b}, B. Rottler⁵², D. Rousseau⁶⁵, G. Rovelli^{71a,71b}, A. Roy¹¹, D. Roy^{33e}, A. Rozanov¹⁰², Y. Rozen¹⁶⁰, X. Ruan^{33e}, T.A. Ruggeri¹, F. Rühr⁵², A. Ruiz-Martinez¹⁷⁴, A. Rummeler³⁶, Z. Rurikova⁵², N.A. Rusakovich⁸⁰, H.L. Russell¹⁰⁴, L. Rustige^{38,47}, J.P. Rutherford⁷, E.M. Rüttinger¹⁴⁹, M. Rybar¹⁴², G. Rybkin⁶⁵, E.B. Rye¹³³, A. Ryzhov¹²³, J.A. Sabater Iglesias⁴⁶, P. Sabatini¹⁷⁴, L. Sabetta^{73a,73b}, S. Sacerdoti⁶⁵, H.F.W. Sadrozinski¹⁴⁵, R. Sadykov⁸⁰, F. Safai Tehrani^{73a}, B. Safarzadeh Samani¹⁵⁶, M. Safdari¹⁵³, P. Saha¹²¹, S. Saha¹⁰⁴, M. Sahinsoy¹¹⁵, A. Sahu¹⁸², M. Saimpert³⁶, M. Saito¹⁶³, T. Saito¹⁶³, H. Sakamoto¹⁶³, D. Salamani⁵⁴, G. Salamanna^{75a,75b}, A. Salnikov¹⁵³, J. Salt¹⁷⁴, A. Salvador Salas¹⁴, D. Salvatore^{41b,41a}, F. Salvatore¹⁵⁶, A. Salvucci^{63a}, A. Salzburger³⁶, J. Samarati³⁶, D. Sammel⁵², D. Sampsonidis¹⁶², D. Sampsonidou^{60d,60c}, J. Sánchez¹⁷⁴, A. Sanchez Pineda^{67a,36,67c}, H. Sandaker¹³³, C.O. Sander⁴⁶, I.G. Sanderswood⁹⁰, M. Sandhoff¹⁸², C. Sandoval^{22b}, D.P.C. Sankey¹⁴³, M. Sannino^{55b,55a}, Y. Sano¹¹⁷, A. Sansoni⁵¹, C. Santoni³⁸, H. Santos^{139a,139b}, S.N. Santpur¹⁸, A. Santra¹⁷⁴, K.A. Saoucha¹⁴⁹, A. Sapronov⁸⁰, J.G. Saraiva^{139a,139d}, O. Sasaki⁸², K. Sato¹⁶⁹, F. Sauerburger⁵², E. Sauvan⁵, P. Savard^{167,ak}, R. Sawada¹⁶³, C. Sawyer¹⁴³, L. Sawyer⁹⁶, I. Sayago Galvan¹⁷⁴, C. Sbarra^{23b}, A. Sbrizzi^{67a,67c}, T. Scanlon⁹⁵, J. Schaarschmidt¹⁴⁸, P. Schacht¹¹⁵, D. Schaefer³⁷, L. Schaefer¹³⁶, U. Schäfer¹⁰⁰, A.C. Schaffer⁶⁵, D. Schaile¹¹⁴, R.D. Schamberger¹⁵⁵, E. Schanet¹¹⁴, C. Scharf¹⁹, N. Scharmberg¹⁰¹, V.A. Schegelsky¹³⁷, D. Scheirich¹⁴², F. Schenck¹⁹, M. Schernau¹⁷¹, C. Schiavi^{55b,55a}, L.K. Schildgen²⁴, Z.M. Schillaci²⁶, E.J. Schioppa^{68a,68b}, M. Schioppa^{41b,41a}, K.E. Schleicher⁵², S. Schlenker³⁶, K.R. Schmidt-Sommerfeld¹¹⁵, K. Schmieden¹⁰⁰, C. Schmitt¹⁰⁰, S. Schmitt⁴⁶, L. Schoeffel¹⁴⁴, A. Schoening^{61b}, P.G. Scholer⁵², E. Schopf¹³⁴, M. Schott¹⁰⁰, J.F.P. Schouwenberg¹¹⁹, J. Schovancova³⁶, S. Schramm⁵⁴, F. Schroeder¹⁸², A. Schulte¹⁰⁰, H-C. Schultz-Coulon^{61a}, M. Schumacher⁵², B.A. Schumm¹⁴⁵, Ph. Schune¹⁴⁴, A. Schwartzman¹⁵³, T.A. Schwarz¹⁰⁶, Ph. Schwemling¹⁴⁴, R. Schwienhorst¹⁰⁷, A. Sciandra¹⁴⁵, G. Sciolla²⁶, F. Scuri^{72a}, F. Scutti¹⁰⁵, L.M. Scyboz¹¹⁵, C.D. Sebastiani⁹¹, K. Sedlaczek⁴⁷, P. Seema¹⁹, S.C. Seidel¹¹⁸, A. Seiden¹⁴⁵, B.D. Seidlitz²⁹, T. Seiss³⁷, C. Seitz⁴⁶, J.M. Seixas^{81b}, G. Sekhniaidze^{70a}, S.J. Sekula⁴², N. Semprini-Cesari^{23b,23a}, S. Sen⁴⁹, C. Serfon²⁹, L. Serin⁶⁵, L. Serkin^{67a,67b}, M. Sessa^{60a}, H. Severini¹²⁸, S. Sevova¹⁵³, F. Sforza^{55b,55a},

A. Sfyra⁵⁴, E. Shabalina⁵³, J.D. Shahinian¹³⁶, N.W. Shaikh^{45a,45b}, D. Shaked Renous¹⁸⁰, L.Y. Shan^{15a},
 M. Shapiro¹⁸, A. Sharma³⁶, A.S. Sharma¹, P.B. Shatalov¹²⁴, K. Shaw¹⁵⁶, S.M. Shaw¹⁰¹, M. Shehade¹⁸⁰,
 Y. Shen¹²⁸, A.D. Sherman²⁵, P. Sherwood⁹⁵, L. Shi⁹⁵, C.O. Shimmin¹⁸³, Y. Shimogama¹⁷⁹,
 M. Shimojima¹¹⁶, J.D. Shinner⁹⁴, I.P.J. Shipsey¹³⁴, S. Shirabe¹⁶⁵, M. Shiyakova^{80,y}, J. Shlomi¹⁸⁰,
 A. Shmeleva¹¹¹, M.J. Shochet³⁷, J. Shojaii¹⁰⁵, D.R. Shope¹⁵⁴, S. Shrestha¹²⁷, E.M. Shrif^{33e}, M.J. Shroff¹⁷⁶,
 E. Shulga¹⁸⁰, P. Sicho¹⁴⁰, A.M. Sickles¹⁷³, E. Sideras Haddad^{33e}, O. Sidiropoulou³⁶, A. Sidoti^{23b,23a},
 F. Siegert⁴⁸, Dj. Sijacki¹⁶, M.Jr. Silva¹⁸¹, M.V. Silva Oliveira³⁶, S.B. Silverstein^{45a}, S. Simion⁶⁵,
 R. Simoniello¹⁰⁰, C.J. Simpson-allsoy²¹, S. Simsek^{12b}, P. Sinervo¹⁶⁷, V. Sinetckii¹¹³, S. Singh¹⁵²,
 S. Sinha^{33e}, M. Sioli^{23b,23a}, I. Siral¹³¹, S.Yu. Sivoklov¹¹³, J. Sjölin^{45a,45b}, A. Skaf⁵³, E. Skorda⁹⁷,
 P. Skubic¹²⁸, M. Slawinska⁸⁵, K. Sliwa¹⁷⁰, V. Smakhtin¹⁸⁰, B.H. Smart¹⁴³, J. Smiesko^{28b}, N. Smirnov¹¹²,
 S.Yu. Smirnov¹¹², Y. Smirnov¹¹², L.N. Smirnova^{113,s}, O. Smirnova⁹⁷, E.A. Smith³⁷, H.A. Smith¹³⁴,
 M. Smizanska⁹⁰, K. Smolek¹⁴¹, A. Smykiewicz⁸⁵, A.A. Snesarev¹¹¹, H.L. Snoek¹²⁰, I.M. Snyder¹³¹,
 S. Snyder²⁹, R. Sobie^{176,aa}, A. Soffer¹⁶¹, A. Søggaard⁵⁰, F. Sohns⁵³, C.A. Solans Sanchez³⁶,
 E.Yu. Soldatov¹¹², U. Soldevila¹⁷⁴, A.A. Solodkov¹²³, A. Soloshenko⁸⁰, O.V. Solovyanov¹²³,
 V. Solovyev¹³⁷, P. Sommer¹⁴⁹, H. Son¹⁷⁰, A. Sonay¹⁴, W. Song¹⁴³, W.Y. Song^{168b}, A. Sopczak¹⁴¹,
 A.L. Sopio⁹⁵, F. Sopkova^{28b}, S. Sottocornola^{71a,71b}, R. Soualah^{67a,67c}, A.M. Soukharev^{122b,122a}, D. South⁴⁶,
 S. Spagnolo^{68a,68b}, M. Spalla¹¹⁵, M. Spangenberg¹⁷⁸, F. Spanò⁹⁴, D. Sperlich⁵², T.M. Spieker^{61a},
 G. Spigo³⁶, M. Spina¹⁵⁶, D.P. Spiteri⁵⁷, M. Spousta¹⁴², A. Stabile^{69a,69b}, B.L. Stamas¹²¹, R. Stamen^{61a},
 M. Stamenkovic¹²⁰, A. Stampekis²¹, E. Stanecka⁸⁵, B. Stanislaus¹³⁴, M.M. Stanitzki⁴⁶, M. Stankaityte¹³⁴,
 B. Stapf¹²⁰, E.A. Starchenko¹²³, G.H. Stark¹⁴⁵, J. Stark⁵⁸, P. Staroba¹⁴⁰, P. Starovoitov^{61a}, S. Stärz¹⁰⁴,
 R. Staszewski⁸⁵, G. Stavropoulos⁴⁴, M. Stegler⁴⁶, P. Steinberg²⁹, A.L. Steinhebel¹³¹, B. Stelzer^{152,168a},
 H.J. Stelzer¹³⁸, O. Stelzer-Chilton^{168a}, H. Stenzel⁵⁶, T.J. Stevenson¹⁵⁶, G.A. Stewart³⁶, M.C. Stockton³⁶,
 G. Stoicea^{27b}, M. Stolarski^{139a}, S. Stonjek¹¹⁵, A. Straessner⁴⁸, J. Strandberg¹⁵⁴, S. Strandberg^{45a,45b},
 M. Strauss¹²⁸, T. Strebler¹⁰², P. Strizenec^{28b}, R. Ströhmer¹⁷⁷, D.M. Strom¹³¹, R. Stroynowski⁴²,
 A. Strubig^{45a,45b}, S.A. Stucci²⁹, B. Stugu¹⁷, J. Stupak¹²⁸, N.A. Styles⁴⁶, D. Su¹⁵³, W. Su^{60d,148,60c},
 X. Su^{60a}, N.B. Suarez¹³⁸, V.V. Sulin¹¹¹, M.J. Sullivan⁹¹, D.M.S. Sultan⁵⁴, S. Sultansoy^{4c}, T. Sumida⁸⁶,
 S. Sun¹⁰⁶, X. Sun¹⁰¹, C.J.E. Suster¹⁵⁷, M.R. Sutton¹⁵⁶, S. Suzuki⁸², M. Svatos¹⁴⁰, M. Swiatlowski^{168a},
 S.P. Swift², T. Swirski¹⁷⁷, A. Sydorenko¹⁰⁰, I. Sykora^{28a}, M. Sykora¹⁴², T. Sykora¹⁴², D. Ta¹⁰⁰,
 K. Tackmann^{46,x}, J. Taenzer¹⁶¹, A. Taffard¹⁷¹, R. Tafirout^{168a}, E. Tagiev¹²³, R.H.M. Taibah¹³⁵,
 R. Takashima⁸⁷, K. Takeda⁸³, T. Takeshita¹⁵⁰, E.P. Takeva⁵⁰, Y. Takubo⁸², M. Talby¹⁰²,
 A.A. Talyshev^{122b,122a}, K.C. Tam^{63b}, N.M. Tamir¹⁶¹, J. Tanaka¹⁶³, R. Tanaka⁶⁵, S. Tapia Araya¹⁷³,
 S. Tapprogge¹⁰⁰, A. Tarek Abouelfadl Mohamed¹⁰⁷, S. Tarem¹⁶⁰, K. Tariq^{60b}, G. Tarna^{27b,e},
 G.F. Tartarelli^{69a}, P. Tas¹⁴², M. Tasevsky¹⁴⁰, E. Tassi^{41b,41a}, G. Tateno¹⁶³, A. Tavares Delgado^{139a},
 Y. Tayalati^{35f}, A.J. Taylor⁵⁰, G.N. Taylor¹⁰⁵, W. Taylor^{168b}, H. Teagle⁹¹, A.S. Tee⁹⁰,
 R. Teixeira De Lima¹⁵³, P. Teixeira-Dias⁹⁴, H. Ten Kate³⁶, J.J. Teoh¹²⁰, K. Terashi¹⁶³, J. Terron⁹⁹,
 S. Terzo¹⁴, M. Testa⁵¹, R.J. Teuscher^{167,aa}, N. Themistokleous⁵⁰, T. Thevenaux-Pelzer¹⁹, D.W. Thomas⁹⁴,
 J.P. Thomas²¹, E.A. Thompson⁴⁶, P.D. Thompson²¹, E. Thomson¹³⁶, E.J. Thorpe⁹³, V.O. Tikhomirov^{111,ag},
 Yu.A. Tikhonov^{122b,122a}, S. Timoshenko¹¹², P. Tipton¹⁸³, S. Tisserant¹⁰², K. Todome^{23b,23a},
 S. Todorova-Nova¹⁴², S. Todt⁴⁸, J. Tojo⁸⁸, S. Tokár^{28a}, K. Tokushuku⁸², E. Tolley¹²⁷, R. Tombs³²,
 K.G. Tomiwa^{33e}, M. Tomoto^{82,117}, L. Tompkins¹⁵³, P. Tornambe¹⁰³, E. Torrence¹³¹, H. Torres⁴⁸,
 E. Torrò Pastor¹⁷⁴, M. Toscani³⁰, C. Toscirì¹³⁴, J. Toth^{102,z}, D.R. Tovey¹⁴⁹, A. Traeet¹⁷, C.J. Treado¹²⁵,
 T. Trefzger¹⁷⁷, F. Tresoldi¹⁵⁶, A. Tricoli²⁹, I.M. Trigger^{168a}, S. Trincaz-Duvoid¹³⁵, D.A. Trischuk¹⁷⁵,
 W. Trischuk¹⁶⁷, B. Trocmé⁵⁸, A. Trofymov⁶⁵, C. Troncon^{69a}, F. Trovato¹⁵⁶, L. Truong^{33c}, M. Trzebinski⁸⁵,
 A. Trzupek⁸⁵, F. Tsai⁴⁶, P.V. Tsiarehka^{108,ae}, A. Tsigotis^{162,v}, V. Tsiskaridze¹⁵⁵, E.G. Tskhadadze^{159a},
 M. Tsopoulou¹⁶², I.I. Tsukerman¹²⁴, V. Tsulaia¹⁸, S. Tsuno⁸², D. Tsybychev¹⁵⁵, Y. Tu^{63b}, A. Tudorache^{27b},
 V. Tudorache^{27b}, A.N. Tuna³⁶, S. Turchikhin⁸⁰, D. Turgeman¹⁸⁰, I. Turk Cakir^{4b,t}, R.J. Turner²¹,
 R. Turra^{69a}, P.M. Tuts³⁹, S. Tzamarias¹⁶², E. Tzovara¹⁰⁰, K. Uchida¹⁶³, F. Ukegawa¹⁶⁹, G. Unal³⁶,

M. Unal¹¹, A. Undrus²⁹, G. Unel¹⁷¹, F.C. Ungaro¹⁰⁵, Y. Unno⁸², K. Uno¹⁶³, J. Urban^{28b}, P. Urquijo¹⁰⁵,
G. Usai⁸, Z. Uysal^{12d}, V. Vacek¹⁴¹, B. Vachon¹⁰⁴, K.O.H. Vadla¹³³, T. Vafeiadis³⁶, A. Vaidya⁹⁵,
C. Valderanis¹¹⁴, E. Valdes Santurio^{45a,45b}, M. Valente^{168a}, S. Valentinetti^{23b,23a}, A. Valero¹⁷⁴, L. Valéry⁴⁶,
R.A. Vallance²¹, A. Vallier³⁶, J.A. Valls Ferrer¹⁷⁴, T.R. Van Daalen¹⁴, P. Van Gemmeren⁶, S. Van Stroud⁹⁵,
I. Van Vulpen¹²⁰, M. Vanadia^{74a,74b}, W. Vandelli³⁶, M. Vandenbroucke¹⁴⁴, E.R. Vandewall¹²⁹,
D. Vannicola^{73a,73b}, R. Vari^{73a}, E.W. Varnes⁷, C. Varni^{55b,55a}, T. Varol¹⁵⁸, D. Varouchas⁶⁵, K.E. Varvell¹⁵⁷,
M.E. Vasile^{27b}, G.A. Vasquez¹⁷⁶, F. Vazeille³⁸, D. Vazquez Furelos¹⁴, T. Vazquez Schroeder³⁶, J. Veatch⁵³,
V. Vecchio¹⁰¹, M.J. Veen¹²⁰, L.M. Veloce¹⁶⁷, F. Veloso^{139a,139c}, S. Veneziano^{73a}, A. Ventura^{68a,68b},
A. Verbytskyi¹¹⁵, V. Vercesi^{71a}, M. Verducci^{72a,72b}, C.M. Vergel Infante⁷⁹, C. Vergis²⁴, W. Verkerke¹²⁰,
A.T. Vermeulen¹²⁰, J.C. Vermeulen¹²⁰, C. Vernieri¹⁵³, P.J. Verschuuren⁹⁴, M.C. Vetterli^{152,ak},
N. Viaux Maira^{146d}, T. Vickey¹⁴⁹, O.E. Vickey Boeriu¹⁴⁹, G.H.A. Viehhauser¹³⁴, L. Vignani^{61b},
M. Villa^{23b,23a}, M. Villaplana Perez¹⁷⁴, E.M. Villhauer⁵⁰, E. Vilucchi⁵¹, M.G. Vinciter³⁴, G.S. Virdee²¹,
A. Vishwakarma⁵⁰, C. Vittori^{23b,23a}, I. Vivarelli¹⁵⁶, M. Vogel¹⁸², P. Vokac¹⁴¹, J. Von Ahnen⁴⁶,
S.E. von Buddenbrock^{33e}, E. Von Toerne²⁴, V. Vorobel¹⁴², K. Vorobev¹¹², M. Vos¹⁷⁴, J.H. Vosseveld⁹¹,
M. Vozak¹⁰¹, N. Vranjes¹⁶, M. Vranjes Milosavljevic¹⁶, V. Vrba^{141,*}, M. Vreeswijk¹²⁰, N.K. Vu¹⁰²,
R. Vuillermet³⁶, I. Vukotic³⁷, S. Wada¹⁶⁹, P. Wagner²⁴, W. Wagner¹⁸², J. Wagner-Kuhr¹¹⁴, S. Wahdan¹⁸²,
H. Wahlberg⁸⁹, R. Wakasa¹⁶⁹, V.M. Walbrecht¹¹⁵, J. Walder¹⁴³, R. Walker¹¹⁴, S.D. Walker⁹⁴,
W. Walkowiak¹⁵¹, V. Wallangen^{45a,45b}, A.M. Wang⁵⁹, A.Z. Wang¹⁸¹, C. Wang^{60a}, C. Wang^{60c}, H. Wang¹⁸,
H. Wang³, J. Wang^{63a}, P. Wang⁴², Q. Wang¹²⁸, R.-J. Wang¹⁰⁰, R. Wang^{60a}, R. Wang⁶, S.M. Wang¹⁵⁸,
W.T. Wang^{60a}, W. Wang^{15c}, W.X. Wang^{60a}, Y. Wang^{60a}, Z. Wang¹⁰⁶, C. Wanotayaroj⁴⁶, A. Warburton¹⁰⁴,
C.P. Ward³², R.J. Ward²¹, N. Warrack⁵⁷, A.T. Watson²¹, M.F. Watson²¹, G. Watts¹⁴⁸, B.M. Waugh⁹⁵,
A.F. Webb¹¹, C. Weber²⁹, M.S. Weber²⁰, S.A. Weber³⁴, S.M. Weber^{61a}, Y. Wei¹³⁴, A.R. Weidberg¹³⁴,
J. Weingarten⁴⁷, M. Weirich¹⁰⁰, C. Weiser⁵², P.S. Wells³⁶, T. Wenaus²⁹, B. Wendland⁴⁷, T. Wengler³⁶,
S. Wenig³⁶, N. Wermes²⁴, M. Wessels^{61a}, T.D. Weston²⁰, K. Whalen¹³¹, A.M. Wharton⁹⁰, A.S. White¹⁰⁶,
A. White⁸, M.J. White¹, D. Whiteson¹⁷¹, B.W. Whitmore⁹⁰, W. Wiedenmann¹⁸¹, C. Wiel⁴⁸, M. Wielers¹⁴³,
N. Wieseotte¹⁰⁰, C. Wiglesworth⁴⁰, L.A.M. Wiik-Fuchs⁵², H.G. Wilkens³⁶, L.J. Wilkins⁹⁴,
D.M. Williams³⁹, H.H. Williams¹³⁶, S. Williams³², S. Willocq¹⁰³, P.J. Windischhofer¹³⁴,
I. Wingerter-Seez⁵, E. Winkels¹⁵⁶, F. Winklmeier¹³¹, B.T. Winter⁵², M. Wittgen¹⁵³, M. Wobisch⁹⁶,
A. Wolf¹⁰⁰, R. Wölker¹³⁴, J. Wollrath⁵², M.W. Wolter⁸⁵, H. Wolters^{139a,139c}, V.W.S. Wong¹⁷⁵,
A.F. Wongel⁴⁶, N.L. Woods¹⁴⁵, S.D. Worm⁴⁶, B.K. Wosiek⁸⁵, K.W. Woźniak⁸⁵, K. Wraight⁵⁷, S.L. Wu¹⁸¹,
X. Wu⁵⁴, Y. Wu^{60a}, J. Wuerzinger¹³⁴, T.R. Wyatt¹⁰¹, B.M. Wynne⁵⁰, S. Xella⁴⁰, J. Xiang^{63c}, X. Xiao¹⁰⁶,
X. Xie^{60a}, I. Xioidis¹⁵⁶, D. Xu^{15a}, H. Xu^{60a}, H. Xu^{60a}, L. Xu²⁹, R. Xu¹³⁶, T. Xu¹⁴⁴, W. Xu¹⁰⁶, Y. Xu^{15b},
Z. Xu^{60b}, Z. Xu¹⁵³, B. Yabsley¹⁵⁷, S. Yacoub^{33a}, D.P. Yallup⁹⁵, N. Yamaguchi⁸⁸, Y. Yamaguchi¹⁶⁵,
A. Yamamoto⁸², M. Yamatani¹⁶³, T. Yamazaki¹⁶³, Y. Yamazaki⁸³, J. Yan^{60c}, Z. Yan²⁵, H.J. Yang^{60c,60d},
H.T. Yang¹⁸, S. Yang^{60a}, T. Yang^{63c}, X. Yang^{60a}, X. Yang^{60b,58}, Y. Yang¹⁶³, Z. Yang^{60a}, W.-M. Yao¹⁸,
Y.C. Yap⁴⁶, H. Ye^{15c}, J. Ye⁴², S. Ye²⁹, I. Yeletsikh⁸⁰, M.R. Yexley⁹⁰, E. Yigitbasi²⁵, P. Yin³⁹, K. Yorita¹⁷⁹,
K. Yoshihara⁷⁹, C.J.S. Young³⁶, C. Young¹⁵³, J. Yu⁷⁹, R. Yuan^{60b,i}, X. Yue^{61a}, M. Zaazoua^{35f},
B. Zabinski⁸⁵, G. Zacharis¹⁰, E. Zaffaroni⁵⁴, J. Zahreddine¹³⁵, A.M. Zaitsev^{123,af}, T. Zakareishvili^{159b},
N. Zakharchuk³⁴, S. Zambito³⁶, D. Zanzi³⁶, S.V. Zeiβner⁴⁷, C. Zeitnitz¹⁸², G. Zemaityte¹³⁴, J.C. Zeng¹⁷³,
O. Zenin¹²³, T. Ženiš^{28a}, D. Zerwas⁶⁵, M. Zgubić¹³⁴, B. Zhang^{15c}, D.F. Zhang^{15b}, G. Zhang^{15b}, J. Zhang⁶,
K. Zhang^{15a}, L. Zhang^{15c}, L. Zhang^{60a}, M. Zhang¹⁷³, R. Zhang¹⁸¹, S. Zhang¹⁰⁶, X. Zhang^{60c}, X. Zhang^{60b},
Y. Zhang^{15a,15d}, Z. Zhang^{63a}, Z. Zhang⁶⁵, P. Zhao⁴⁹, Y. Zhao¹⁴⁵, Z. Zhao^{60a}, A. Zhemchugov⁸⁰,
Z. Zheng¹⁰⁶, D. Zhong¹⁷³, B. Zhou¹⁰⁶, C. Zhou¹⁸¹, H. Zhou⁷, M. Zhou¹⁵⁵, N. Zhou^{60c}, Y. Zhou⁷,
C.G. Zhu^{60b}, C. Zhu^{15a,15d}, H.L. Zhu^{60a}, H. Zhu^{15a}, J. Zhu¹⁰⁶, Y. Zhu^{60a}, X. Zhuang^{15a}, K. Zhukov¹¹¹,
V. Zhulanov^{122b,122a}, D. Zieminska⁶⁶, N.I. Zimine⁸⁰, S. Zimmermann^{52,*}, Z. Zinonos¹¹⁵, M. Ziolkowski¹⁵¹,
L. Živković¹⁶, G. Zobernig¹⁸¹, A. Zoccoli^{23b,23a}, K. Zoch⁵³, T.G. Zorbas¹⁴⁹, R. Zou³⁷, L. Zwalinski³⁶.

- ¹Department of Physics, University of Adelaide, Adelaide; Australia.
- ²Physics Department, SUNY Albany, Albany NY; United States of America.
- ³Department of Physics, University of Alberta, Edmonton AB; Canada.
- ⁴(^a)Department of Physics, Ankara University, Ankara; (^b)Istanbul Aydin University, Application and Research Center for Advanced Studies, Istanbul; (^c)Division of Physics, TOBB University of Economics and Technology, Ankara; Turkey.
- ⁵LAPP, Université Grenoble Alpes, Université Savoie Mont Blanc, CNRS/IN2P3, Annecy; France.
- ⁶High Energy Physics Division, Argonne National Laboratory, Argonne IL; United States of America.
- ⁷Department of Physics, University of Arizona, Tucson AZ; United States of America.
- ⁸Department of Physics, University of Texas at Arlington, Arlington TX; United States of America.
- ⁹Physics Department, National and Kapodistrian University of Athens, Athens; Greece.
- ¹⁰Physics Department, National Technical University of Athens, Zografou; Greece.
- ¹¹Department of Physics, University of Texas at Austin, Austin TX; United States of America.
- ¹²(^a)Bahcesehir University, Faculty of Engineering and Natural Sciences, Istanbul; (^b)Istanbul Bilgi University, Faculty of Engineering and Natural Sciences, Istanbul; (^c)Department of Physics, Bogazici University, Istanbul; (^d)Department of Physics Engineering, Gaziantep University, Gaziantep; Turkey.
- ¹³Institute of Physics, Azerbaijan Academy of Sciences, Baku; Azerbaijan.
- ¹⁴Institut de Física d'Altes Energies (IFAE), Barcelona Institute of Science and Technology, Barcelona; Spain.
- ¹⁵(^a)Institute of High Energy Physics, Chinese Academy of Sciences, Beijing; (^b)Physics Department, Tsinghua University, Beijing; (^c)Department of Physics, Nanjing University, Nanjing; (^d)University of Chinese Academy of Science (UCAS), Beijing; China.
- ¹⁶Institute of Physics, University of Belgrade, Belgrade; Serbia.
- ¹⁷Department for Physics and Technology, University of Bergen, Bergen; Norway.
- ¹⁸Physics Division, Lawrence Berkeley National Laboratory and University of California, Berkeley CA; United States of America.
- ¹⁹Institut für Physik, Humboldt Universität zu Berlin, Berlin; Germany.
- ²⁰Albert Einstein Center for Fundamental Physics and Laboratory for High Energy Physics, University of Bern, Bern; Switzerland.
- ²¹School of Physics and Astronomy, University of Birmingham, Birmingham; United Kingdom.
- ²²(^a)Facultad de Ciencias y Centro de Investigaciones, Universidad Antonio Nariño, Bogotá; (^b)Departamento de Física, Universidad Nacional de Colombia, Bogotá, Colombia; Colombia.
- ²³(^a)INFN Bologna and Università di Bologna, Dipartimento di Fisica; (^b)INFN Sezione di Bologna; Italy.
- ²⁴Physikalisches Institut, Universität Bonn, Bonn; Germany.
- ²⁵Department of Physics, Boston University, Boston MA; United States of America.
- ²⁶Department of Physics, Brandeis University, Waltham MA; United States of America.
- ²⁷(^a)Transilvania University of Brasov, Brasov; (^b)Horia Hulubei National Institute of Physics and Nuclear Engineering, Bucharest; (^c)Department of Physics, Alexandru Ioan Cuza University of Iasi, Iasi; (^d)National Institute for Research and Development of Isotopic and Molecular Technologies, Physics Department, Cluj-Napoca; (^e)University Politehnica Bucharest, Bucharest; (^f)West University in Timisoara, Timisoara; Romania.
- ²⁸(^a)Faculty of Mathematics, Physics and Informatics, Comenius University, Bratislava; (^b)Department of Subnuclear Physics, Institute of Experimental Physics of the Slovak Academy of Sciences, Kosice; Slovak Republic.
- ²⁹Physics Department, Brookhaven National Laboratory, Upton NY; United States of America.
- ³⁰Departamento de Física, Universidad de Buenos Aires, Buenos Aires; Argentina.
- ³¹California State University, CA; United States of America.

- ³²Cavendish Laboratory, University of Cambridge, Cambridge; United Kingdom.
- ³³(^a)Department of Physics, University of Cape Town, Cape Town; (^b)iThemba Labs, Western Cape; (^c)Department of Mechanical Engineering Science, University of Johannesburg, Johannesburg; (^d)University of South Africa, Department of Physics, Pretoria; (^e)School of Physics, University of the Witwatersrand, Johannesburg; South Africa.
- ³⁴Department of Physics, Carleton University, Ottawa ON; Canada.
- ³⁵(^a)Faculté des Sciences Ain Chock, Réseau Universitaire de Physique des Hautes Energies - Université Hassan II, Casablanca; (^b)Faculté des Sciences, Université Ibn-Tofail, Kénitra; (^c)Faculté des Sciences Semlalia, Université Cadi Ayyad, LPHEA-Marrakech; (^d)Moroccan Foundation for Advanced Science Innovation and Research (MAScIR), Rabat; (^e)LPMR, Faculté des Sciences, Université Mohamed Premier, Oujda; (^f)Faculté des sciences, Université Mohammed V, Rabat; Morocco.
- ³⁶CERN, Geneva; Switzerland.
- ³⁷Enrico Fermi Institute, University of Chicago, Chicago IL; United States of America.
- ³⁸LPC, Université Clermont Auvergne, CNRS/IN2P3, Clermont-Ferrand; France.
- ³⁹Nevis Laboratory, Columbia University, Irvington NY; United States of America.
- ⁴⁰Niels Bohr Institute, University of Copenhagen, Copenhagen; Denmark.
- ⁴¹(^a)Dipartimento di Fisica, Università della Calabria, Rende; (^b)INFN Gruppo Collegato di Cosenza, Laboratori Nazionali di Frascati; Italy.
- ⁴²Physics Department, Southern Methodist University, Dallas TX; United States of America.
- ⁴³Physics Department, University of Texas at Dallas, Richardson TX; United States of America.
- ⁴⁴National Centre for Scientific Research "Demokritos", Agia Paraskevi; Greece.
- ⁴⁵(^a)Department of Physics, Stockholm University; (^b)Oskar Klein Centre, Stockholm; Sweden.
- ⁴⁶Deutsches Elektronen-Synchrotron DESY, Hamburg and Zeuthen; Germany.
- ⁴⁷Lehrstuhl für Experimentelle Physik IV, Technische Universität Dortmund, Dortmund; Germany.
- ⁴⁸Institut für Kern- und Teilchenphysik, Technische Universität Dresden, Dresden; Germany.
- ⁴⁹Department of Physics, Duke University, Durham NC; United States of America.
- ⁵⁰SUPA - School of Physics and Astronomy, University of Edinburgh, Edinburgh; United Kingdom.
- ⁵¹INFN e Laboratori Nazionali di Frascati, Frascati; Italy.
- ⁵²Physikalisches Institut, Albert-Ludwigs-Universität Freiburg, Freiburg; Germany.
- ⁵³II. Physikalisches Institut, Georg-August-Universität Göttingen, Göttingen; Germany.
- ⁵⁴Département de Physique Nucléaire et Corpusculaire, Université de Genève, Genève; Switzerland.
- ⁵⁵(^a)Dipartimento di Fisica, Università di Genova, Genova; (^b)INFN Sezione di Genova; Italy.
- ⁵⁶II. Physikalisches Institut, Justus-Liebig-Universität Giessen, Giessen; Germany.
- ⁵⁷SUPA - School of Physics and Astronomy, University of Glasgow, Glasgow; United Kingdom.
- ⁵⁸LPSC, Université Grenoble Alpes, CNRS/IN2P3, Grenoble INP, Grenoble; France.
- ⁵⁹Laboratory for Particle Physics and Cosmology, Harvard University, Cambridge MA; United States of America.
- ⁶⁰(^a)Department of Modern Physics and State Key Laboratory of Particle Detection and Electronics, University of Science and Technology of China, Hefei; (^b)Institute of Frontier and Interdisciplinary Science and Key Laboratory of Particle Physics and Particle Irradiation (MOE), Shandong University, Qingdao; (^c)School of Physics and Astronomy, Shanghai Jiao Tong University, Key Laboratory for Particle Astrophysics and Cosmology (MOE), SKLPPC, Shanghai; (^d)Tsun-Dao Lee Institute, Shanghai; China.
- ⁶¹(^a)Kirchhoff-Institut für Physik, Ruprecht-Karls-Universität Heidelberg, Heidelberg; (^b)Physikalisches Institut, Ruprecht-Karls-Universität Heidelberg, Heidelberg; Germany.
- ⁶²Faculty of Applied Information Science, Hiroshima Institute of Technology, Hiroshima; Japan.
- ⁶³(^a)Department of Physics, Chinese University of Hong Kong, Shatin, N.T., Hong Kong; (^b)Department of Physics, University of Hong Kong, Hong Kong; (^c)Department of Physics and Institute for Advanced

- Study, Hong Kong University of Science and Technology, Clear Water Bay, Kowloon, Hong Kong; China.
- ⁶⁴Department of Physics, National Tsing Hua University, Hsinchu; Taiwan.
- ⁶⁵IJCLab, Université Paris-Saclay, CNRS/IN2P3, 91405, Orsay; France.
- ⁶⁶Department of Physics, Indiana University, Bloomington IN; United States of America.
- ⁶⁷(^a)INFN Gruppo Collegato di Udine, Sezione di Trieste, Udine; (^b)ICTP, Trieste; (^c)Dipartimento Politecnico di Ingegneria e Architettura, Università di Udine, Udine; Italy.
- ⁶⁸(^a)INFN Sezione di Lecce; (^b)Dipartimento di Matematica e Fisica, Università del Salento, Lecce; Italy.
- ⁶⁹(^a)INFN Sezione di Milano; (^b)Dipartimento di Fisica, Università di Milano, Milano; Italy.
- ⁷⁰(^a)INFN Sezione di Napoli; (^b)Dipartimento di Fisica, Università di Napoli, Napoli; Italy.
- ⁷¹(^a)INFN Sezione di Pavia; (^b)Dipartimento di Fisica, Università di Pavia, Pavia; Italy.
- ⁷²(^a)INFN Sezione di Pisa; (^b)Dipartimento di Fisica E. Fermi, Università di Pisa, Pisa; Italy.
- ⁷³(^a)INFN Sezione di Roma; (^b)Dipartimento di Fisica, Sapienza Università di Roma, Roma; Italy.
- ⁷⁴(^a)INFN Sezione di Roma Tor Vergata; (^b)Dipartimento di Fisica, Università di Roma Tor Vergata, Roma; Italy.
- ⁷⁵(^a)INFN Sezione di Roma Tre; (^b)Dipartimento di Matematica e Fisica, Università Roma Tre, Roma; Italy.
- ⁷⁶(^a)INFN-TIFPA; (^b)Università degli Studi di Trento, Trento; Italy.
- ⁷⁷Institut für Astro- und Teilchenphysik, Leopold-Franzens-Universität, Innsbruck; Austria.
- ⁷⁸University of Iowa, Iowa City IA; United States of America.
- ⁷⁹Department of Physics and Astronomy, Iowa State University, Ames IA; United States of America.
- ⁸⁰Joint Institute for Nuclear Research, Dubna; Russia.
- ⁸¹(^a)Departamento de Engenharia Elétrica, Universidade Federal de Juiz de Fora (UFJF), Juiz de Fora; (^b)Universidade Federal do Rio De Janeiro COPPE/EE/IF, Rio de Janeiro; (^c)Instituto de Física, Universidade de São Paulo, São Paulo; Brazil.
- ⁸²KEK, High Energy Accelerator Research Organization, Tsukuba; Japan.
- ⁸³Graduate School of Science, Kobe University, Kobe; Japan.
- ⁸⁴(^a)AGH University of Science and Technology, Faculty of Physics and Applied Computer Science, Krakow; (^b)Marian Smoluchowski Institute of Physics, Jagiellonian University, Krakow; Poland.
- ⁸⁵Institute of Nuclear Physics Polish Academy of Sciences, Krakow; Poland.
- ⁸⁶Faculty of Science, Kyoto University, Kyoto; Japan.
- ⁸⁷Kyoto University of Education, Kyoto; Japan.
- ⁸⁸Research Center for Advanced Particle Physics and Department of Physics, Kyushu University, Fukuoka ; Japan.
- ⁸⁹Instituto de Física La Plata, Universidad Nacional de La Plata and CONICET, La Plata; Argentina.
- ⁹⁰Physics Department, Lancaster University, Lancaster; United Kingdom.
- ⁹¹Oliver Lodge Laboratory, University of Liverpool, Liverpool; United Kingdom.
- ⁹²Department of Experimental Particle Physics, Jožef Stefan Institute and Department of Physics, University of Ljubljana, Ljubljana; Slovenia.
- ⁹³School of Physics and Astronomy, Queen Mary University of London, London; United Kingdom.
- ⁹⁴Department of Physics, Royal Holloway University of London, Egham; United Kingdom.
- ⁹⁵Department of Physics and Astronomy, University College London, London; United Kingdom.
- ⁹⁶Louisiana Tech University, Ruston LA; United States of America.
- ⁹⁷Fysiska institutionen, Lunds universitet, Lund; Sweden.
- ⁹⁸Centre de Calcul de l'Institut National de Physique Nucléaire et de Physique des Particules (IN2P3), Villeurbanne; France.
- ⁹⁹Departamento de Física Teórica C-15 and CIAFF, Universidad Autónoma de Madrid, Madrid; Spain.
- ¹⁰⁰Institut für Physik, Universität Mainz, Mainz; Germany.

- ¹⁰¹School of Physics and Astronomy, University of Manchester, Manchester; United Kingdom.
- ¹⁰²CPPM, Aix-Marseille Université, CNRS/IN2P3, Marseille; France.
- ¹⁰³Department of Physics, University of Massachusetts, Amherst MA; United States of America.
- ¹⁰⁴Department of Physics, McGill University, Montreal QC; Canada.
- ¹⁰⁵School of Physics, University of Melbourne, Victoria; Australia.
- ¹⁰⁶Department of Physics, University of Michigan, Ann Arbor MI; United States of America.
- ¹⁰⁷Department of Physics and Astronomy, Michigan State University, East Lansing MI; United States of America.
- ¹⁰⁸B.I. Stepanov Institute of Physics, National Academy of Sciences of Belarus, Minsk; Belarus.
- ¹⁰⁹Research Institute for Nuclear Problems of Byelorussian State University, Minsk; Belarus.
- ¹¹⁰Group of Particle Physics, University of Montreal, Montreal QC; Canada.
- ¹¹¹P.N. Lebedev Physical Institute of the Russian Academy of Sciences, Moscow; Russia.
- ¹¹²National Research Nuclear University MEPhI, Moscow; Russia.
- ¹¹³D.V. Skobeltsyn Institute of Nuclear Physics, M.V. Lomonosov Moscow State University, Moscow; Russia.
- ¹¹⁴Fakultät für Physik, Ludwig-Maximilians-Universität München, München; Germany.
- ¹¹⁵Max-Planck-Institut für Physik (Werner-Heisenberg-Institut), München; Germany.
- ¹¹⁶Nagasaki Institute of Applied Science, Nagasaki; Japan.
- ¹¹⁷Graduate School of Science and Kobayashi-Maskawa Institute, Nagoya University, Nagoya; Japan.
- ¹¹⁸Department of Physics and Astronomy, University of New Mexico, Albuquerque NM; United States of America.
- ¹¹⁹Institute for Mathematics, Astrophysics and Particle Physics, Radboud University/Nikhef, Nijmegen; Netherlands.
- ¹²⁰Nikhef National Institute for Subatomic Physics and University of Amsterdam, Amsterdam; Netherlands.
- ¹²¹Department of Physics, Northern Illinois University, DeKalb IL; United States of America.
- ¹²²^(a) Budker Institute of Nuclear Physics and NSU, SB RAS, Novosibirsk; ^(b) Novosibirsk State University Novosibirsk; Russia.
- ¹²³Institute for High Energy Physics of the National Research Centre Kurchatov Institute, Protvino; Russia.
- ¹²⁴Institute for Theoretical and Experimental Physics named by A.I. Alikhanov of National Research Centre "Kurchatov Institute", Moscow; Russia.
- ¹²⁵Department of Physics, New York University, New York NY; United States of America.
- ¹²⁶Ochanomizu University, Otsuka, Bunkyo-ku, Tokyo; Japan.
- ¹²⁷Ohio State University, Columbus OH; United States of America.
- ¹²⁸Homer L. Dodge Department of Physics and Astronomy, University of Oklahoma, Norman OK; United States of America.
- ¹²⁹Department of Physics, Oklahoma State University, Stillwater OK; United States of America.
- ¹³⁰Palacký University, RCPTM, Joint Laboratory of Optics, Olomouc; Czech Republic.
- ¹³¹Institute for Fundamental Science, University of Oregon, Eugene, OR; United States of America.
- ¹³²Graduate School of Science, Osaka University, Osaka; Japan.
- ¹³³Department of Physics, University of Oslo, Oslo; Norway.
- ¹³⁴Department of Physics, Oxford University, Oxford; United Kingdom.
- ¹³⁵LPNHE, Sorbonne Université, Université de Paris, CNRS/IN2P3, Paris; France.
- ¹³⁶Department of Physics, University of Pennsylvania, Philadelphia PA; United States of America.
- ¹³⁷Konstantinov Nuclear Physics Institute of National Research Centre "Kurchatov Institute", PNPI, St. Petersburg; Russia.
- ¹³⁸Department of Physics and Astronomy, University of Pittsburgh, Pittsburgh PA; United States of

America.

¹³⁹(*a*) Laboratório de Instrumentação e Física Experimental de Partículas - LIP, Lisboa; (*b*) Departamento de Física, Faculdade de Ciências, Universidade de Lisboa, Lisboa; (*c*) Departamento de Física, Universidade de Coimbra, Coimbra; (*d*) Centro de Física Nuclear da Universidade de Lisboa, Lisboa; (*e*) Departamento de Física, Universidade do Minho, Braga; (*f*) Departamento de Física Teórica y del Cosmos, Universidad de Granada, Granada (Spain); (*g*) Dep Física and CEFITEC of Faculdade de Ciências e Tecnologia, Universidade Nova de Lisboa, Caparica; (*h*) Instituto Superior Técnico, Universidade de Lisboa, Lisboa; Portugal.

¹⁴⁰Institute of Physics of the Czech Academy of Sciences, Prague; Czech Republic.

¹⁴¹Czech Technical University in Prague, Prague; Czech Republic.

¹⁴²Charles University, Faculty of Mathematics and Physics, Prague; Czech Republic.

¹⁴³Particle Physics Department, Rutherford Appleton Laboratory, Didcot; United Kingdom.

¹⁴⁴IRFU, CEA, Université Paris-Saclay, Gif-sur-Yvette; France.

¹⁴⁵Santa Cruz Institute for Particle Physics, University of California Santa Cruz, Santa Cruz CA; United States of America.

¹⁴⁶(*a*) Departamento de Física, Pontificia Universidad Católica de Chile, Santiago; (*b*) Universidad Andres Bello, Department of Physics, Santiago; (*c*) Instituto de Alta Investigación, Universidad de Tarapacá; (*d*) Departamento de Física, Universidad Técnica Federico Santa María, Valparaíso; Chile.

¹⁴⁷Universidade Federal de São João del Rei (UFSJ), São João del Rei; Brazil.

¹⁴⁸Department of Physics, University of Washington, Seattle WA; United States of America.

¹⁴⁹Department of Physics and Astronomy, University of Sheffield, Sheffield; United Kingdom.

¹⁵⁰Department of Physics, Shinshu University, Nagano; Japan.

¹⁵¹Department Physik, Universität Siegen, Siegen; Germany.

¹⁵²Department of Physics, Simon Fraser University, Burnaby BC; Canada.

¹⁵³SLAC National Accelerator Laboratory, Stanford CA; United States of America.

¹⁵⁴Physics Department, Royal Institute of Technology, Stockholm; Sweden.

¹⁵⁵Departments of Physics and Astronomy, Stony Brook University, Stony Brook NY; United States of America.

¹⁵⁶Department of Physics and Astronomy, University of Sussex, Brighton; United Kingdom.

¹⁵⁷School of Physics, University of Sydney, Sydney; Australia.

¹⁵⁸Institute of Physics, Academia Sinica, Taipei; Taiwan.

¹⁵⁹(*a*) E. Andronikashvili Institute of Physics, Iv. Javakhishvili Tbilisi State University, Tbilisi; (*b*) High Energy Physics Institute, Tbilisi State University, Tbilisi; Georgia.

¹⁶⁰Department of Physics, Technion, Israel Institute of Technology, Haifa; Israel.

¹⁶¹Raymond and Beverly Sackler School of Physics and Astronomy, Tel Aviv University, Tel Aviv; Israel.

¹⁶²Department of Physics, Aristotle University of Thessaloniki, Thessaloniki; Greece.

¹⁶³International Center for Elementary Particle Physics and Department of Physics, University of Tokyo, Tokyo; Japan.

¹⁶⁴Graduate School of Science and Technology, Tokyo Metropolitan University, Tokyo; Japan.

¹⁶⁵Department of Physics, Tokyo Institute of Technology, Tokyo; Japan.

¹⁶⁶Tomsk State University, Tomsk; Russia.

¹⁶⁷Department of Physics, University of Toronto, Toronto ON; Canada.

¹⁶⁸(*a*) TRIUMF, Vancouver BC; (*b*) Department of Physics and Astronomy, York University, Toronto ON; Canada.

¹⁶⁹Division of Physics and Tomonaga Center for the History of the Universe, Faculty of Pure and Applied Sciences, University of Tsukuba, Tsukuba; Japan.

¹⁷⁰Department of Physics and Astronomy, Tufts University, Medford MA; United States of America.

- ¹⁷¹Department of Physics and Astronomy, University of California Irvine, Irvine CA; United States of America.
- ¹⁷²Department of Physics and Astronomy, University of Uppsala, Uppsala; Sweden.
- ¹⁷³Department of Physics, University of Illinois, Urbana IL; United States of America.
- ¹⁷⁴Instituto de Física Corpuscular (IFIC), Centro Mixto Universidad de Valencia - CSIC, Valencia; Spain.
- ¹⁷⁵Department of Physics, University of British Columbia, Vancouver BC; Canada.
- ¹⁷⁶Department of Physics and Astronomy, University of Victoria, Victoria BC; Canada.
- ¹⁷⁷Fakultät für Physik und Astronomie, Julius-Maximilians-Universität Würzburg, Würzburg; Germany.
- ¹⁷⁸Department of Physics, University of Warwick, Coventry; United Kingdom.
- ¹⁷⁹Waseda University, Tokyo; Japan.
- ¹⁸⁰Department of Particle Physics and Astrophysics, Weizmann Institute of Science, Rehovot; Israel.
- ¹⁸¹Department of Physics, University of Wisconsin, Madison WI; United States of America.
- ¹⁸²Fakultät für Mathematik und Naturwissenschaften, Fachgruppe Physik, Bergische Universität Wuppertal, Wuppertal; Germany.
- ¹⁸³Department of Physics, Yale University, New Haven CT; United States of America.
- ^a Also at Borough of Manhattan Community College, City University of New York, New York NY; United States of America.
- ^b Also at Center for High Energy Physics, Peking University; China.
- ^c Also at Centro Studi e Ricerche Enrico Fermi; Italy.
- ^d Also at CERN, Geneva; Switzerland.
- ^e Also at CPPM, Aix-Marseille Université, CNRS/IN2P3, Marseille; France.
- ^f Also at Département de Physique Nucléaire et Corpusculaire, Université de Genève, Genève; Switzerland.
- ^g Also at Departament de Física de la Universitat Autònoma de Barcelona, Barcelona; Spain.
- ^h Also at Department of Financial and Management Engineering, University of the Aegean, Chios; Greece.
- ⁱ Also at Department of Physics and Astronomy, Michigan State University, East Lansing MI; United States of America.
- ^j Also at Department of Physics and Astronomy, University of Louisville, Louisville, KY; United States of America.
- ^k Also at Department of Physics, Ben Gurion University of the Negev, Beer Sheva; Israel.
- ^l Also at Department of Physics, California State University, East Bay; United States of America.
- ^m Also at Department of Physics, California State University, Fresno; United States of America.
- ⁿ Also at Department of Physics, California State University, Sacramento; United States of America.
- ^o Also at Department of Physics, King's College London, London; United Kingdom.
- ^p Also at Department of Physics, St. Petersburg State Polytechnical University, St. Petersburg; Russia.
- ^q Also at Department of Physics, University of Fribourg, Fribourg; Switzerland.
- ^r Also at Dipartimento di Matematica, Informatica e Fisica, Università di Udine, Udine; Italy.
- ^s Also at Faculty of Physics, M.V. Lomonosov Moscow State University, Moscow; Russia.
- ^t Also at Giresun University, Faculty of Engineering, Giresun; Turkey.
- ^u Also at Graduate School of Science, Osaka University, Osaka; Japan.
- ^v Also at Hellenic Open University, Patras; Greece.
- ^w Also at Institutio Catalana de Recerca i Estudis Avancats, ICREA, Barcelona; Spain.
- ^x Also at Institut für Experimentalphysik, Universität Hamburg, Hamburg; Germany.
- ^y Also at Institute for Nuclear Research and Nuclear Energy (INRNE) of the Bulgarian Academy of Sciences, Sofia; Bulgaria.
- ^z Also at Institute for Particle and Nuclear Physics, Wigner Research Centre for Physics, Budapest; Hungary.

- aa* Also at Institute of Particle Physics (IPP); Canada.
- ab* Also at Institute of Physics, Azerbaijan Academy of Sciences, Baku; Azerbaijan.
- ac* Also at Instituto de Fisica Teorica, IFT-UAM/CSIC, Madrid; Spain.
- ad* Also at Istanbul University, Dept. of Physics, Istanbul; Turkey.
- ae* Also at Joint Institute for Nuclear Research, Dubna; Russia.
- af* Also at Moscow Institute of Physics and Technology State University, Dolgoprudny; Russia.
- ag* Also at National Research Nuclear University MEPhI, Moscow; Russia.
- ah* Also at Physics Department, An-Najah National University, Nablus; Palestine.
- ai* Also at Physikalisches Institut, Albert-Ludwigs-Universität Freiburg, Freiburg; Germany.
- aj* Also at The City College of New York, New York NY; United States of America.
- ak* Also at TRIUMF, Vancouver BC; Canada.
- al* Also at Università di Napoli Parthenope, Napoli; Italy.
- am* Also at University of Chinese Academy of Sciences (UCAS), Beijing; China.
- * Deceased